論文 / 著書情報
Article / Book Information

題目(和文)	大規模基地局連携を用いた動的カバレッジ制御を実現する高度なセルラネットワークアーキテクチャに関する研究
Title(English)	Efficient architecture of cellular networks for dynamic cell structuring with large-scale base station cooperation
著者(和文)	E.RezagahRoya
Author(English)	Roya Rezagah
出典(和文)	学位:博士（工学）, 学位授与機関:東京工業大学, 報告番号:甲第9629号, 授与年月日:2014年9月25日, 学位の種別:課程博士, 審査員:鈴木　博,安藤　真,府川　和彦,古谷　之綱,秋葉　重幸,阪口　啓
Citation(English)	Degree:, Conferring organization: Tokyo Institute of Technology, Report number:甲第9629号, Conferred date:2014/9/25, Degree Type:Course doctor, Examiner:,,,,,
学位種別(和文)	博士論文
Type(English)	Doctoral Thesis

EFFICIENT ARCHITECTURE OF CELLULAR NETWORKS FOR DYNAMIC CELL STRUCTURING WITH LARGE-SCALE BASE STATION COOPERATION

A Dissertation

Presented to the Department of Electrical and Electronic Engineering,

Graduate School of Science and Engineering

of Tokyo Institute of Technology

in Partial Fulfillment of the Requirements for the Degree of

Doctor of Engineering

by

Roya Ebrahim Rezagah

August 2014

EFFICIENT ARCHITECTURE OF CELLULAR NETWORKS FOR DYNAMIC CELL STRUCTURING WITH LARGE-SCALE BASE STATION COOPERATION

Abstract- This research focuses on a heterogeneous wireless cellular network consisting of small cells within macro cells. The thesis aims to provide a development direction to utilize the network resources to the utmost extent. It is started with random non coordinated networks. The main limiting factor in a non coordinated network is the interference. Then step by step, more advanced schemes are added to the network to reduce or eliminate the interference and improve network's performance. At first, full coordination is added to the network. It is shown that although such a coordination improves the system rate in some scenarios, it cannot fit to the dynamics of the traffic demand in a cellular network. Therefore, a more advanced scheme is introduced. In this scheme dynamic coverage control of BSs alongside large scale clusters direct idle network resources from sparse areas to the congestion areas. This method is especially beneficial when there are some distinct congestion zones in the network. This scheme can achieve several times higher capacity than the previous schemes. In addition, by introducing rank adaptation in the large scale clusters the system rate can be increased even more. Then gain in the system rate can be more than 100 percent depending on the scenario and environment. This huge gain is a motivation for further study on the aspects and issues of the practical implementation. The last part of the thesis discusses the required measurement and signaling scheme for the practical implementation based on the concept of C/U splitting and signaling schemes that are currently considered in 3GPP standardization. This can insure the feasibility of the scheme.

ACKNOWLEDGEMENTS

My deepest gratitude goes to my research advisor, Associate Professor Kei Sakaguchi for his patience, motivation, enthusiasm, and for his unique insight. Without his help and guidance, none of this research could be accomplished. I should also thank Professor Kiyomichi Araki for his continuous support in all stages of the student life and research. Also my special gratitude to Professor Hiroshi Suzuki who supported my study after Professor Kiyomichi Araki's retirement. Also, I would like to thank the rest of my thesis examination committee whose comments and advices helped me a lot in improving the quality of this thesis: Professor Kazuhiko Fukawa, Professor Makoto Ando, Professor Shigeyuki Akiba and Professor Yukitsuna Furuya. My sincere thanks also goes to Assistant Professor Gia Khanh Tran who is always available for the students and has a major role in running the laboratory smoothly.

Thanks to my research advisor, Associate Professor Kei Sakaguchi, I had the chance to meet and work with many experts and experienced people from different companies and incorporations. I should specially thank to Dr. Satoshi Konishi from KDDI Inc. and Mr. Shinobu Nanba from KDDI R&D labs. Regular contact and meetings with these experts was a guideline to keep the research in a correct direction. Also, I should thank Mr. Toshiaki Yamamoto from KDDI R&D labs. who kindly provided critical support and advise in this research.

During the study in Araki-Sakaguchi lab. I was blessed with a nice and friendly environment and colleagues. I am grateful to all of them. However, I should explicitly thank the doctoral student Hidekazu Shimodaira, for his cooperation in all stages of this research.

Finally my deep gratitude to my family who are the true light of my life. I am thankful to their constant support and encouragement in every moment of my life.

Finally, it should be mentioned that a part of this research is done as a project named Milimeter-Wave Evolution for Backhaul and Access (MiWEBA) under international cooperation program of ICT-2013 EU-Japan supported by FP7 in EU and MIC in Japan.

TABLE OF CONTENTS

Acknowledgements . . . iii
Table of Contents . . . v
List of Tables . . . vii
List of Figures . . . viii
List of Abbreviations . . . x

1 Introduction **1**
1.1 Current status and advances in cellular networks . . . 1
1.1.1 Coordinated multipoint (CoMP) . . . 4
1.1.2 Centralized radio access network (C-RAN) . . . 7
1.2 Objectives of the thesis . . . 8
1.3 Thesis structure . . . 11

2 Capacity in random non-cooperative networks **13**
2.1 Introduction . . . 13
2.2 Network scenario . . . 14
2.3 System rate analysis . . . 17
2.4 Numerical results . . . 23
2.5 Conclusion . . . 26

3 Capacity in a cooperative cellular network **27**
3.1 Introduction . . . 27
3.2 System model . . . 28
3.2.1 Downlink communication model . . . 28
3.2.2 Antenna gain and path loss model . . . 30
3.3 Numerical results . . . 33
3.3.1 Uniform user distribution . . . 35
3.3.2 Hotspot . . . 37
3.4 Conclusion . . . 39

4 Dynamic cell structuring and large-scale cooperation **40**
4.1 Introduction . . . 40
4.2 System rate analysis . . . 41
4.3 Clustering mechanism for large scale CoMP . . . 47
4.3.1 Optimization of antenna beam angles . . . 50
4.3.2 Optimal BS selection for the clusters . . . 54
4.4 Numerical results and discussion . . . 55
4.4.1 Capacity trend versus cluster size . . . 57
4.4.2 Effect of shadowing . . . 59
4.4.3 Effect of hotspot size . . . 60
4.4.4 Two-hotspot scenario . . . 63
4.4.5 Rank adaptation . . . 66
4.5 Conclusion . . . 71

5 Protocol for dynamic cluster formation **74**
5.1 Introduction . . . 74
5.1.1 The concept of C/U splitting . . . 75
5.1.2 Positioning in LTE . . . 76
5.2 Scenario and objectives . . . 77
5.3 Selection of SC-BSs for control signal transmissions . . . 83
5.4 Optimal cluster formation . . . 87
5.5 Numerical results . . . 92
5.6 Conclusion . . . 92

6 Conclusion **96**
6.1 Achievements of the thesis at a glance . . . 96
6.2 Open issues and future study . . . 98

A PDF of the eigenvalues of a Wishart matrix **100**

B Publications **101**
B.1 Publications related to this thesis . . . 101
B.1.1 Journal papers . . . 101
B.1.2 Book chapter . . . 101
B.1.3 Conference paper . . . 102
B.1.4 Technical report . . . 102
B.2 Others . . . 102

Bibliography **104**

LIST OF TABLES

1.1 Characteristics of different schemes of CoMP 6

3.1 Parameters for numerical evaluations 36

4.1 Summary of the clustering algorithm 53
4.2 Parameters for numerical evaluations 56

5.1 Positioning methods in LTE and their accuracies 76
5.2 The algorithm of SC-BS selection for control signal transmission . 86

LIST OF FIGURES

1.1 Schematic curves that show the relation of data traffic demand and the area and time. . . . 3
1.2 Three different CoMP schemes: (a)dynamic point selection (DPS), (b)coordinated scheduling/ beamforming (CS/CB), (c)joint transmission (JT) . . . 5
1.3 (a) Architecture of a network of distinct standalone BSs, (b) C-RAN architecture . . . 7
1.4 Dynamic transfer of network resources to dense areas. . . . 10

2.1 The scenario for a random non-cooperative network . . . 16
2.2 (a) Hexagonal small cell, (b) a lattice network with hexagonal small cells, (c) a random network with the same netwrok radius, R, and the same density of SC-BSs. . . . 24
2.3 System rate of a non-coordinated random network versus normalized network radius, R/d. . . . 25

3.1 Demonstration of (a) horizontal and (b) vertical beam patterns and corresponding angles. . . . 31
3.2 The scenario of a regular lattice network, with network radius R and inter-site distance od d. . . . 34
3.3 Effect of sectoral antennas and full BS cooperation on the system rate in a network with uniform user distribution. . . . 37
3.4 System rate for the hotspot scenario in non-coordinated and full cooperation cases. . . . 38

4.1 A large cluster to serve users in a hotspot zone. . . . 42
4.2 Modeling a cooperative cluster as a distributed MIMO which consists of a single aggregated BS with $K_{\mathrm{BS}}M_{\mathrm{T}}$ distributed antennas to K_{UE} user equipments. . . . 43
4.3 A cluster of 5 tiers around the dense area of the central cell. . . . 57
4.4 System rate vs. number of tiers in the clusters for single hotspot case as shown in Fig. 4.3. . . . 58
4.5 Shadowing degrades the system rate. . . . 60
4.6 A certain cluster is considered and the radius of the hotspot is considered to vary from zero to $4d$. . . . 61
4.7 Effect of the hotspot radius on the system rate . . . 62
4.8 Two dense areas in the network and the proposed clusters with optimal beam directions around them; vertical tilt angles in degrees are also written beside corresponding BSs. . . . 64
4.9 Average system rate of the proposed scheme and conventional scheme versus number of tiers in the clusters. The scenarios and corresponding parameters, D and d, are shown in Figs. 4.3 and 4.8. Here, P_t = 30 dBm for all cases. . . . 66

4.10 System rate vs. K_{UE} for a 3-tier cluster in the single hotspot scenario (K_{BS} = 21). 67
4.11 Optimal K_{UE} vs. number of BSs in the cluster, K_{BS}, in the single hotspot scenario. 68
4.12 Effect of the rank adaptation for the single hotspot case. 69
4.13 Optimal clusters with rank optimization for the two-hotspot scenario. 70
4.14 Optimal K_{UE} vs. number of BSs in the cluster, K_{BS}, for the two-hotspot scenario shown in Fig. 4.13. 71
4.15 Effect of the rank adaptation for the two-hotspot scenario shown in Fig. 4.13. 72

5.1 The concept of C/U splitting 75
5.2 Scenario: There is a macro cell and several SC-BSs within the macro cell. The macro cell area is tiled by hexagonal small areas. 78
5.3 The protocol to detect the hotspot zones and its position with regard to the dynamic coverage control phase and cluster formation. 79
5.4 (a) A scenario with a single hotspot zone; (b) the macro BS recognizes tentative hotspot zones based on the estimated locations of UEs. 80
5.5 A SC-BS may use different antenna tilt angles to transmit control signals in order to target different tiers around it. 82
5.6 For a tentative hotspot, a list of SC-BSs in tiers around it are considered. Signal transmissions from these SC-BSs can cover some areas in the tentative hotspot control. 84
5.7 Several SC-BSs are selected to transmit reference signal (RS) to different tiers around them. 87
5.8 The protocol to obtain optimal antenna direction for a SC-BS. . . . 88
5.9 The protocol to obtain optimal antenna direction for a SC-BS in case when the prior knowledge of the calibrated RF pattern of the SC-BS in the whole area is available. 90
5.10 Optimal antenna beam directions: horizontal sector is shown in the figure and vertical tilt angle is written beside it. 91
5.11 The order at which the BSs are going to be considered for the cluster. 93
5.12 The result of cell structuring and large scale clustering for the scenario of Fig. 5.4. 94

LIST OF ABBREVIATIONS

A-GNSS	Autonomous and assisted Global Navigation Satellite Systems
BD	Block Diagonalization
BS	Base Station
CoMP	Coordinated Multipoint
C-plane	Control plane
C-RAN	centralized Radio Access Network
CRS	Cell-specific Reference Signal
CS/CB	Coordinated Scheduling/ Coordinated Beamforming
DL	Downlink
DPS	Dynamic Point Selection
E-CID	Enhanced Cell ID
e-NodeB	Enhanced NodeB
GPS	Global Positioning System
JT	Joint Transmission
LTE	Long-Term Evolution
LTE-A	Long-Term Evolution-Advanced
MAC	Medium Access Control
OTDOA	Observed Time Difference Of Arrival
PRS	Position Reference Signal
RRC	Radio Resource Control
RS	Reference Signal
RSRP	Reference Signal Received Power
SC transmission	Single Cell transmission
SC-BS	Small Cell Base Station
UE	User Equipment
UL	Uplink
U-plane	User plane
UTDOA	Uplink Time Difference-of-Arrival

CHAPTER 1

INTRODUCTION

1.1 Current status and advances in cellular networks

International Mobile Telecommunications-Advanced (IMT-Advanced) are requirements issued by the ITU-R in 2008 for 4G mobile phone and Internet access service. Long-Term Evolution-Advanced (LTE-A) is a mobile communication standard that is standardized by 3rd Generation Partnership Project (3GPP). LTE-A is a major enhancement of the Long Term Evolution (LTE) standard and aims to satisfy the requirements of 4G defined by IMT-A. Nowadays, a rapid increase in wireless cellular networks is observed. In 2013, the global mobile data traffic grew 81 percent and it is anticipated that by 2018 it will reach nearly 11-fold increase over 2013. Another interesting observation is that in 2013, 30 percent of the data traffic was 4G, although only 2.9 percent of current mobile connections are 4G [1].

The growing demand for the data traffic in cellular networks seems to be a persistent problem. Furthermore, when a more advanced network with higher capacity becomes available the schema of the traffic demand may change and the network users start to use more capacity. This trend of data traffic demand motivates the constant efforts for introducing and implementing more efficient networks with higher capacity. The capacity enhancement can be addressed and studied in three different axes:

- use of new bands and increasing the bandwidth,
- employing communication techniques with higher spectral efficiency,

- and densification, which means installing and exploiting more BS antennas in the network.

For instance, introducing mm-wave and recent measurement and modeling of outdoor and indoor mm-wave channels aim to advance the capacity of wireless network by allocating more bandwidth to the communication. The use of mm-wave or any other new band in cellular networks requires a huge effort not only in technical side, but also in standardization and regulation side. However, the wide unused bandwidths have the potential to provide a huge capacity for wireless communication. Therefore, despite all the difficulties, the idea of using new bands in cellular networks remains as a practical and efficient solution.

In the second direction, higher order modulations are examples that aim to increase the spectral efficiency. Base station (BS) cooperation also can be categorized in the group of techniques that increase the spectral efficiency by reducing interference for the cell edge users. In a cellular network, the users in cell-edge areas suffer from high interference from neighboring cells and hence, are forced to communicate at a reduced data rate. Coordinated multipoint (CoMP) is a technique that has been proposed to address this issue by implementing cooperation among neighboring BSs [2-5]. This technique has been adopted in 3GPP standardization as well [6]. In addition, "centralized radio access network" (C-RAN) has been introduced as an architecture that facilitates the implementation of CoMP in the cellular networks. Since both CoMP and C-RAN are very essential to the study in this thesis, in the end of this section they are defined explicitly in distinct subsections.

In the third direction, different schemes and scenarios of densification are studied. Densification or using more antennas can be implemented in two ways. One

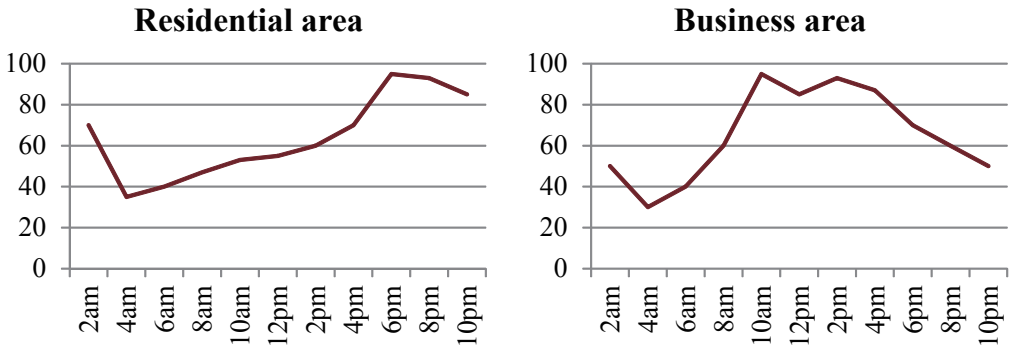

Figure 1.1: Schematic curves that show the relation of data traffic demand and the area and time.

way is to add more antenna to each BS and the other one is to install more BSs in the area. Increasing the number of antennas of a BS eventually leads to the massive MIMO techniques which seems inevitable at least for mm-wave communications. However, recent studies suggest that adding more antennas in each BS does not fill out the need for more BSs in the area. Therefore the trend of cellular networks is towards a heterogeneous architecture consisting of a macro BS with a large number of antennas and a dense deployment of small cells within macro cell area [10]-[12]. Also 3GPP standardization follows the same trend. Specifically, the efficient deployment of small cells is becoming an important part of the 3GPP discussions [13]-[15].

So far we have discussed the trends and techniques of increasing the capacity of cellular networks. However, there is another issue in cellular networks that rises from the nonuniform time-fluctuating user distribution in the network area. In general, the user distribution is not necessarily uniform and some hotspots or user-dense areas are seen in some areas. Also, in typical cellular networks the density of users in different areas (e.g. residential areas, business areas, ...) changes based on the time of the day (Fig. 1.1). To answer the traffic demand with a speci-

fied quality of service, the simplest method is to design the network for the worst case. Especially when cell coverage is static and fixed, each UE can connect only to one or a few local BSs, and therefore the network should be installed according to the most crowded time in each area. However, such a design does not utilize available resources efficiently. In other words, during the periods that the area is less crowded, some network resources remain idle or unused. Thus, the wireless network resource cannot be utilized to the most extent. In this case, the only possible adaptation is to reduce power consumption by turning off BSs in some areas at times when there is no traffic [19]. However the pre-installed network resources that remain idle cannot transfer to the crowded area. In this thesis, this issue is addressed by a novel architecture that benefits from cell structuring as well as CoMP. However, before proceeding to introduce objective of this thesis, in this section the concept of CoMP and C-RAN are briefly explained.

1.1.1 Coordinated multipoint (CoMP)

The main idea of CoMP is to form a distributed MIMO system among cooperative base stations (BSs) and perform cooperative multi-user transmission in order to mitigate interference for user equipments (UE) specially in the cell-edge areas. The theoretical performance gain of CoMP has already been proven [7]. In spite of various technical challenges, e.g. [8], the non-negligible gain of CoMP motivates the consideration of CoMP as an attractive solution for the cellular networks (e.g. [6]).

Three different schemes are considered for CoMP as demonstrated in Fig. 1.2:

- Dynamic point selection (DPS)

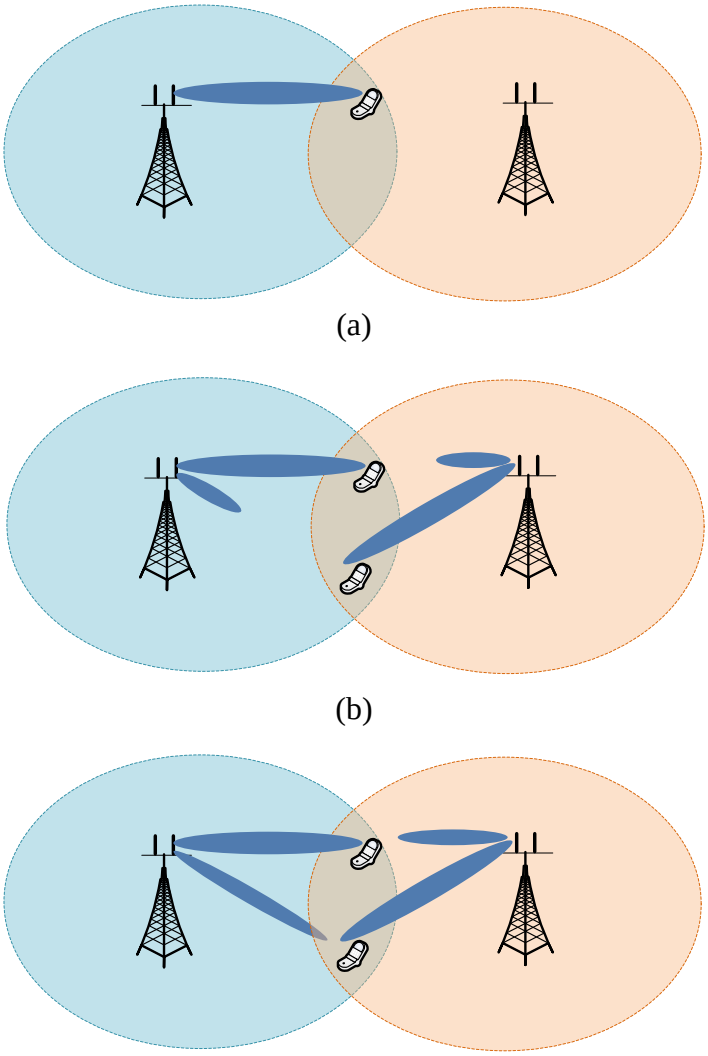

Figure 1.2: Three different CoMP schemes: (a)dynamic point selection (DPS), (b)coordinated scheduling/ beamforming (CS/CB), (c)joint transmission (JT)

- Coordinated scheduling/ beamforming (CS/CB)
- Joint transmission (JT)

In DPS, the data for the UE must be shared among coordinated BSs and the serving cell is dynamically selected so that the UE always receives the best signal.

Table 1.1: Characteristics of different schemes of CoMP

CoMP scheme	DPS	CS/CB	JT
Channel information	unshared	shared	shared
Users' data	shared	unshared	shared
Interference cancellation	muting	beam/ power control	antenna weight
Distributed MIMO gain	diversity	multiplexing	diversity/ multiplexing

CS/CB is a different CoMP scheme that does not require data sharing among coordinated BSs. The data is exclusively available to the serving cell and only that cell transmits to the UE. However scheduling and beamforming is coordinated among cooperative BSs to mitigate interference. Joint transmission (JT) is the third CoMP scheme. In JT coordinated BSs jointly transmit data to the UE. JT is the most complicated CoMP scheme that requires data as well as channel state information be shared among cooperative BSs.

The characteristics of each of CoMP schemes are summarized in Table 1.1. An important technical challenge in implementation of CoMP is the requirement for a backhaul that is capable of transferring required channel information/ user data among BSs in a timely manner. C-RAN architecture provides a suitable backhaul that supports this data sharing and facilitates the joint processing and cooperative communication for several BSs.

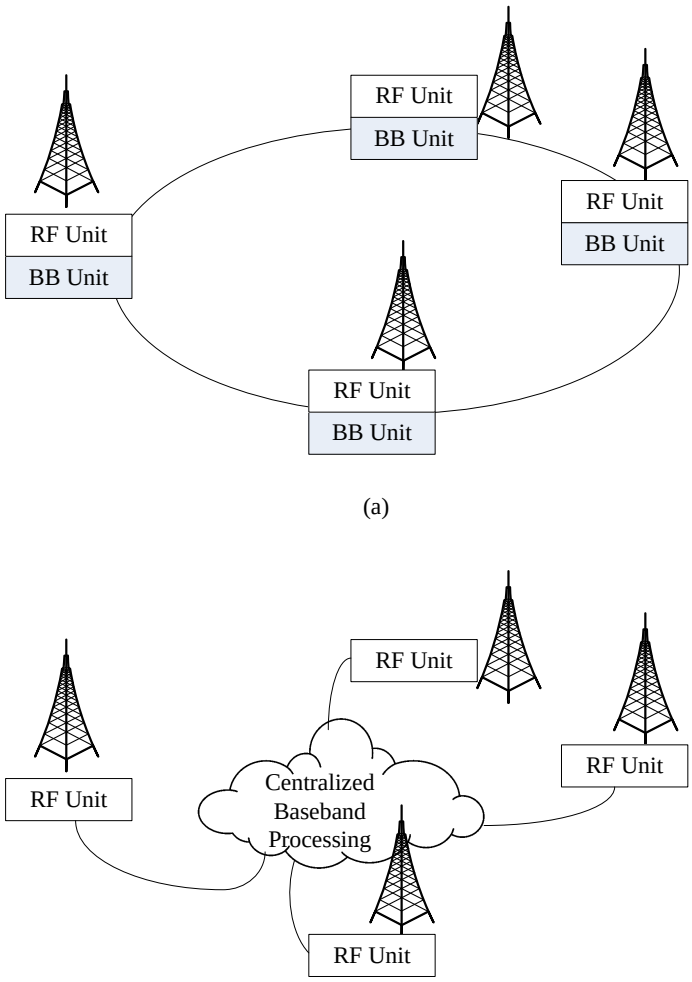

Figure 1.3: (a) Architecture of a network of distinct standalone BSs, (b) C-RAN architecture

1.1.2 Centralized radio access network (C-RAN)

Basically a BS can be a standalone entity consisting of baseband (BB) and RF units. The distinct standalone BSs connect to a backhaul that controls and supports resource allocation in the network area. However, in contrast to this architecture, centralized radio access network (C-RAN) refers to a newer configuration

in which the baseband processing component of BSs is separated from the radio head and all baseband processing is integrated to form a centralized baseband cloud [9]. In other words, the BSs are reduced to radio heads and all the signal processing and data sharing happens in the central baseband processing unit that is connected to the radio heads via high speed links. The structure of C-RAN facilitates the implementation of CoMP. Depending on the scheme, CoMP requires data and/or channel information to be shared among coordinated BSs (Table 1.1). This architecture is shown in Fig. 1.3.

The C-RAN is an interesting architecture in heterogeneous networks (HetNets) in which several small cell BSs (SC-BSs) are deployed within the area of a macro cell. In such HetNets, the SC-BSs can be remote radio heads and all BB processes can be managed and controlled by the macro BS. Macro BS can provide a reliable coverage for the control plane and resource management, while SC-BSs provide high data rates for the nearby users. In such networks the interference among neighboring SC-BSs can be mitigated by CoMP. Such a HetNet architecture with a C-RAN that supports CoMP among SC-BSs is basis of a large portion of this thesis.

1.2 Objectives of the thesis

In this thesis, a HetNet cellular network is considered and the architecture is developed step by step. The ultimate goal is to construct an architecture that utilizes the network resources to the utmost extent. As mentioned in the previous section, the issue of the increasing data traffic demand can be addressed in three directions of: more bandwidth, more efficient communication schemes and densification. The solution that is followed in this thesis can be categorized as a combination of a

more efficient communication scheme and densification. The densification that is considered here is to deploy a number of SC-BSs within a macro cell area. Then, by means of coordination among small cells the interference is eliminated and a huge capacity is obtained. In other words, a dense network of SC-BSs covers an area in an orchestrated manner to utilize their resources to the utmost extent.

The thesis begins by considering the simplest case in which SC-BSs are standalone BSs that do not cooperate to each other. The performance of this scheme can be used as the basis for comparison for more advanced schemes. In next steps, the cooperation among SC-BSs and orchestrated operation of SC-BSs are introduced. The orchestrated operation of SC-BSs relies not only on the large scale CoMP among SC-BSs, but also on the adaptive coverage or the cell structure of each SC-BS (Fig. 1.4). The adaptive coverage of a BS is in contrast to the studies on cellular networks which assume that the coverage range of each BS is fixed and therefore, BSs mainly communicate to the nearby users (eg. [16]-[18]). However, it is of a great importance to introduce adaptive coverage in cellular networks because the fixed rigid transmission range of BSs will result in the waste of the idle network resources in sparse/ vacant areas. Besides, from the technological point of view, it is possible to deploy BSs or SC-BSs that are capable of adapting their coverage. The coverage of a BS can be shifted by controlling the antenna beam direction. Especially, changing the vertical tilt angle of a BS's antenna affects the transmission range. If the coverage of BSs is fixed the BSs/SC-BSs required to be deployed in each area according to the worst case or the busiest time in that area. Quite the contrary, here the idea is to dynamically transfer idle network resources to the dense areas by dynamic cell structuring along with large scale CoMP among SC-BSs.

CoMP was originally introduced to improve the performance for cell-edge

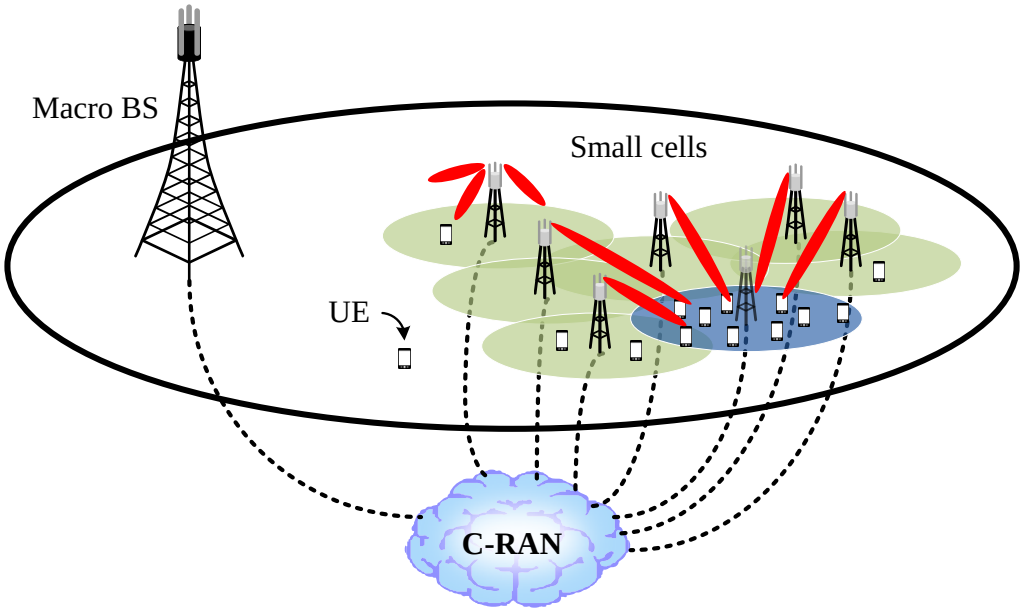

Figure 1.4: Dynamic transfer of network resources to dense areas.

users, however, here the idea is extended to large scale cooperation among several SC-BSs that are not necessarily near to each other. Basically, C-RAN architecture assists the implementation of large scale CoMP. Prior to implementation of such a system, it is necessary to characterize the fundamental limits of large scale CoMP scheme and distinguish the theoretical limits from current technological limits [16], [17]. Also, some system design issues such as clustering influence the achievable performance of large scale CoMP [18]. In this thesis an efficient architecture for large scale CoMP in an orchestrated network of SC-BSs is introduced and evaluated in various scenarios and under different circumstances. This scheme responds to network traffic demands and dynamically fits the cells' structures and cooperative clusters to the traffic congestion areas. The numerical evaluations show that if the large-scale clusters and the coverages of SC-BSs are dynamically optimized according to the traffic demand several times higher capacity is

obtained compared to the networks of cooperating SC-BSs without dynamic coverage. Here it is assumed that the macro BS and all SC-BSs are connected to a perfect C-RAN backhaul and therefore the formation of any cooperative cluster with arbitrary SC-BSs is feasible.

Beside a scheme for cell structuring and coordination, it is necessary to introduce a method for practical implementation. Therefore, in this thesis a protocol is introduced to realize the dynamic coverage control and large-scale cluster formation. This protocol provides the signaling and measurements required to setup the orchestrated network. In the protocol, it is tried to use the signaling and positioning that are currently available in 3GPP standards as much as possible. This guarantees the feasibility of the proposed scheme.

1.3 Thesis structure

The purpose of this thesis is to develop the architecture of a wireless cellular network step by step. In general a nonuniform user distribution is assumed. Especially the cases in which a few distinct congestion zones exist in the network area are considered and the network performance is examined with each architecture. A HetNet which consists of a macro cell and several SC-BSs in the macro cell area is assumed. First in chapter 2 the capacity in a random non-coordinated network of SC-BSs is analyzed. Then in chapter 3 coordination is added to the system and it is shown that the coordination is not sufficient to form an orchestrated network that directs idle resources to the congestion areas. Therefore, in chapter 4 dynamic cell structuring is combined to the clustering mechanism and the theoretical bounds of its performance are studied. In this chapter the effect of several

factors such as cluster size, shadowing and rank adaptation are examined. The performance gain of this architecture over the large-scale CoMP scheme of chapter 3 shows the importance of concurrent dynamic coverage control of SC-BSs and optimal CoMP cluster formation. However, this scheme requires dynamic measurements of several factors of the network and user distribution. Therefore, in chapter 5, the practical aspects are discussed. In this chapter a protocol is proposed to dynamically follow the user distribution and form optimal clusters seamlessly. The proposed protocol tries to follow 3GPP signaling and protocols as much as possible. This will assure the feasibility of the practical implementation of our proposed scheme. Finally, chapter 6 summarizes the results and holds some concluding remarks.

CHAPTER 2

CAPACITY IN RANDOM NON-COOPERATIVE NETWORKS

2.1 Introduction

In this chapter, a network of small cells with a random architecture is studied and its performance is examined. This study can be used as the basis for comparison with more advanced architectures and schemes in the subsequent chapters.

Here a random network consists of several SC-BSs or pico-cells that are randomly distributed in the area. No coordination among SC-BSs is available and each SC-BS independently communicates to some nearby UEs. This architecture is similar to wireless ad hoc networks and therefore, some geometrical and mathematical models of ad hoc networks can be applied to analyze it. There are quite a lot of studies in the literature that concentrate on the total capacity of an ad hoc network or the per node transmission capacity, e.g. [32]-[36], [43]-[45], or more recent studies of [47]-[52]. Although this approach does not discuss fairness or how the total capacity is divided among the nodes, it gives an insight to the overall performance of the network. In [32]-[36] the asymptotic capacity or the order of the capacity has been determined. Particularly, reference [32] is one of the pioneering studies that model and examine the asymptotic capacity of a static ad hoc network. Authors of [32] show that, the throughput for every node is of the order of $1/\sqrt{N}$, where N is the number of nodes in the network. References [43]-[45] follow the same definition for capacity as introduced in [32] and investigate the scaling laws of network and the total capacity as a function of number of nodes.

Asymptotic results are very common in the case of ah hoc networks, however in this chapter, the capacity of a random non-cooperative network is deter-

mined with the assumptions and parameters of a typical cellular network of small cells. Although this scenario is similar to an ad hoc network, suitable modeling is necessary to analyze the capacity of a random non-cooperative scheme in a HetNet. In fact, the model and the analysis metric should be selected and defined so that they can function as the basis for comparison for more advanced cellular networks that will be analyzed in the subsequent chapters. Therefore in this chapter, first a model of the network is described and the capacity is defined and formulated. Then, the statistics of the received signal to interference power ratio (SIR) is extracted and the cumulative distribution function (CDF) of SIR is analytically derived. This expression directly results in a closed form solution for the total network capacity. In the end, the capacity is studied both analytically and by simulation.

2.2 Network scenario

In this section the network scenario is described. The objective is to facilitate the mathematical analysis while maintaining the generality of a typical network. Hereafter in this chapter the term "BS" refers to a standalone SC-BS that can independently communicate to some UE.

It is assumed that the BSs and UEs are randomly located in the network coverage area with uniform distribution. To make the mathematical analysis more tractable, the network area is considered as a planar circular disk with radius R as shown in Fig. 2.1. This makes it easier to formulate the CDF of the distance of each

BS to the center of the network, r:

$$F_r(x) = \text{Prob.}\{r \leq x\} = \begin{cases} 0, & \text{if } x < 0 \\ \frac{\pi x^2}{\pi R^2}, & \text{if } 0 \leq x \leq R \\ 1, & \text{if } x > R \end{cases} \tag{2.1}$$

where, Prob.$\{A\}$ is the probability of event A.

Therefore, the polar coordinates of each BS, (r, θ), will have the following probability density functions (PDF) [37]:

$$\begin{cases} f_r(r) = \frac{\mathrm{d}F_r(r)}{\mathrm{d}r} = \frac{2r}{R^2}, & 0 \leq x \leq R \\ f_\theta(\theta) = \frac{1}{2\pi}, & 0 \leq \theta < 2\pi \end{cases} \tag{2.2}$$

where, r is the distance from the origin and θ is the angle between the positive x-axis and the ray from the origin to the location of the BS.

It is also assumed that every BS uses an omnidirectional antenna and randomly chooses its receiver from UEs no closer than ϵ and no farther than D with equal probability (Fig. 2.1). Therefore, the probability that the j^{th} BS chooses a UE within $\rho \geq \epsilon$ distance away is proportional to the number of UEs in the disk centered at BS_j with radius from ϵ to ρ. Since the UEs are also uniformly distributed in the coverage area we can write:

$$F_d(\rho) = \text{Prob.}\{d \leq \rho\} = \begin{cases} 0, & \text{if } \rho < \epsilon \\ \frac{\pi\rho^2 - \pi\epsilon^2}{\pi D^2 - \pi\epsilon^2}, & \text{if } \epsilon < \rho \leq D \\ 1, & \text{if } \rho > D \end{cases} \tag{2.3}$$

where, $F_d(\rho)$ is the CDF of the distance between a BS to its intended UE.

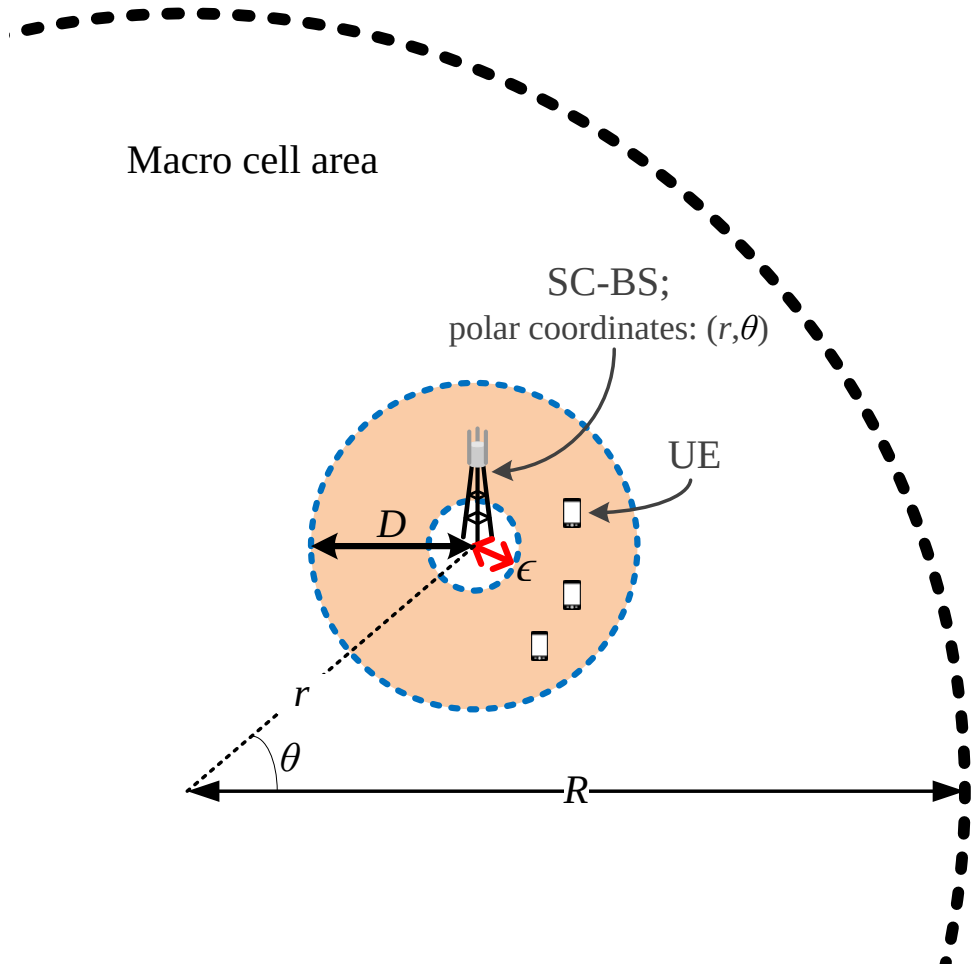

Figure 2.1: The scenario for a random non-cooperative network

No interference coordination among BSs is considered. There are K_{BS} small cell base stations and each of them communicates to one UE independently. Each BS has got M_{T} antennas for transmission and each UE is equipped with M_{R} antennas for reception. There is a single user MIMO communication between each BS_j ($1 \leq j \leq K_{\mathrm{BS}}$) and its corresponding UE:

$$\mathbf{y}_j = \mathbf{H}_{jj}\mathbf{x}_j + \sum_{\substack{k=1 \\ k \neq j}}^{K_{\mathrm{BS}}} \mathbf{H}_{jk}\mathbf{x}_k + \mathbf{n}_j \tag{2.4}$$

where, $\mathbf{x}_j \in \mathbb{C}^{M_{\mathrm{T}}}$ is the transmitted vector by BS_j and $\mathbf{y}_j \in \mathbb{C}^{M_{\mathrm{R}}}$ is the vector received by UE_j ($1 \leq j \leq K_{\mathrm{BS}}$). Also, $\mathbf{H}_{jk} \in \mathbb{C}^{M_{\mathrm{R}} \times M_{\mathrm{T}}}$ is the MIMO channel matrix between the

k^{th} BS and the j^{th} UE. Rayleigh flat fading is assumed in the channel. In the right side of Eq. (2.4), the second term is the interference at the receiver, and $\mathbf{n}_j \in \mathbb{C}^{M_R}$ is the noise.

In the analytical approximation, an interference-limited environment is assumed where the noise power is negligible compared to the interference. In other words, in the analysis, signal-to-interference-power-ratio (SIR) is considered instead of signal-to-interference-plus-noise-power-ratio (SINR). Neglecting noise in the presence of interference is a usual assumption in ad hoc networks. In fact, every ad hoc network can be interference-limited if all transmission powers are high enough [46]. Here, analogous to ad hoc networks, this assumption is used to facilitate the mathematical analysis.

2.3 System rate analysis

This section presents a formulation of the capacity in random non-coordinated cellular network.

To define the total capacity of the network, we start by characterizing the rate function, R_j, which is the communication rate of a single wireless link, i.e the the link between BS_j ($1 \leq j \leq K_{\text{BS}}$) and its corresponding UE [42]. The rate function can be defined in various forms according to the capabilities of the transmitters and receivers in the network. This function is upper bounded by the Shannon rate. Here the best case is considered and the rate function is set to its upper bound. For the link between BS_j and its corresponding UE that is described in Eq. (2.4),

the rate function is as follows:

$$R_j = \sum_{i=1}^{q} \log_2(1 + \lambda_i \gamma_j), \quad \text{[bps/Hz]} \tag{2.5}$$

where, γ_j is the received SINR in the link between j^{th} BS and its corresponding UE. In this equation, λ_i $(1 \leq i \leq q)$ are the eigenvalues of $\mathbf{H}_{jj}^{\text{H}}\mathbf{H}_{jj}$ and q is the rank of MIMO channel:

$$q = \min(M_{\text{T}}, M_{\text{R}}) \tag{2.6}$$

The PDF of λ_i $(1 \leq i \leq q)$ is characterized by the eigenvalues of the transmit correlation matrix, $\boldsymbol{\Upsilon}$ [23], [24] as explained in Appendix A:

$$\boldsymbol{\Upsilon} = \frac{1}{M_{\text{R}}} \text{E}\left\{\mathbf{H}_{jj}^{\text{H}}\mathbf{H}_{jj}\right\} = \mathbf{I}_{M_{\text{T}}}. \tag{2.7}$$

In Appendix A, the vector of all eigenvalues of $\mathbf{H}_{jj}^{\text{H}}\mathbf{H}_{jj}$ is considered as $\underline{\lambda} = \left[\lambda_1, \lambda_2, \cdots, \lambda_q\right]^{\text{T}}$ $(\lambda_1 \geq \lambda_2 \geq \cdots \geq \lambda_q)$ and their joint PDF $f_{\underline{\lambda}}(\underline{\lambda})$ is obtained.

In Eq. (2.5), γ_j and λ_i $(1 \leq i \leq q)$ are random variables. The average rate of each link is defined as the expected value of its communication rate:

$$\overline{R}_j = \int_0^{\infty} \int_{\lambda_q}^{\infty} \cdots \int_{\lambda_3}^{\infty} \int_{\lambda_2}^{\infty} R_j f_{\text{SINR}_j}(\gamma_j) f_{\underline{\lambda}}(\underline{\lambda}) \text{d}\gamma_j \text{d}\underline{\lambda}, \quad \text{[bps/Hz]} \tag{2.8}$$

where, $f_{\text{SINR}_j}(\gamma_j)$ is the PDF of the received SINR, γ_j.

The average system rate of a wireless network, $\overline{R}$, can be defined as the sum of the average capacities of all simultaneously active links. Because of the symmetry of the network scenario, the PDF of the received SINR can be considered the same for all the UEs: $f_{\text{SINR}_j}(\gamma) = f_{\gamma}(\gamma)$ $(\forall j)$. As a result, the average system rate of the network with K_{BS} base stations is:

$$\overline{R} = K_{\text{BS}}\, \overline{R}_j \tag{2.9}$$

where, $\overline{R}_j$ is substituted from Eq. (2.8). In Eq. (2.8) all terms are already known, except the PDF of SINR, $f_{\text{SINR}}(\gamma)$. In the rest of this section, the effect of noise is neglected and an approximation closed form is obtained for the CDF of SIR. Then, using that approximation, the PDF of SIR is estimated and replaced in Eq. (2.8) to estimate the system rate.

In order to characterize the CDF of SIR, we begin with the definition of the SIR. There are K_{BS} pairs of transmitter-receivers in the network. And, with no loss in generality, the first pair can be taken as the intended pair for which the receiver's SIR is written as:

$$\text{SIR} = \frac{\left(P_t G / r_1^{\alpha}\right)}{\sum_{i=2}^{K_{\text{BS}}} \left(P_t G / r_i^{\alpha}\right)} = \frac{1/r_1^{\alpha}}{\sum_{i=2}^{K_{\text{BS}}} \left(1/r_i^{\alpha}\right)} \tag{2.10}$$

where, P_t is the power of each transmitter and G reflects the effects of any constant gain in all links such as the gains of BSs' and UEs' antennas' that are assumed to be omnidirectional. Also, r_1 is the distance between the intended BS (BS_1) and the the corresponding UE (UE_1) and r_i ($2 \leq i \leq K_{\text{BS}}$) is distance from the i^{th} BS to UE_1. A free space path loss model is considered in all interfering paths as well as the desired link with path loss exponent of α [41]. It should be mentioned that this model is consistent with the distance-dependent path loss model in 3GPP (e.g. [6]).

The interfering power at the receiver, I, is defined as follows:

$$I = \sum_{i=2}^{K_{\text{BS}}} (1/r_i^{\alpha}) \tag{2.11}$$

In [39] and [40], it has been suggested that using the law of large numbers, I can be replaced by $(K_{\text{BS}} - 1)\text{E}(1/r^{\alpha})$ where E{.} stands for the expected value. However, instead of replacing I by its mean, here the probability distribution of I is approximated to obtain more accurate analytical results. Monte Carlo simulation for most

common values of α (i.e. $2 \leq \alpha \leq 4$ [41]), shows that the variance of I is too large. Therefore, we use logarithm and consider powers and SIR in dB scale. We define I_{dB} as follows:

$$I_{\text{dB}} = 10 \log_{10}(I) = 10 \log_{10}\left(\sum_{i=2}^{K_{\text{BS}}} \frac{1}{r_i^{\alpha}}\right) \tag{2.12}$$

In the Monte Carlo simulation it is observed that I_{dB} tends to follow some sort of extreme value distribution. In fact, since r_i varies in a wide range from ϵ to R ($\epsilon << R$), in the above equation the smallest r_i or in other words, the nearest interferer has the dominant effect. This motivates us to approximate the summation by this dominant part. It should be noted that the larger the value of α is, the more accurate this approximate is. Later, by comparing the analytic results with the simulation, it will be seen that this approximation is accurate enough to estimate the capacity. Consequently, we approximate I_{dB} as follows:

$$I_{\text{dB}} \simeq 10 \log_{10}\left(\max_{i\,(1\leq i\leq K_{\text{BS}})}\left(\frac{1}{r_i^{\alpha}}\right)\right) = 10 \log_{10}\left(\left(\min_{i\,(1\leq i\leq K_{\text{BS}})}(r_i)\right)^{-\alpha}\right) \tag{2.13}$$

Hence, the CDF of I_{dB} can be estimated as:

$$\begin{aligned} F_{I_{\text{dB}}}(x) =& \text{Prob.}\{I_{\text{dB}} \leq x\} \\ \simeq& \text{Prob.}\left\{10 \log_{10}\left(\left(\min_{i\,(2\leq i\leq K_{\text{BS}})}(r_i)\right)^{-\alpha}\right) \leq x\right\} \\ =& \text{Prob.}\left\{r_i \geq 10^{-\frac{x}{10\alpha}} \quad \forall i, 2 \leq i \leq K_{\text{BS}}\right\} \\ =& \prod_{i=2}^{K_{\text{BS}}}\left(1 - F_{r_i}\left(10^{-\frac{x}{10\alpha}}\right)\right) \end{aligned} \tag{2.14}$$

In Eq. (2.14), $F_{r_i}(.)$ is the CDF of the distance between each BS_i ($\forall i \neq 1$) and UE_1. In general, $F_{r_i}(.)$ depends on the network scenario. When the network radius, R, is large, UE_1 can be considered as the center of the network [38]. With this assumption, interfering BSs are uniformly distributed around UE_1 and their distances to

it, vary from a minimum value, ϵ, to a maximum value, R, where ϵ is the minimum distance between a BS to any UE in the network. In such a case, the distance from the i^{th} ($2 \leq i \leq K_{\text{BS}}$) BS to UE_1, r_i, has the following distribution function:

$$F_{r_i}(r) = \text{Prob.}\{r_i \leq r\} = \begin{cases} 0, & \text{if } r < \epsilon \\ \frac{\pi x^2 - \pi\epsilon^2}{\pi R^2 - \pi\epsilon^2}, & \text{if } \epsilon \leq r \leq R \\ 1, & \text{if } r > R \end{cases} \tag{2.15}$$

Combining Eqs. (2.14) and (2.15), $F_{I_{\text{dB}}}$ is estimated as follows:

$$F_{I_{\text{dB}}}(x) \simeq \left(\frac{R^2 - 10^{-\frac{x}{5\alpha}}}{R^2 - \epsilon^2}\right)^{(K_{\text{BS}}-1)}, \quad -10\ \log_{10} R \leq x \leq -10\ \log_{10} \epsilon \tag{2.16}$$

Afterwards, the SIR is considered in dB scale and its CDF is characterized. According to Eq. (2.10), SIR_{dB} is obtained as:

$$SIR_{\text{dB}} = -10\alpha \log_{10}(r_1) - I_{\text{dB}} \tag{2.17}$$

Therefore, the CDF of SIR_{dB} is defined as:

$$F_\gamma(\gamma) = \text{Prob.}\{SIR_{\text{dB}} \leq \gamma\} = \text{Prob.}\left\{r_1 \geq 10^{-\frac{\gamma + I_{\text{dB}}}{10\alpha}}\right\} \tag{2.18}$$

Hence:

$$\begin{aligned} F_\gamma(\gamma) &= \int_{-\infty}^{\infty} \text{Prob.}\left\{r_1 \geq 10^{-\frac{\gamma+x}{10\alpha}}\right\} f_{I_{\text{dB}}}(x)\text{d}x \\ &= \int_{-\infty}^{\infty} \left(1 - F_d\left(10^{-\frac{\gamma+x}{10\alpha}}\right)\right) f_{I_{\text{dB}}}(x)\text{d}x \end{aligned} \tag{2.19}$$

where, $F_d(.)$ is defined in Eq. (2.3) and $f_{I_{\text{dB}}}(.)$ is the PDF of I_{dB} which is by definition, the derivative of the CDF in Eq. (2.16). By replacing corresponding functions and maintaining boundaries in $F_d(.)$ and $f_{I_{\text{dB}}}(.)$, the CDF of SIR_{dB} is obtained as:

$$F_\gamma(\gamma) = \begin{cases} 0, & \text{if } \gamma \leq 10\alpha \log_{10}(\frac{\epsilon}{D}) \\ \left[H\left(D^2 p\right) - H(\epsilon^2)\right] - \\ \frac{p^{-1}}{D^2 - \epsilon^2} \times \left[G\left(D^2 p\right) - G(\epsilon^2)\right], & \text{if } 10\alpha \log_{10}\left(\frac{\epsilon}{D}\right) < \gamma \leq 0 \\ \left[H\left(\epsilon^2 p\right) - H(\epsilon^2)\right] + \\ \frac{D^2}{D^2 - \epsilon^2}\left[H(m) - H\left(\epsilon^2 p\right)\right] - \\ \frac{p^{-1}}{D^2 - \epsilon^2}\left[G(m) - G\left(\epsilon^2 p\right)\right] & \text{if } 0 < \gamma \leq 10\alpha \log_{10}\left(\frac{R}{\epsilon}\right) \\ 1, & \text{if } \gamma > 10\alpha \log_{10}\left(\frac{R}{\epsilon}\right) \end{cases} \tag{2.20}$$

where p and m are defined as:

$$p \stackrel{\text{def}}{=} 10^{\frac{\gamma}{5\alpha}}$$

$$m \stackrel{\text{def}}{=} \min\left\{R^2, D^2\ p\right\}$$

And functions $H(.)$ and $G(.)$ are defined as:

$$H(x) \stackrel{\text{def}}{=} -\frac{\left(R^2 - x\right)^{(K_{\text{BS}}-1)}}{\left(R^2 - \epsilon^2\right)^{(K_{\text{BS}}-1)}}$$

$$G(x) \stackrel{\text{def}}{=} -\frac{(K_{\text{BS}}-1)}{\left(\epsilon^2 - R^2\right)^{(K_{\text{BS}}-1)}}\left[\frac{\left(x - R^2\right)^{K_{\text{BS}}}}{K_{\text{BS}}} + \frac{R^2\left(x - R^2\right)^{(K_{\text{BS}}-1)}}{K_{\text{BS}} - 1}\right]$$

Equation (2.20) for $F_\gamma(\gamma)$ is a closed form that can be used to approximate the PDF of SINR as follows:

$$f_{\text{SINR}_j}(\gamma_j) \simeq f_\gamma(\gamma) = \frac{\mathrm{d}F_\gamma(\gamma)}{\mathrm{d}\gamma}; \quad \forall j \tag{2.21}$$

The result of Eq. (2.21) can be replaced in Eqs. (2.8) and (2.9), to calculate the average system rate of the network.

2.4 Numerical results

In this section the system rate of a non-coordinated random network of SC-BSs is examined versus the network size. At first it is assumed that the locations of SC-BSs is random. The density of BSs is assumed to be $1/A$, where A is the area of a hexagonal small cell as shown in Fig. 2.2(a). This assumption keeps the average number of BSs in the random network equal to the number of BSs in a lattice network with hexagonal small cells as demonstrated in Fig. 2.2. To keep the consistency with 3GPP specifications, the path loss exponent, α is set to 3.67 (see Table 3.1 or [6]). Also, it is assumed that each SC-BS and UE are equipped with two antennas for transmission and reception, respectively: $M_{\mathrm{T}} = M_{\mathrm{R}} = 2$.

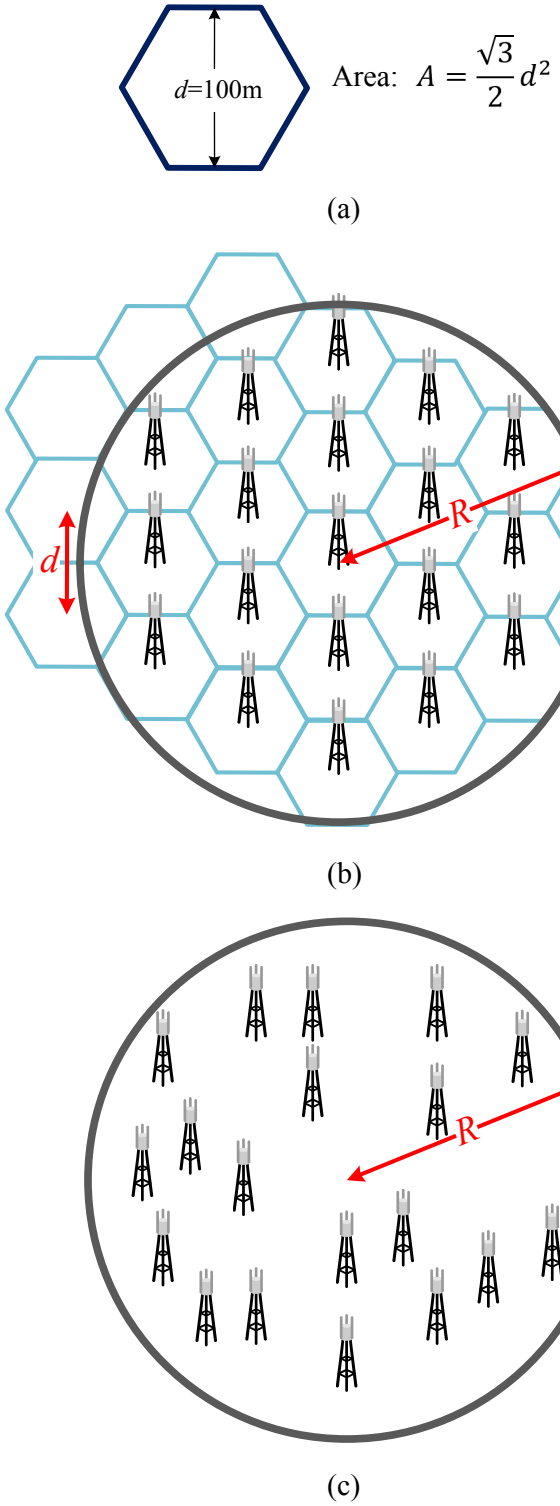

Figure 2.2: (a) Hexagonal small cell, (b) a lattice network with hexagonal small cells, (c) a random network with the same netwrok radius, R, and the same density of SC-BSs.

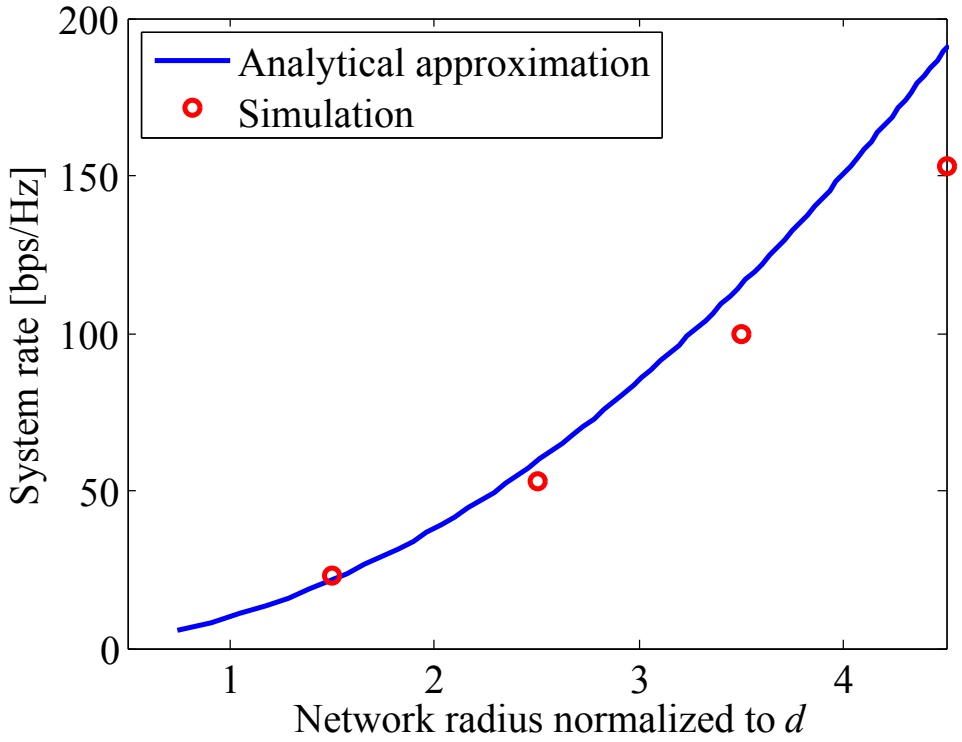

Figure 2.3: System rate of a non-coordinated random network versus normalized network radius, R/d.

The system rate of the network is shown in Fig. 2.3 for a uniform user distribution. In this figure, a gap between analytical approximation and the simulation result is observed. In the analytical approximation, among all interfering signals, only the strongest one that is coming from the nearest transmitter is taken into account and all other interferences and noise are neglected. The larger is the network, the more interfering transmitters exist and therefore the less accurate is the approximation. However, the approximation can always be used to obtain an upper bound on the system rate.

Figure 2.3 shows that the system rate increases quadratically with the network radius. On the other hands, since the distribution of BSs is uniform, the number

of BSs increases quadratically with the network radius, and therefore, the system rate increases linearly with the number of BSs.

In Fig. 2.3 the result is plotted versus the network radius. In fact, the capacity can be studied in different aspects. For example, an interesting study is to examine the per BS capacity. However, the objective of this chapter is to provide a basis for comparison for more developed cellular network architectures in the subsequent chapters. These architectures aim to provide an efficient scheme for nonuniform user distributions with some congestion areas. For nonuniform user distributions instead of the capacity in each small cell or per BS capacity, the sum rate or system rate will be studied as the performance metric. Thus the same metric has been considered in this chapter.

2.5 Conclusion

In this chapter the capacity of a random non-coordinated network was modeled and analyzed. An analytical upper bound was provided for the system rate and the system rate versus network size was examined in a uniform user distribution environment. In such a network, the main factor that restricts the capacity is interference. Use of the sectoral/ directional antennas in SC-BSs can reduce the interference and increase the system rate. Besides, by implementing cooperation among SC-BSs the interference can be further eliminated. The numerical results of this chapter can be used to examine the gain of these two mechanisms. Both mechanisms are described and modeled in the next chapter.

CHAPTER 3

CAPACITY IN A COOPERATIVE CELLULAR NETWORK

3.1 Introduction

As in the previous chapter, this chapter focuses on a HetNet cellular network in which there are several SC-BSs within a macro cell area. However in this chapter two mechanisms for interference reduction/elimination are added to the network. These mechanisms are the use of sectoral antennas and BSs' coordination. Sectoral antennas at SC-BSs directs a larger portion of the power towards the intended UE while reduces the interference in other directions. On the other hand, with SC-BSs' coordination a cluster of SC-BSs performs joint transmission (JT) CoMP to fully eliminate the interference.

In this chapter these mechanisms are described and modeled in detail and then the performance gain is examined for different user distribution scenarios. As expected, the interference reduction/elimination improves the performance of the network. However, for a nonuniform user distribution in which there are some congestion areas in the network surrounded by sparse areas, the gain is marginal. In other words, the aforementioned interference reduction/elimination mechanisms are still insufficient to utilize network resources to the utmost extent.

This chapter starts with the description of the system model. Then the system rate is evaluated and compared to the previous chapter the non-coordinated random network of the previous chapter. In the end, the merits and shortcomings of the considered interference reduction/elimination are discussed.

3.2 System model

This chapter deals with SC-BSs within a macro cell area that are equipped with directional antennas. Also, all the SC-BSs are connected to a C-RAN and can participate in a cooperative JT cluster. Hereafter, in this chapter the term "BS" refers to the SC-BS.

In this section, first the model for the downlink communication in a cooperative cluster is presented in a distinct subsection. It is assumed that a cooperative cluster performs block diagonalization (BD) to fully eliminate interference within a cluster. Then in another, a 3-dimensional model for a sectoral/directional antenna is described. This model is similar to the model accepted in 3GPP [6].

3.2.1 Downlink communication model

Here a cluster is a set of K_{BS} base stations ($j = 1, ..., K_{\mathrm{BS}}$) that perform joint transmission (JT) CoMP to a set of K_{UE} ($K_{\mathrm{UE}} \leq K_{\mathrm{BS}}$) user equipments ($i = 1, ..., K_{\mathrm{UE}}$). Also, each base station (BS) uses M_{T} antennas for transmission and each user is equipped with M_{R} antennas for reception ($M_{\mathrm{R}} \leq M_{\mathrm{T}}$).

It is assumed that the channel from each base station (BS) in the cluster to each user equipment (UE) is known in a baseband central processing unit that processes and distributes the data to be transmitted on the set of antennas of all BSs of the cluster. This communication is modeled as follows:

$$\mathbf{y} = \mathbf{HQTs} + \mathbf{n}_{\mathrm{intf}} + \mathbf{n} \tag{3.1}$$

In the above equation:

- $\mathbf{s} = [\mathbf{s}_1{}^{\mathrm{T}}, ..., \mathbf{s}_{K_{\mathrm{UE}}}{}^{\mathrm{T}}]^{\mathrm{T}} \in \mathbb{C}^{M_{\mathrm{R}}K_{\mathrm{UE}}}$ is the aggregated transmit streams to K_{UE} users;
- $\mathbf{y} = [\mathbf{y}_1{}^{\mathrm{T}}, ..., \mathbf{y}_{K_{\mathrm{UE}}}{}^{\mathrm{T}}]^{\mathrm{T}} \in \mathbb{C}^{M_{\mathrm{R}}K_{\mathrm{UE}}}$ is the aggregated receive signal vector of K_{UE} users;
- $\mathbf{H} \in \mathbb{C}^{M_{\mathrm{R}}K_{\mathrm{UE}} \times M_{\mathrm{T}}K_{\mathrm{BS}}}$ is the aggregated channel matrix between cooperative BSs and CoMP users:

$$\mathbf{H} = \left[\mathbf{H}_1^{\mathrm{T}}, \cdots, \mathbf{H}_{K_{\mathrm{UE}}}^{\mathrm{T}}\right]^{\mathrm{T}} \tag{3.2}$$

  where $\mathbf{H}_i = [\mathbf{H}_{i1}, \cdots, \mathbf{H}_{iK_{\mathrm{BS}}}] \in \mathbb{C}^{M_{\mathrm{R}} \times M_{\mathrm{T}}K_{\mathrm{BS}}}$ is the channel from all cluster BSs to the i^{th} user which is composed of $\mathbf{H}_{ij} \in \mathbb{C}^{M_{\mathrm{R}} \times M_{\mathrm{T}}}$, the channel from the j^{th} BS to the i^{th} user. Rayleigh flat fading is considered in the channel.
- $\mathbf{Q}=[\mathbf{Q}_1, \mathbf{Q}_2, \cdots, \mathbf{Q}_{K_{\mathrm{UE}}}]$ is a block diagonalization (BD) precoding matrix, with: $\mathbf{Q}_i \in \mathbb{C}^{M_{\mathrm{T}}K_{\mathrm{BS}} \times [M_{\mathrm{T}}K_{\mathrm{BS}} - M_{\mathrm{R}}(K_{\mathrm{UE}}-1)]}$,
  such that: $\widetilde{\mathbf{H}} \overset{\mathrm{def}}{=} \mathbf{HQ} = \mathrm{diag}\left[\widetilde{\mathbf{H}}_1, \cdots, \widetilde{\mathbf{H}}_{K_{\mathrm{UE}}}\right]$,
  where: $\widetilde{\mathbf{H}}_i \in \mathbb{C}^{M_{\mathrm{R}} \times [M_{\mathrm{T}}K_{\mathrm{BS}} - M_{\mathrm{R}}(K_{\mathrm{UE}}-1)]}$ is the effective channel matrix for user i;
- $\mathbf{T}=\left[\widetilde{\mathbf{T}}_1^{\mathrm{T}}, \cdots, \widetilde{\mathbf{T}}_{K_{\mathrm{UE}}}^{\mathrm{T}}\right]^{\mathrm{T}} = \widetilde{\mathbf{V}}\mathbf{P}_{\mathbf{s}}$ is the aggregated precoding matrix of SVD-MIMO, where $\widetilde{\mathbf{V}} = \left[\widetilde{\mathbf{V}}_1^{\mathrm{T}}, \cdots, \widetilde{\mathbf{V}}_{K_{\mathrm{UE}}}^{\mathrm{T}}\right]^{\mathrm{T}} \in \mathbb{C}^{K_{\mathrm{UE}}[M_{\mathrm{T}}K_{\mathrm{BS}} - M_{\mathrm{R}}(K_{\mathrm{UE}}-1)] \times M_{\mathrm{R}}K_{\mathrm{UE}}}$ is the aggregated right singular matrix ($\widetilde{\mathbf{V}}_i$ is the right singular matrix of $\widetilde{\mathbf{H}}_i$) and the diagonal matrix $\mathbf{P}_{\mathbf{s}} \in \mathbb{R}^{M_{\mathrm{R}}K_{\mathrm{UE}} \times M_{\mathrm{R}}K_{\mathrm{UE}}}$ is a power allocation matrix for each stream;
- $\mathbf{n}_{\mathrm{intf}} = [\mathbf{n}_{\mathrm{intf},1}{}^{\mathrm{T}}, \cdots, \mathbf{n}_{\mathrm{intf},K_{\mathrm{UE}}}^{\mathrm{T}}]^{\mathrm{T}} \in \mathbb{C}^{M_{\mathrm{R}}K_{\mathrm{UE}}}$ denotes the aggregated interference from non-cooperating BSs and BSs of other clusters. Also $\mathbf{n} = [\mathbf{n}_1{}^{\mathrm{T}}, \cdots, \mathbf{n}_{K_{\mathrm{UE}}}^{\mathrm{T}}]^{\mathrm{T}} \in \mathbb{C}^{M_{\mathrm{R}}K_{\mathrm{UE}}}$ is the noise vector, where $\mathrm{E}\{\mathbf{n}_i\mathbf{n}_i^{\mathrm{H}}\} = \sigma^2\mathbf{I}_{M_{\mathrm{R}}}$ and σ^2 is the noise power.

The instantaneous spectral efficiency of the i^{th} user is then given by:

$$\begin{aligned} R_i = \chi \log_2 \Big\{ & \det\Big(\mathbf{I}_{M_{\mathrm{R}}} + \widetilde{\mathbf{H}}_i\widetilde{\mathbf{T}}_i\widetilde{\mathbf{T}}_i^{\mathrm{H}}\widetilde{\mathbf{H}}_i^{\mathrm{H}} \times \\ & \left[\sigma^2\mathbf{I}_{M_{\mathrm{R}}} + \mathrm{E}\left\{\mathbf{n}_{\mathrm{intf},i}\mathbf{n}_{\mathrm{intf},i}{}^{\mathrm{H}}\right\}\right]^{-1}\Big)\Big\} \end{aligned} \tag{3.3}$$

where χ is the bandwidth efficiency coefficient.

3.2.2 Antenna gain and path loss model

The channel from the j^{th} BS to the i^{th} user, $\mathbf{H}_{ij}$, can be decomposed into two terms:

$$\mathbf{H}_{ij} = \sqrt{\pi_{ij}}\mathbf{F}_{ij} \tag{3.4}$$

$\mathbf{F}_{ij} \in \mathbf{C}^{M_{\mathbf{R}} \times M_{\mathbf{T}}}$ models the i.i.d. Rayleigh flat fading with unit power. And, π_{ij} is the average path power gain between the j^{th} BS and the i^{th} user. We consider antenna gain as well as path loss to model π_{ij} as follows:

$$\pi_{ij} = \frac{G\left(\phi_j, \theta_j, \mathbf{\Psi}(\text{BS}_j), \mathbf{\Psi}(\text{UE}_i)\right)}{L\left(\|\mathbf{\Psi}(\text{BS}_j) - \mathbf{\Psi}(\text{UE}_i)\|\right)} \tag{3.5}$$

$\mathbf{\Psi}(.) = [\psi_{\text{x}}(.), \psi_{\text{y}}(.), \psi_{\text{z}}(.)]$ denotes the 3-dimensional location vector of BSs and UEs. Thus, $\|\mathbf{\Psi}(\text{BS}_j) - \mathbf{\Psi}(\text{UE}_i)\|$ is in fact the distance between the transmitter and the receiver and $L(\|\mathbf{\Psi}(\text{BS}_j) - \mathbf{\Psi}(\text{UE}_i)\|)$ is the distance-dependent path loss from the j^{th} BS to the i^{th} user. Also, $G(\phi_j, \theta_j, \mathbf{\Psi}(\text{BS}_j), \mathbf{\Psi}(\text{UE}_i))$ is the antenna gain of the j^{th} BS towards the i^{th} user. Furthermore, $\phi_j \left(-\pi \leq \phi_j \leq \pi\right)$ and $\theta_j \left(0 \leq \theta_j \leq \frac{\pi}{2}\right)$ are the horizontal direction and the vertical tilt of the BS's antenna respectively as demonstrated in Figs. 3.1(a) and (b).

A 3-dimensional (3D) model is considered for the antenna gain [20]. This model also conforms to 3GPP specifications for BS antennas [21]. In this model, we are dealing with one main lobe whose directions in horizontal and vertical plane are characterized by the angles ϕ_j and θ_j respectively. Outside the main lobe, a constant gain is assumed; but, for users locating in the main lobe, the antenna gain in horizontal plane (G_{h}) and vertical plane (G_{v}) should be calculated. To obtain G_{v} and G_{h}, the relative angles of the user and the antenna main lobe must be calculated.

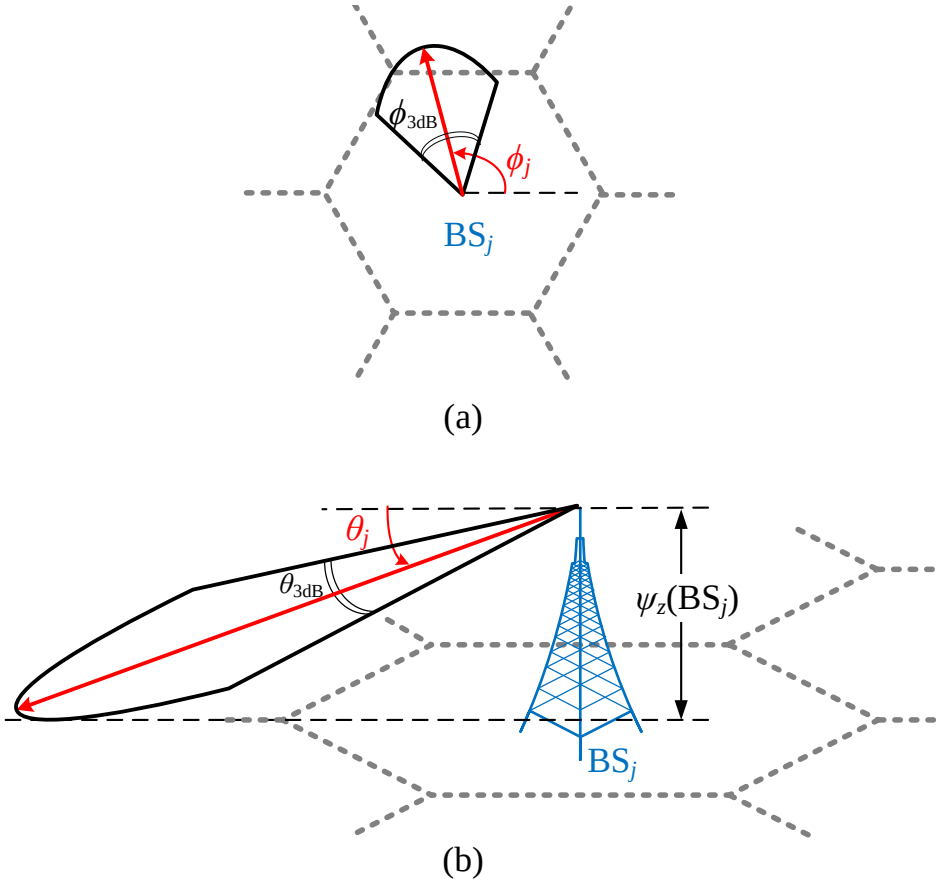

Figure 3.1: Demonstration of (a) horizontal and (b) vertical beam patterns and corresponding angles.

In the horizontal plane, the relative angle between BS_j and UE_i is obtained as:

$$\Delta\phi_{ij} = \text{atan2}\left(\psi_y(UE_i) - \psi_y(BS_j), \psi_x(UE_i) - \psi_x(BS_j)\right) - \phi_j \tag{3.6}$$

where, ϕ_j is the horizontal direction of the main lobe of BS_j. Also atan2(y, x) is the arctangent function with two input arguments which returns the result in $(-\pi, \pi]$:

$$\text{atan2}(y,x) \stackrel{\text{def}}{=} \begin{cases} \text{atan}(y,x), & \text{if } x > 0 \\ \text{atan}(y,x) + \pi, & \text{if } x < 0,\ y \geq 0 \\ \text{atan}(y,x) - \pi, & \text{if } x < 0,\ y < 0 \\ \pi/2 & \text{if } x = 0,\ y > 0 \\ -\pi/2 & \text{if } x = 0,\ y < 0 \\ \text{undefined}, & \text{if } x = 0,\ y = 0 \end{cases}$$

Then the antenna horizontal gain is:

$$G_{\text{h}}(\Delta\phi_{ij})[\text{dB}] = -\min\left(c\left(\frac{\Delta\phi_{ij}}{\phi_{\text{3dB}}}\right)^2, A_{\text{h}}\right) \tag{3.7}$$

where, ϕ_{3dB} is the 3dB beam-width of the main lobe in horizontal plane and c and A_{h} determine the gains in the main lobe and side lobe in horizontal plane respectively.

Similarly, in the vertical plane, the relative angle between BS_j and UE_i is obtained as follows:

$$\Delta\theta_{ij} = \text{atan}\left(\frac{\psi_{\text{z}}(\text{BS}_j) - \psi_{\text{z}}(\text{UE}_i)}{\Delta D_{ij}}\right) - \theta_j \tag{3.8}$$

where θ_j is the vertical direction of the main lobe of BS_j and ΔD_{ij} is the relative distance between BS_j and UE_i in the horizontal plane:

$$\Delta D_{ij} = \sqrt{\left(\psi_{\text{x}}(\text{BS}_j) - \psi_{\text{x}}(\text{UE}_i)\right)^2 + \left(\psi_{\text{y}}(\text{BS}_j) - \psi_{\text{y}}(\text{UE}_i)\right)^2}$$

Then the antenna vertical gain is:

$$G_{\text{v}}(\Delta\theta_{ij})[\text{dB}] = -\min\left(c\left(\frac{\Delta\theta_{ij}}{\theta_{\text{3dB}}}\right)^2, A_{\text{v}}\right) \tag{3.9}$$

where, θ_{3dB} is the 3dB beam-width of the main lobe in vertical plane. Also A_{v} determines the antenna power gain in the side lobe in the vertical plane.

Now the overall antenna gain, which appears in Eq. (3.5), can be calculated in dB units by combining Eq. (3.7) and Eq. (3.9):

$$G\left(\phi_j, \theta_j, \mathbf{\Psi}(\mathrm{BS}_j), \mathbf{\Psi}(\mathrm{UE}_i)\right)_{[\mathrm{dB}]} =$$

$$G_{\mathrm{o\ [dBi]}} - \min\left(-\left(G_{\mathrm{h}}(\Delta\phi_{ij})_{[\mathrm{dB}]} + G_{\mathrm{v}}(\Delta\theta_{ij})_{[\mathrm{dB}]}\right), A_{\mathrm{h}}\right) \tag{3.10}$$

where a constant G_{o} is also added as the normalization factor so that the average gain of the antenna becomes $1/4\pi$ to guarantee unit transmission power. Also, A_{h} is the same as in Eq. (3.7).

To conclude this section, Eqs. (3.4) and (3.5) relate the user rate in Eq. (3.3) to the BS's antenna parameters as well as location.

3.3 Numerical results

A lattice network of BSs is considered as shown in Fig. 3.2 where there is a BS in each hexagonal small cell. The network radius varies from d to $4d$, where d is the inter-site distance. The case of non-coordinated random network with the same density of BSs is considered as the basis for the comparison. In this case neither sectoral antenna, nor BS cooperation is available. This case has already been analyzed in chapter 2.

For all numerical evaluations, the parameters are selected similar to the 3GPP specifications for small cells. The only exception is that in in 3GPP an omnidirectional antenna is considered for SC-BSs. This omnidirectional model, is replaced by the sectorized antenna model of macro BSs [21]. All parameters are listed in Table 3.1.

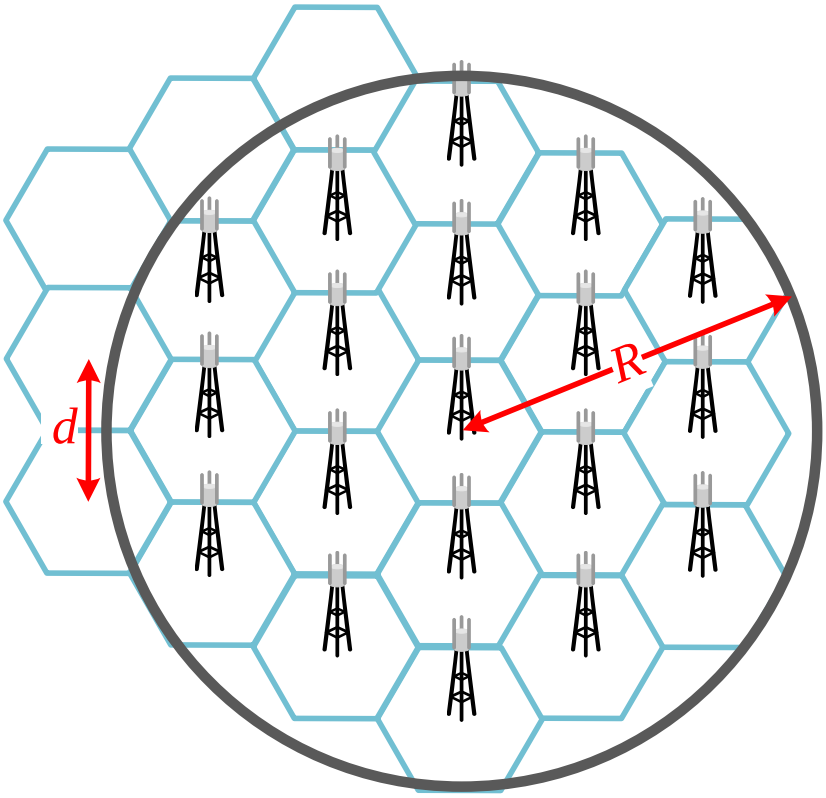

Figure 3.2: The scenario of a regular lattice network, with network radius R and inter-site distance od d.

The effect of CoMP is also evaluated in the section. The CoMP communication model has been characterized in subsection 3.2.1. In the case of coordinated network, it is assumed that full cooperation is available. In other words, all BSs join a cooperative cluster and jointly transmit to several UEs. As Fig. 3.2 shows, the number of BSs in the network is a function of the network radius. Also, the number of UEs for the multiuser communication in a CoMP cluster is selected to be equal to the number of BSs in the cluster.

Two different cases for UE distributions are examined. In one case UEs are distributed uniformly in the network area. On the other hand, in the second case an example of a nonuniform user distribution is considered. In this case, it is assumed

that all UEs are located in a limited congestion area which is called a hotspot and there is no UE in the rest of the network area. This latter scenario provides a foundation to study the effectiveness of a network architecture in adapting to the user distribution. In this scenario, a large portion of the network is empty of users, and the resources of the BSs within those areas are wasted unless a mechanism is added to direct idle resources to the congestion area.

3.3.1 Uniform user distribution

It is assumed that UEs are randomly located in the network area with uniform distribution. The the improvements due to sectoral antenna and BS coordination are shown in Fig. 3.3. The case of Non-coordinated network with omnidirectional transmissions is the case that was studied in chapter 2 and evaluated in Fig. 2.3.

As expected, the use of sectoral/ directional antennas improves the system rate. In Fig. 3.3 it is observed that performance gain of sectoral/ directional antennas is not constant. In fact by the increase of the network radius the gain of sectoral/ directional antennas slightly increases. This can be explained by the fact that when the network size increases, more BSs are transmitting in the network area and the interference becomes more severe. Thus, in this circumstance the use of an interference reduction method is more beneficial.

As expected, addition of full cooperation among all BSs further improves the system rate. The number of UEs that are picked for multiuser transmission is equal to the number of BSs in the cooperative cluster. For every multiuser joint transmission, one UE is selected randomly in each small hexagonal cell. Therefore, the user scheduling and the number of UEs is exactly the same as the non-coordinated

Table 3.1: Parameters for numerical evaluations

Inter-site distance (d)	100 m
Number of Transmit antennas Number of Receive antennas	2 2
Antenna height	5 m
Normalization factor of the antenna gain (G_{o})	 14 dBi
Antenna horizontal pattern, G_{h}	$-\min\left(c\ \left(\frac{\phi-\phi_{\mathrm{o}}}{\phi_{3\mathrm{dB}}}\right)^2, A_{\mathrm{h}}\right)$ ϕ_{o} is the horizontal beam direction of a BS; $c = 12$, $A_{\mathrm{h}} = 25$ dB, $\phi_{3\mathrm{dB}} = 70^{\mathrm{o}}$
Antenna vertical pattern, G_{v}	$-\min\left(c\ \left(\frac{\theta-\theta_{\mathrm{o}}}{\theta_{3\mathrm{dB}}}\right)^2, A_{\mathrm{v}}\right)$ $\theta_{\mathrm{o}} = 15^{\mathrm{o}}$ $c = 12$, $A_{\mathrm{v}} = 20$ dB, $\theta_{3\mathrm{dB}} = 10^{\mathrm{o}}$
Distance-dependent path loss, L	$140.7 + 36.7\log_{10}(\mathit{distance}[\mathrm{km}])$
Transmit power	30 dBm
Noise power	-100 dBm

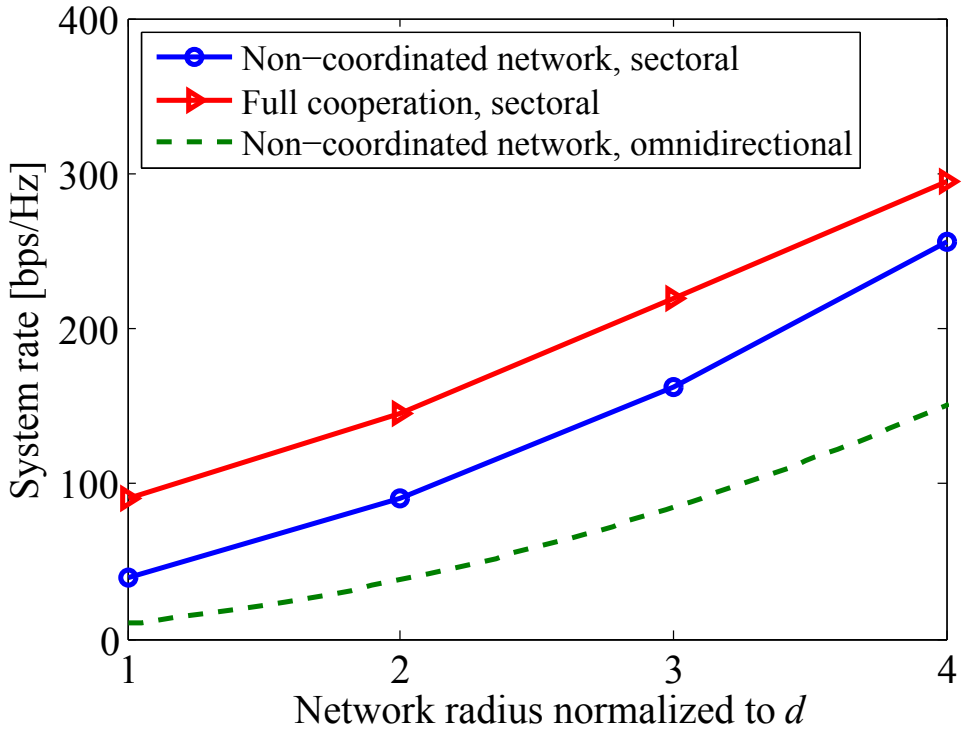

Figure 3.3: Effect of sectoral antennas and full BS cooperation on the system rate in a network with uniform user distribution.

cases. Full cooperation eliminates the remaining interference and increases the system rate.

3.3.2 Hotspot

Here a hotspot means a small limited area with a high density of UEs. As an example for the numerical evaluation, a hotspot is considered in the central hexagonal small cell. It is assumed that all users are located in the area of one small cell in the center of the network. The system rate versus network radius is shown in Fig. 3.4. In both non-coordinated and full cooperation cases random scheduling is applied and the users are randomly selected. However, in the case of full co-

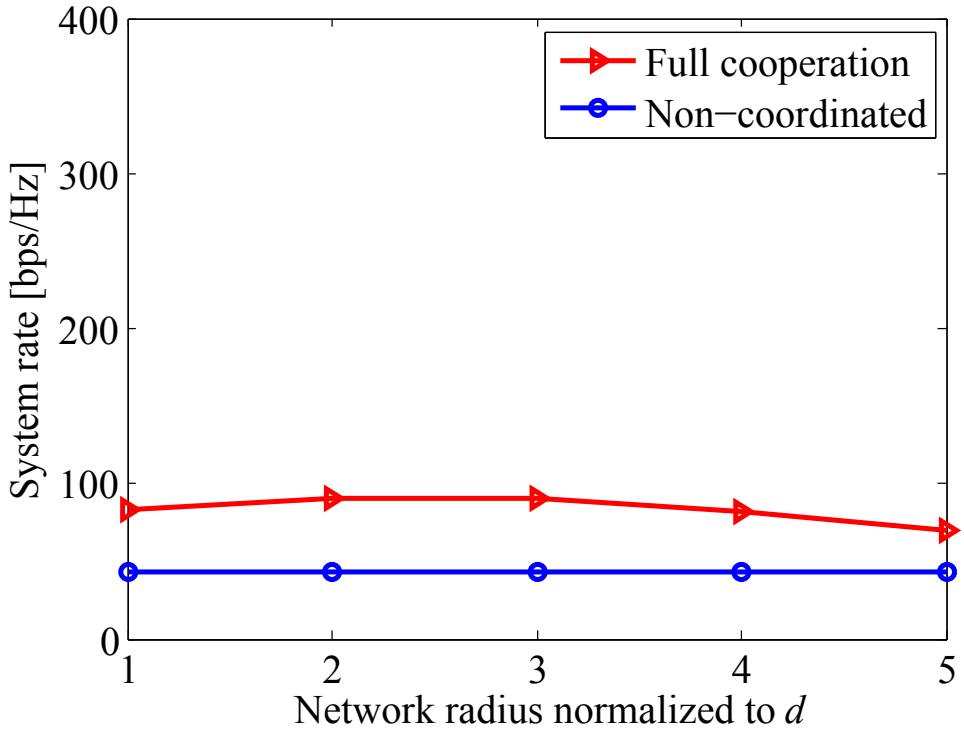

Figure 3.4: System rate for the hotspot scenario in non-coordinated and full cooperation cases.

operation the number of UEs that are selected for the multiuser communication is equal to the number of cooperating BSs in the cluster. On the other hand, in the non-coordinated case each BS selects one UE randomly from the UEs in its range. However, most of the BSs do not have any UEs in their range and cannot contribute to the communications. In both cases, all BSs use sectoral antennas. Except for the user distribution, all other parameters are the same as previous subsection. Also, the scale of Fig. 3.4 is selected similar to Fig. 3.3 to facilitate the comparison of the performance of the system for different user distributions.

When the radius of the network is increased, more BSs will be available in the network. However, in the non-coordinated case, BSs that are not located near

the hotspot do not communicate to the UEs. On the other hand, by means of full cooperation, non-local BSs can contribute to the system rate by adding to the multiplexing gain. By addition of each BS to the cooperative cluster, the number of UEs for multiuser communication is incremented by 1. Nonetheless, the received power from far BSs is very low due to distance-dependent path loss. It is observed that using far BSs in the cooperative cluster can have a destructive effect on the system rate. In other words, full cooperation does not use idle network resources in the congestion areas efficiently.

3.4 Conclusion

In this chapter the system models of BS cooperation and sectoral/ directional antennas were described. These systems are used for interference reduction/ elimination. The performance gain due to these mechanisms were studied in two different network scenario. In the case of uniform user distribution a steady improvement was observed. However, in the case of a hotspot, the performance is limited. It is observed that these mechanisms do not efficiently adapt to nonuniform user distributions. To solve this problem, in the next chapter a more advanced scheme is developed that implements cell structuring and cooperation concurrently to dynamically transfer network resources to hotspot areas.

CHAPTER 4

DYNAMIC CELL STRUCTURING AND LARGE-SCALE COOPERATION

4.1 Introduction

In this chapter a nonuniform user distribution with congestion areas is considered and the architecture of the HetNet cellular network is developed in way that it can adapt to the user distribution. In practical networks, the users' distribution in the network area fluctuates during a day. For example residential areas and business areas may have different user distributions during different periods of time. To be more explicit, in some time periods the business area may be crowded, while the traffic demand is very low in the residential area. This observation is the motivation behind the study and design of a flexible cellular network that is capable of dynamically transferring idle network resources from sparse areas to the crowded areas that are called hotspot zones.

When the coverages of BSs/ SC-BSs are static and fixed some network resources remain unused in sparse areas while the hotspot zones require more resources. In the previous chapter, full cooperation among BSs was studied. Full cooperation improves the performance by eliminating the interference, however it cannot transfer and reuse the resources of a far away BS/ SC-BS in the hotspot zone.

The objective of this chapter is to introduce a flexible scheme that is able to dynamically direct idle network resources to the hotspots. In this chapter dynamic cell structuring is performed concurrent to the full cooperation. Here the term "cell structuring" refers to the dynamically change the coverage of SC-BSs. It is assumed that in the HetNet all SC-BSs are connected to the C-RAN and can adjust

their antenna beam directions and perform joint transmission CoMP in a cluster. In the rest of this chapter, the general term of "BS" refers to a SC-BSs within a macro cell area that is connected to the C-RAN.

In brief, large optimal cooperative clusters are formed around hotspots. A cluster is a group of SC-BSs that cooperatively perform joint transmission (JT) to several UEs. The set of SC-BSs for each cluster and the antennas' beam angles of each SC-BS are optimized so that the system rate of the network is maximized. Thus at first, the system rate is analyzed and a mathematical framework for calculation of the system rate in a cooperative cluster is developed. Then, the optimization problem for cluster formation is defined and solved, and in the end the trend of performance variation versus cluster size is studied and its limitations are determined. Numerical results using 3GPP specifications show that this scheme attains several times higher capacity compared to both non-coordinated transmission and full cooperation without dynamic coverage control.

4.2 System rate analysis

In practical cellular networks, the user distribution is not uniform and congeries of users appear in some areas that are called hotspots. In this thesis large clusters are proposed to utilize resources in the hotspots more efficiently as demonstrated in Fig. 4.1. In this chapter, maximizing the system rate will be used as the optimization objective for cell structuring and cluster formation. System rate is defined as the average sum rate of all users in the network. Monte Carlo simulation can be implemented to obtain this performance metric through various snapshots of the network. However, in order to use this metric as an optimization objective, it is of

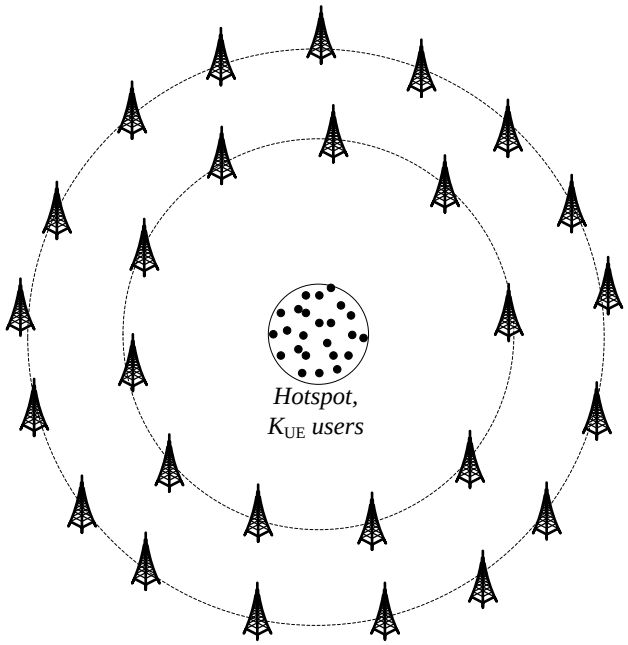

Figure 4.1: A large cluster to serve users in a hotspot zone.

great importance to develop an analytical framework to estimate it without Monte Carlo iterations.

The goal of this section is to calculate the system rate of a cooperative cluster communicating to users in a small dense zone. A cluster is a set of K_{BS} base stations that perform joint transmission (JT) CoMP to a set of K_{UE} UEs. The channel from each BS to each UE is assumed to be known at a baseband central processing unit which processes and distributes the transmission data over the set of antennas of all BSs of the cluster. Therefore, the whole cluster can be modeled as a broadcast channel that consists of a single aggregated BS with $K_{\mathrm{BS}}M_{\mathrm{T}}$ distributed antennas to K_{UE} user equipments (Fig. 4.2).

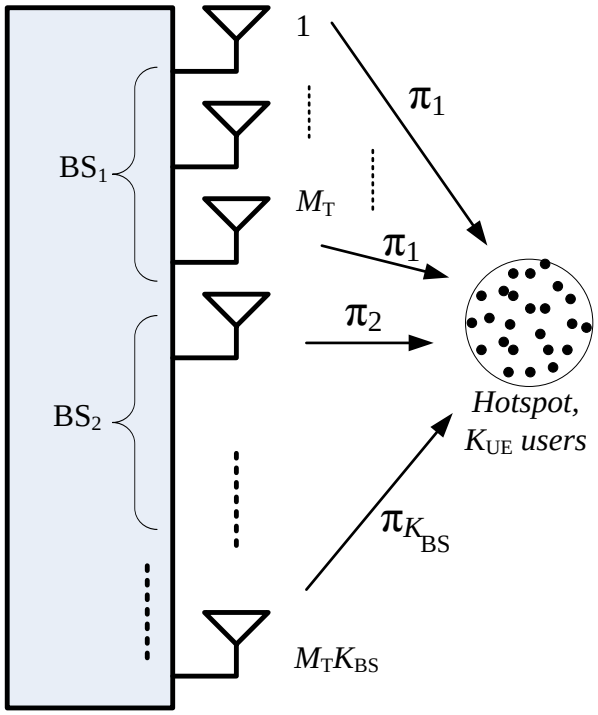

Figure 4.2: Modeling a cooperative cluster as a distributed MIMO which consists of a single aggregated BS with $K_{\mathrm{BS}} M_{\mathrm{T}}$ distributed antennas to K_{UE} user equipments.

First of all, the received signal of the i^{th} user is expressed as follows:

$$\mathbf{y}_i = \mathbf{F}_i \mathbf{\Pi}_i^{\frac{1}{2}} \mathbf{Q}_i \mathbf{x} + \mathbf{n}_{\mathrm{intf},\, i} + \mathbf{n}_i \tag{4.1}$$

where, $\mathbf{x} = \mathbf{T}\mathbf{s} \in \mathbb{C}^{M_{\mathrm{T}} K_{\mathrm{BS}} - M_{\mathrm{R}}(K_{\mathrm{UE}}-1)}$ is the coded vector that is transmitted over all BSs' antennas, $\mathbf{y}_i \in \mathbb{C}^{M_{\mathrm{R}}}$ is the received signal and $\mathbf{n}_{\mathrm{intf},\, i}$ and $\mathbf{n}_i \in \mathbb{C}^{M_{\mathrm{R}}}$ are the corresponding interference and additive noise of the i^{th} user, respectively. Also, P is

calculated by the sum of powers from K_{BS} BSs as:

$$\begin{aligned} \mathbf{P} &= \mathrm{E}\left\{\mathbf{Q}_i \mathbf{x}\mathbf{x}^{\mathrm{H}} \mathbf{Q}_i^{\mathrm{H}}\right\}, \\ P &= \mathrm{tr}\left(\mathbf{P}\right) = \sum_{j=1}^{K_{\mathrm{BS}}} P_j, \end{aligned} \tag{4.2}$$

where P_j is the transmit power from j^{th} BS. The block diagonalization matrix, $\mathbf{Q}_i$, is considered to be normalized to maintain the transmit power limit.

In Eq. (4.1), the MIMO channel matrix from all BSs' antennas to user i, is considered as $\mathbf{H}_i = \mathbf{F}_i \mathbf{\Pi}_i^{\frac{1}{2}} \in \mathbb{C}^{M_{\mathrm{R}} \times M_{\mathrm{T}} K_{\mathrm{BS}}}$; where, $\mathbf{F}_i \in \mathbb{C}^{M_{\mathrm{R}} \times M_{\mathrm{T}} K_{\mathrm{BS}}}$ models the i.i.d. Rayleigh flat fading with unit power; and $\mathbf{\Pi}_i \in \mathbb{R}^{M_{\mathrm{T}} K_{\mathrm{BS}} \times M_{\mathrm{T}} K_{\mathrm{BS}}}$ is the diagonal matrix of path power gains from all BSs' antennas towards user i which are obtained from Eq. (3.5).

$$\mathbf{\Pi}_i = \mathrm{diag}\left(\pi_{i1}, \cdots, \pi_{iK_{\mathrm{BS}}}\right) \otimes \mathbf{I}_{M_{\mathrm{T}}} \tag{4.3}$$

Since all users of a cluster are assumed to be located in a small area, $\mathbf{\Pi}_i$ is assumed to be almost the same for all users: $\mathbf{\Pi}_i = \mathbf{\Pi}, (1 \leq i \leq K_{\mathrm{UE}})$. For the elements related to the BSs that are very close to the hotspot area, this assumption may be inaccurate. However, it leads to a mathematically tractable framework; and later, our numerical evaluations show that the analytical result matches to the simulation results and can safely be used to predict the trend.

Furthermore, according to Eq. (3.1), the block diagonalization precoding matrix $\mathbf{Q}_i$ is selected such that:

$$\left[\mathbf{H}_1^{\mathrm{T}}, ..., \mathbf{H}_{(i-1)}^{\mathrm{T}}, \mathbf{H}_{(i+1)}^{\mathrm{T}}, ..., \mathbf{H}_{K_{\mathrm{UE}}}^{\mathrm{T}}\right]^{\mathrm{T}} \mathbf{Q}_i = \mathbf{0} \tag{4.4}$$

Equation (4.4) can be rewritten as follows:

$$\left[\mathbf{F}_1^{\mathrm{T}}, ..., \mathbf{F}_{(i-1)}^{\mathrm{T}}, \mathbf{F}_{(i+1)}^{\mathrm{T}}, ..., \mathbf{F}_{K_{\mathrm{UE}}}^{\mathrm{T}}\right]^{\mathrm{T}} \mathbf{\Pi}^{\frac{1}{2}} \mathbf{Q}_i = \mathbf{0} \tag{4.5}$$

This modeling enables us to decompose the precoding matrix $\mathbf{Q}_i$ into two terms:

$$\mathbf{Q}_i = \mathbf{D}_i \mathbf{U}_i \tag{4.6}$$

where $\mathbf{D}_i \in \mathbb{C}^{M_T K_{BS} \times M_T K_{BS}}$ is a diagonal matrix to cancel $\mathbf{\Pi}^{1/2}$ term and $\mathbf{U}_i \in \mathbb{C}^{M_T K_{BS} \times [M_T K_{BS} - M_R(K_{UE}-1)]}$ is a unitary matrix that nullifies the interference of other users' signals:

$$\begin{aligned} \mathbf{D}_i &= \left(\frac{M_T K_{BS}}{\mathrm{tr}\left(\mathbf{\Pi}^{-1}\right)}\right)^{\frac{1}{2}} \mathbf{\Pi}^{-\frac{1}{2}} \\ &\left[\mathbf{F}_1^T, ..., \mathbf{F}_{(i-1)}^T, \mathbf{F}_{(i+1)}^T, ..., \mathbf{F}_{K_{UE}}^T\right]^T \mathbf{U}_i = \mathbf{0} \end{aligned} \tag{4.7}$$

It should be noted that the normalization coefficient in $\mathbf{D}_i$ is calculated so that the BD matrix, $\mathbf{Q}_i$, does not affect the total transmit power. Therefore, the communication model of Eq. (4.1) can be considered as follows:

$$\mathbf{y}_i = \left(\frac{M_T K_{BS}}{\mathrm{tr}\left(\mathbf{\Pi}^{-1}\right)}\right)^{\frac{1}{2}} \mathbf{F}_i \mathbf{U}_i \mathbf{x} + \mathbf{n}_{\mathrm{intf},\, i} + \mathbf{n}_i \tag{4.8}$$

In our scenario there is a large cluster in which a large number of BSs cooperatively communicate to users in a small dense area. Thus, user selection diversity is not effective, and users are considered to be selected randomly. Such a block diagonalization (BD) multi-user CoMP transmission can be converted into equivalent parallel single-user CoMP transmission model [5], [22]. To be more explicit, with random user scheduling in a cluster, the block diagonalization matrix corresponding to user i ($1 \le i \le K_{UE}$), $\mathbf{U}_i$, will be an orthonormal matrix independent of the own channel coefficients, $\mathbf{F}_i$ [5]. This feature makes the effective channel matrix, $\widetilde{\mathbf{H}}_i = \mathbf{F}_i \mathbf{U}_i \in \mathbb{C}^{M_R \times [M_T K_{BS} - M_R(K_{UE}-1)]}$, a random matrix with the following average correlation matrix, $\mathbf{\Upsilon}_i$:

$$\begin{aligned} \mathbf{\Upsilon}_i &= \frac{1}{M_R} \mathrm{E}\left\{\widetilde{\mathbf{H}}_i^H \widetilde{\mathbf{H}}_i\right\} \\ &= \frac{1}{M_R} \mathrm{E}\left\{\mathbf{U}_i^H \, \mathbf{F}_i{}^H \mathbf{F}_i \mathbf{U}_i\right\} \\ &= \mathbf{I}_{M_T K_{BS} - M_R(K_{UE}-1)}. \end{aligned} \tag{4.9}$$

The instantaneous matrix, $\widetilde{\mathbf{H}}_i^H \widetilde{\mathbf{H}}_i$ is a Wishart matrix with eigenvalues λ_l ($l = 1, 2, ..., M_R$) where the probability density function (PDF) of λ_l's is characterized

by the eigenvalues of the transmit correlation matrix, Υ_i [23], [24] as explained in Appendix A. Especially, note that this PDF is a function of the dimensions of $\widetilde{\mathbf{H}}_i$ and therefore is affected by M_{R}, M_{T}, K_{UE} and K_{BS}.

Eventually, the MIMO transmission for user i can be converted into M_{R} equivalent parallel streams each with SINR of γ_{il} ($1 \leq l \leq M_{\mathrm{R}}$):

$$\gamma_{il} = \lambda_l \overline{\gamma}_i \tag{4.10}$$

where $\overline{\gamma}_i$ is the average received SINR of the i^{th} user in the cluster which can be assumed to be the same for all users within a hotspot ($\overline{\gamma}_i = \overline{\gamma}$, $1 \leq i \leq K_{\mathrm{UE}}$):

$$\overline{\gamma} = \left(\frac{M_{\mathrm{T}} K_{\mathrm{BS}}}{\mathrm{tr}\left(\mathbf{\Pi}^{-1}\right)} \right) \frac{P/K_{\mathrm{UE}}}{\sigma^2 + \sigma^2_{\mathrm{intf}}} \tag{4.11}$$

It should be mentioned that in Eq. (4.11), the interference is treated as noise. To be more explicit, there are a large number of interfering signals from BSs out of the cluster and the overall interference matrix ($\mathbf{n}_{\mathrm{intf}}$ in Eq. (3.1)) becomes a random matrix with i.i.d elements. The term $\mathrm{E}\left\{\mathbf{n}_{\mathrm{intf},i}\mathbf{n}_{\mathrm{intf},i}{}^{\mathrm{H}}\right\}$ in Eq. (3.3) can be replaced by $\sigma^2_{\mathrm{intf},\,i}\mathbf{I}_{M_{\mathrm{R}}}$, where $\sigma^2_{\mathrm{intf},\,i}$ is the total interfering power that user i receives. It can be assumed that $\sigma^2_{\mathrm{intf},\,i} \cong \sigma^2_{\mathrm{intf}}$ for all users in the same hotspot:

$$\sigma^2_{\mathrm{intf}} = \sum_{\forall \mathrm{BS}_k \notin h} P_k \pi_{hk}, \tag{4.12}$$

where, P_k is the transmit power of a BS_k that is not a member of the cooperative cluster h. Also, π_{hk} is the path power gain from that BS to the hotspot h.

Finally, the average sum rate of the cluster is calculated as follows:

$$\begin{aligned} \overline{R} &= \chi \mathrm{E}\left\{ \sum_{i=1}^{K_{\mathrm{UE}}} \sum_{k=1}^{M_{\mathrm{R}}} \log_2\left(1+\gamma_{ik}\right) \right\} \\ &\overset{\text{Jensen}}{\leq} \chi \sum_{i=1}^{K_{\mathrm{UE}}} \sum_{k=1}^{M_{\mathrm{R}}} \log_2\left(1+\mathrm{E}\{\gamma_{ik}\}\right) \\ &= \chi K_{\mathrm{UE}} \sum_{k=1}^{M_{\mathrm{R}}} \log_2\left(1+\overline{\gamma}\,\mathrm{E}\{\lambda_l\}\right) \end{aligned} \tag{4.13}$$

where, Jensen's inequality [25] is applied to obtain an upper bound for the average sum rate. Also, $\overline{\gamma}$ is substituted from Eq. (4.11). Furthermore, as explained in Appendix 1, $\mathrm{E}\{\lambda_l\}$ is obtained according to the PDF of a Wishart matrix with the average correlation matrix of Υ_i that has been derived in Eq. (4.9). Note that in Eq. (4.13), K_{UE} not only appears as a coefficient, but also affects $\mathrm{E}\{\lambda_l\}$ through affecting the dimensions of Υ_i.

4.3 Clustering mechanism for large scale CoMP

Applying the analytic tool of section 4.2, in this section we propose a novel cell structuring and BS clustering method in order to utilize network resources more efficiently. When there are some dense hotspot zones in the network area, this method can multiply the capacity compared to conventional schemes. This gain in capacity comes from transferring idle resources of sparse areas to the crowded areas.

The idea is to focus on each hotspot zone and form a cluster around that zone. We add BSs to the cluster tier by tier. A tier is a virtual ring around the zone of interest which consists of BSs that potentially produce almost equal power in the hotspot. It should be emphasized that here a tier is a geometrical parameter and does not contain any hierarchical interpretation. An example of a cluster with five tiers is shown in Fig. 4.3. This figure represents a single hotspot zone at the center and a cluster around it. In this scenario, all users are located in one central cell and the rest of the network area is empty of users. With no loss of generality, in the first tier at the center of the cluster, three sectors are coordinated as intra-site CoMP to maintain consistency with current 3GPP specifications. Note that the

conventional 3GPP system is equivalent to a 1-tier cluster. In general, every BS that joins a cluster can increase the sum rate for the corresponding hotspot, but on the other hand, produces interference in other hotspots. The general problem can be formulated as follows.

Before going to the details about clustering, we have to extend several notations to be able to describe multiple hotspots or clusters at the same time. The matrix $\mathbf{\Pi}^{h\bar{h}}$ is defined as the path power gain matrix between the BSs of cluster $\bar{h}$ and the UEs in hotspot h:

$$\mathbf{\Pi}^{h\bar{h}} = \text{diag}\left(\pi_1^{h\bar{h}}, \cdots, \pi_{K_{\text{BS}}^{\bar{h}}}^{h\bar{h}}\right) \otimes \mathbf{I}_{M_{\text{T}}} \tag{4.14}$$

The number of hotspots or equivalently the number of clusters in the network is denoted by $\mathcal{H}$. The transmit power matrix and the total power of the h^{th} cluster ($1 \leq h \leq \mathcal{H}$) are denoted by $\mathbf{P}^h$ and P^h, respectively. Also the power of the j^{th} BS in cluster h is denoted by P_j^h. The objective function to be maximized is the average system rate of the whole network. The parameters to be optimized are the indices j of the BSs of each cluster h and the horizontal direction (ϕ_j) and vertical tilt (θ_j) angles of the antenna (sector) of each BS_j.

The cluster for a hotspot is initiated as a 1-tier cluster consisting of the BSs within the hotspot area. Afterwards, the following optimization problem should be solved to add the k^{th} tier ($k \geq 2$) to each cluster. Note that in general, the index of the tier, k, can be different for different hotspots.

$$\begin{aligned}\left[(\widehat{\phi}_j, \widehat{\theta}_j)_{\forall j \in \{\widehat{j}\}}, \left(\{\widehat{j}\}_k^h\right)_{\forall h,\ \forall k}\right] = \\ \arg \max_{(\phi_j, \theta_j), \{j\}_k^h} \left(\sum_{h=1}^{\mathcal{H}} \max_{1 \leq K_{\text{UE}}^h \leq K_{\text{BS}}^h} \overline{R}^h \right)\end{aligned} \tag{4.15}$$

Here, $\{j\}_k^h$ is a set of indices of candidate BSs of k^{th} tier in cluster h and $\{\widehat{j}\}_k^h$ denotes

the set of indices of optimal BSs to be added to the cluster h:

$$\sum_{k} \left| \{\widehat{j}\}_k^h \right| = K_{\mathrm{BS}}^h \tag{4.16}$$

Also, $\overline{R}^h$ is the average sum rate in hotspot h. An upper bound on $\overline{R}^h$ has been provided in Eq. (4.13). The horizontal direction (ϕ_j) and vertical tilt (θ_j) angles of the antenna of each BS_j change the power-gain matrix in Eq. (4.14) whose elements are obtained through Eq. (3.5). Therefore, they affect the system rate by changing SINR, $\overline{\gamma}$.

In Eq. (4.15), $\overline{R}^h$ can be substituted with either Monte Carlo simulation or the analytical estimation. Our numerical evaluation shows that both result in the same optimal clusters. Using the upper bound of Eq. (4.13) instead of Monte Carlo estimation reduces the computational cost significantly. However, still the optimization problem of Eq. (4.15) is a complicated problem that contains several optimization parameters. This problem can be decomposed into simpler problems based on the characteristics of the network. In fact, different network parameters vary in different time scales. The propagation channel changes quickly and therefore the block diagonalization (BD) weights (**Q** in Eq. (3.1)) are to be updated every few milliseconds. In contrast, a cluster is formed in a totally slower time scale. Hence, cluster formation is accomplished based on averaging over short term parameters including BD weights and user scheduling. Furthermore, antenna beam angles are long term parameters that are optimized very slowly to follow the slow changes and shifts of hotspots during a day.

The rest of this section deals with the problem of forming the optimal clusters. In brief, at the first stage all available BSs are treated as candidates for the clusters and the optimum beam angles for each candidate are specified. Then, the optimal clusters are formed around the hotspots. The mathematical details are described in

subsections 4.3.1 and 4.3.2 and in the end the clustering algorithm is summarized in Table 4.1.

4.3.1 Optimization of antenna beam angles

In usual networks the locations of hotspots do not change rapidly. Besides, the purpose of controlling antennas' beam directions is to adapt the coverage of BSs to the hotspots' locations. Therefore, the optimization of the beam angles can be accomplished independently in a different time scale. Antennas' beam angles affect the system rate or capacity by changing the received powers in the hotspots. All BSs of the k^{th} tier around the h^{th} hotspot are considered as candidate BSs for the h^{th} cluster. However, since K_{BS}^{h} is not determined yet, for each cluster a single user in the center of the hotspot is considered: $K_{\text{UE}}^{h} = 1, \forall h$. For any candidate base station (e.g. BS_j), the optimum angles $(\widehat{\phi}_j, \widehat{\theta}_j)$ are determined from the following equation:

$$\left(\widehat{\phi}_j, \widehat{\theta}_j\right) = \arg \max_{\phi_j, \theta_j} \left(\Gamma_j(\phi_j, \theta_j)\right) \tag{4.17}$$

$\Gamma_j(\phi_j, \theta_j)$ can be defined as any function whose maximization is equivalent to maximizing the system rate.

$$\begin{aligned}
\left(\widehat{\phi}_j, \widehat{\theta}_j\right) &= \arg \max_{\phi_j, \theta_j} \left(\sum_{h=1}^{\mathcal{H}} \overline{R}^{h}\right) \\
&\leq \arg \max_{\phi_j, \theta_j} \left(\sum_{h=1}^{\mathcal{H}} \log_2\left(1 + \overline{\gamma}^{h}(\phi_j, \theta_j)\right)\right) \\
&= \arg \max_{\phi_j, \theta_j} \left(\prod_{h=1}^{\mathcal{H}} \left(1 + \overline{\gamma}^{h}(\phi_j, \theta_j)\right)\right) \\
&\simeq \arg \max_{\phi_j, \theta_j} \left(\prod_{h=1}^{\mathcal{H}} \left(\overline{\gamma}^{h}(\phi_j, \theta_j)\right)\right)
\end{aligned} \tag{4.18}$$

where, $\overline{\gamma}^h$ is the average received SINR for users in cluster h, and according to Eq. (4.11) it is related to (ϕ_j, θ_j) through the matrix $\mathbf{\Pi}^{hh}$. In this equation, Jensen's inequality has been applied for simplification. Also, for simpler notation, the equations are written for the case of $M_{\mathrm{T}} = M_{\mathrm{R}} = 1$. However, extension to the general case is straightforward.

Assume that the j^{th} BS is a candidate for cluster h ($1 \le h \le \mathcal{H}$) and its transmit power is P_j^h. Therefore, the j^{th} BS is contributing to the received signal for users in hotspot h. On the other hand, it is producing interference for the users in all other hotspots. Then the objective function of Eq. (4.18) is calculated by replacing $\overline{\gamma}^h$ from Eq. (4.11) as follows:

$$\prod_{h=1}^{\mathcal{H}} \overline{\gamma}^h(\phi_j, \theta_j) = \left(\frac{\frac{P_j^h + \sum_{i \neq j} P_i^h}{\left(\pi_j^{hh}\right)^{-1} + \sum_{i \neq j} \left(\pi_i^{hh}\right)^{-1}}}{\sigma^2 + \sum_{\bar{h} \neq h} \mathbf{\Pi}^{h\bar{h}} \mathbf{P}^{\bar{h}}} \right) \times \prod_{\bar{h} \neq h}^{\mathcal{H}} \left(\frac{\frac{P^{\bar{h}}}{\mathrm{tr}\left(\mathbf{\Pi}^{\bar{h}\bar{h}}\right)^{-1}}}{\sigma^2 + \sum_{\tilde{h} \neq \bar{h}, h} \mathrm{tr}\left(\mathbf{\Pi}^{\bar{h}\tilde{h}} \mathbf{P}^{\tilde{h}}\right) + P_j^h \pi_j^{h\bar{h}} + \sum_{i \neq j} P_i^h \pi_i^{h\bar{h}}} \right) \tag{4.19}$$

Equation (4.19) can be decomposed as:

$$\prod_{h=1}^{\mathcal{H}} \overline{\gamma}^h(\phi_j, \theta_j) = \beta \;\; \Gamma_j(\phi_j, \theta_j) \tag{4.20}$$

where β is a coefficient that contains all factors that are independent of BS_j, and $\Gamma_j(\phi_j, \theta_j)$ is the maximization objective function as follows:

$$\Gamma_j(\phi_j, \theta_j) = \frac{\Gamma_{\mathrm{num},j}(\phi_j, \theta_j)}{\Gamma_{\mathrm{den},j}(\phi_j, \theta_j)} \tag{4.21}$$

where the numerator and denominator are defined as:

$$\Gamma_{\mathrm{num},j}(\phi_j, \theta_j) = \left(\frac{P_j^h + \sum_{i \neq j} P_i^h}{\left(\pi_j^{hh}\right)^{-1} + \sum_{i \neq j} \left(\pi_i^{hh}\right)^{-1}} \right), \tag{4.22}$$

$$\Gamma_{\mathrm{den},j}(\phi_j, \theta_j) = \prod_{\bar{h} \neq h}^{\mathcal{H}} \left(\sigma^2 + \sum_{\tilde{h} \neq \bar{h}, h} \mathrm{tr}\left(\mathbf{\Pi}^{\bar{h}\tilde{h}} \mathbf{P}^{\tilde{h}}\right) + P_j^h \pi_j^{h\bar{h}} + \sum_{i \neq j} P_i^h \pi_i^{h\bar{h}} \right)$$

Equations (4.17) and (4.21) associate the optimum beam direction of any candidate BS, e.g. BS_j, to all clusters and the signal power and interferences that each of them produces. Hereafter, in our numerical evaluations we replace the maximization metric $\Gamma_j(\phi_j, \theta_j)$ with a suboptimal metric, $\widetilde{\Gamma}_j(\phi_j, \theta_j)$, that can be calculated for each BS independently. Such a metric is obtained by neglecting the effect of all BSs other than the candidate BS. In the numerator of $\Gamma_j(\phi_j, \theta_j)$ the only factor that is a function of the optimization parameters, (ϕ_j, θ_j), is $\left(\pi_j^{hh}\right)^{-1}$. Therefore at the first step, the maximization problem is approximated as:

$$\arg \max_{\phi_j, \theta_j} \left(\Gamma_j(\phi_j, \theta_j)\right) \simeq \arg \max_{\phi_j, \theta_j} \left(\frac{P_j^h \pi_j^{hh}}{\Gamma_{\text{den},j}(\phi_j, \theta_j)}\right) \tag{4.23}$$

In the above equation $\left(\pi_j^{hh}\right)^{-1}$ has been replaced with $P_j^h \pi_j^{hh}$. Since P_j is independent of (ϕ_j, θ_j), this replacement does not change the result, but it assigns the physical meaning of the received signal power to the optimization objective.

Similarly in $\Gamma_{\text{den},j}(\phi_j, \theta_j)$, only $\pi_j^{h\bar{h}}$ is dependent on (ϕ_j, θ_j). Therefore, the maximization problem is further approximated as:

$$\arg \max_{\phi_j, \theta_j} \left(\Gamma_j(\phi_j, \theta_j)\right) \simeq \arg \max_{\phi_j, \theta_j} \left(\frac{\pi_j^{hh} P_j^h}{\prod_{\bar{h} \neq h} \pi_j^{\bar{h}h} P_j^h}\right) \tag{4.24}$$

In this maximization metric the numerator is the signal power that is received from BS_j in the corresponding hotspot, and the denominator is the total interference that this BS produces in all other hotspots. Using these approximations, every BS_j can calculate and tune its beam angle independently. Finally, we define the metric $\widetilde{\Gamma}_j(\phi_j, \theta_j)$ as follows:

$$\widetilde{\Gamma}_j(\phi_j, \theta_j) \stackrel{\text{def}}{=} \frac{\pi_j^{hh} P_j^h}{\prod_{\bar{h} \neq h} \pi_j^{\bar{h}h} P_j^h} \tag{4.25}$$

And the suboptimal beam directions are obtained as:

$$\left(\widetilde{\phi}_j, \widetilde{\theta}_j\right) = \arg \max_{\phi_j, \theta_j} \left(\widetilde{\Gamma}_j(\phi_j, \theta_j)\right) \tag{4.26}$$

Table 4.1: Summary of the clustering algorithm

1. Initialization:
   1.1. Initialize clusters as 1-tier clusters;
   $\forall h$ initialize K_{BS}^{h} accordingly.

2. Addition of tier $k > 1$ to the cluster h ($\forall h$):
   2.1. Obtain $(\widetilde{\phi}_j, \widetilde{\theta}_j)$, $\forall j \in \{j\}_k^h$ according to Eq. (4.26);
   2.2. Sort candidate BSs, $\{j\}_k^h$, according to $\widetilde{\Gamma}_j(\widetilde{\phi}_j, \widetilde{\theta}_j)$ of Eq. (4.25);
   2.3. Consider all the sorted BSs one by one:
      2.3.1. Calculate the metric of Eq. (4.28) with and without the candidate BS.
      2.3.2. If the metric is higher when the candidate BS is included:
      add the candidate BS to the cluster;
      update the cluster size:$K_{\mathrm{BS}}^{h} = K_{\mathrm{BS}}^{h} + 1$
   2.4. If in step 2.3, no BS of tier k is added to the cluster,
   stop adding more tiers to this cluster;
   otherwise increase k by 1 for this cluster, and repeat step 2.

By considering $\widetilde{\Gamma}_j(\phi_j, \theta_j)$ as the optimization metric, all BSs are able to adjust their beam angles simultaneously and independently. Although Eq. (4.25) is a suboptimal metric, the numerical evaluations in the next section demonstrate the remarkable performance gain due to such an optimization mechanism. It is interesting to note that the metric $\widetilde{\Gamma}_j(\phi_j, \theta_j)$ is also similar to the signal-to-leakage-noise ratio (SLNR) that is used as the figure of merit in [26] for precoding purposes.

4.3.2 Optimal BS selection for the clusters

Once the optimal beam direction of each BS is determined, the optimal BSs should be picked from tier k ($k \geq 2$) so that the system rate of the whole network is maximized. Therefore, Eq. (4.15) is modified as follows:

$$\left(\{\widehat{j}\}_k^h\right)_{\forall h,\, \forall k} = \arg \max_{\{j\}_k^h} \left(\sum_{h=1}^{\mathcal{H}} \max_{1 \leq K_{\mathrm{UE}}^h \leq K_{\mathrm{BS}}^h} \overline{R}^h \right)_{|\, (\widetilde{\phi}_j, \widetilde{\theta}_j)\ \forall j} \tag{4.27}$$

where $\overline{R}^h$ is obtained in Eq. (4.13). The system rate is the summation of $\overline{R}^h$'s of all hotspots with the previously calculated beam angles. Therefore, the optimization metric is calculated as follows:

$$\begin{aligned} &\left(\sum_{h=1}^{\mathcal{H}} \max_{1 \leq K_{\mathrm{UE}}^h \leq K_{\mathrm{BS}}^h} \overline{R}^h \right)_{|\, (\widetilde{\phi}_j, \widetilde{\theta}_j)\ \forall j} = \\ &\sum_{h=1}^{\mathcal{H}} \left(\max_{1 \leq K_{\mathrm{UE}}^h \leq K_{\mathrm{BS}}^h} K_{\mathrm{UE}}^h \sum_{l=1}^{M_{\mathrm{R}}} \log_2 \left(1 + \overline{\gamma}^h(\widetilde{\phi}_j, \widetilde{\theta}_j) \mathrm{E}\{\lambda_l\} \right) \right) \end{aligned} \tag{4.28}$$

where $\overline{R}^h$ has been replaced by the upper bound approximation that is obtained by applying Jensen's inequality in Eq. (4.13).

For each cluster h, $\{j\}_k^h$ (the candidate BSs in tier k) are sorted according to their $\widetilde{\Gamma}_j(\widetilde{\phi}_j, \widetilde{\theta}_j)$ of Eq. (4.25). In other words, the BSs that are capable of producing higher power to interference ratio with adjusting their beam direction, are given priority to join the corresponding cluster. Then the candidate BSs are considered one by one, and the optimization metric of Eq. (4.28) is calculated with and without each candidate BS. A candidate BS is added to the corresponding cluster only when its addition increases the system rate. It should be noted that K_{BS}^h, is affected by $\{\widehat{j}\}_k^h$ as stated in Eq. (4.16). Also for the calculation of the metric, the sum rate of each cluster, $\overline{R}^h$ $\forall h$, is calculated for all possible values of K_{UE}^h ($1 \leq K_{\mathrm{UE}}^h \leq K_{\mathrm{BS}}^h$) and among the calculated sum rates the maximum is selected. The overall clustering algorithm is summarized in Table 4.1.

4.4 Numerical results and discussion

A practical cellular network scenario consists of a hotspot in a limited area with sparse users in all other areas of the network. In such a case, a possible solution is to serve the sparse users by the macro BS (or a few resource blocks of some of the SC-BSs). Then, large optimal clusters of small cells are formed around hotspot zones to direct the resources of SC-BSs towards the hotspots. The details of the exact performance of this scenario is not discussed here. Instead, scenarios with isolated hotspot zones surrounded by vacant areas are examined in this section.

We start with a special scenario in which all users are gathered in one cell area to demonstrate the performance of the proposed scheme of section 4.3. In the conventional system, BSs' vertical tilt angles are fixed and equal to 15^{o}, and BSs communicate only to their local users. In fact, when all users are aggregated in a single hotspot cell, the conventional system only exploits the three BSs of the first tier of Fig. 4.3. Obviously, such a system wastes idle resources of vacant areas. Unlike the conventional scheme, the proposed clustering includes several tiers in a cooperative cluster and transfers their resources to the user congestion area by means of beam direction control.

For all numerical evaluations, the parameters are selected similar to 3GPP specifications for pico cells except that the omnidirectional antennas are replaced by sectorized antennas of macro BSs [21]. These parameters are listed in Table 4.2.

In all cases random user scheduling is assumed. Particularly, for a cooperative cluster around a hotspot, K_{UE} users are selected randomly for the multiuser communication. Except in subsection 4.4.5, in all other evaluations, K_{UE} is set to its maximum value: $K_{\mathrm{UE}} = K_{\mathrm{BS}}$. In general K_{UE} may vary between 1 and K_{BS}. In

Table 4.2: Parameters for numerical evaluations

Inter-site distance (d)	100 m
Number of Transmit antennas Number of Receive antennas	2 2
Antenna height	5 m
Normalization factor of the antenna gain (G_{o})	14 dBi
Antenna horizontal pattern, G_{h}	$-\min\left(c\ \left(\frac{\phi-\phi_{\mathrm{o}}}{\phi_{3\mathrm{dB}}}\right)^2, A_{\mathrm{h}}\right)$ ϕ_{o} is the horizontal beam direction of a BS; $c = 12$, $A_{\mathrm{h}} = 25$ dB, $\phi_{3\mathrm{dB}} = 70^{\mathrm{o}}$
Antenna vertical pattern, G_{v}	$-\min\left(c\ \left(\frac{\theta-\theta_{\mathrm{o}}}{\theta_{3\mathrm{dB}}}\right)^2, A_{\mathrm{v}}\right)$ θ_{o} is the vertical beam tilt angle of a BS; ($\theta_{\mathrm{o}} = 15^{\mathrm{o}}$ in 3GPP) $c = 12$, $A_{\mathrm{v}} = 20$ dB, $\theta_{3\mathrm{dB}} = 10^{\mathrm{o}}$
Distance-dependent path loss, L	$140.7 + 36.7\log_{10}(\mathit{distance}[\mathrm{km}])$
Shadowing standard deviation Inter-site correlation	8dB 0.5
Transmit power	Two cases: 24 and 30 dBm
Noise power	−100 dBm

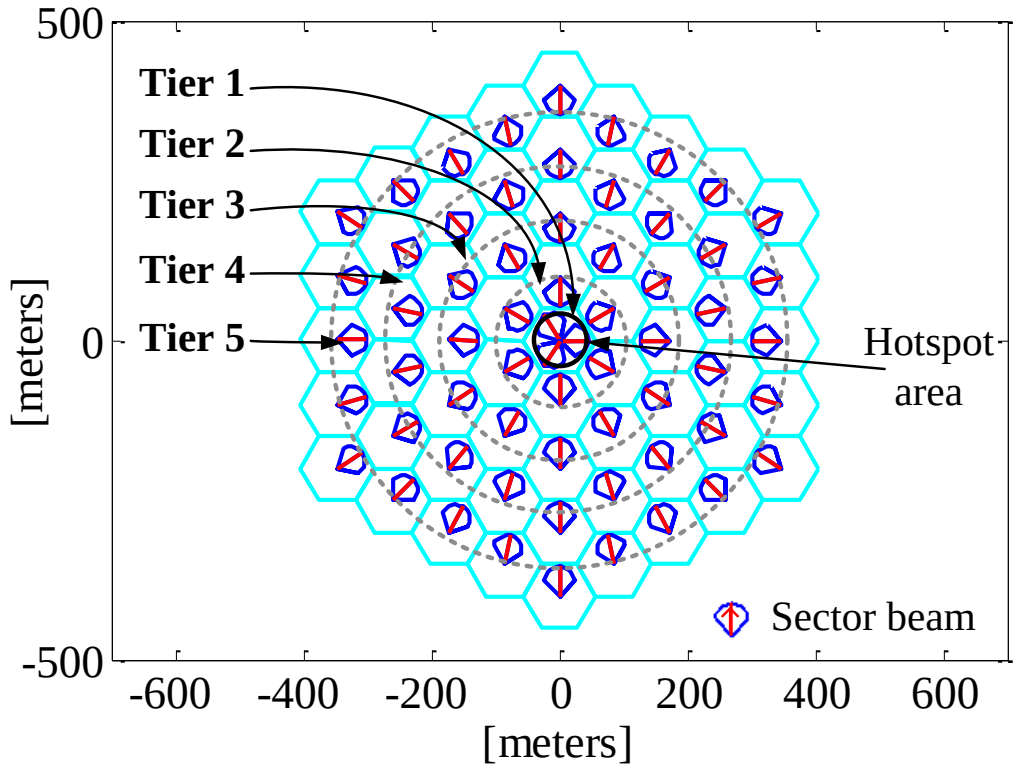

Figure 4.3: A cluster of 5 tiers around the dense area of the central cell.

subsection 4.4.5 is considered as an optimization parameter and for each case the number UEs for multiuser communication is selected in a way that the system rate is maximized.

4.4.1 Capacity trend versus cluster size

The scenario and the proposed cluster is shown in Fig. 4.3. In this scenario, there is no UE outside the cluster. Therefore, cluster BSs are allowed to tune their sector beam direction and tilt angle toward the hotspot with no restriction.

The system rate versus the number of tiers in the cluster is shown in Fig. 4.4.

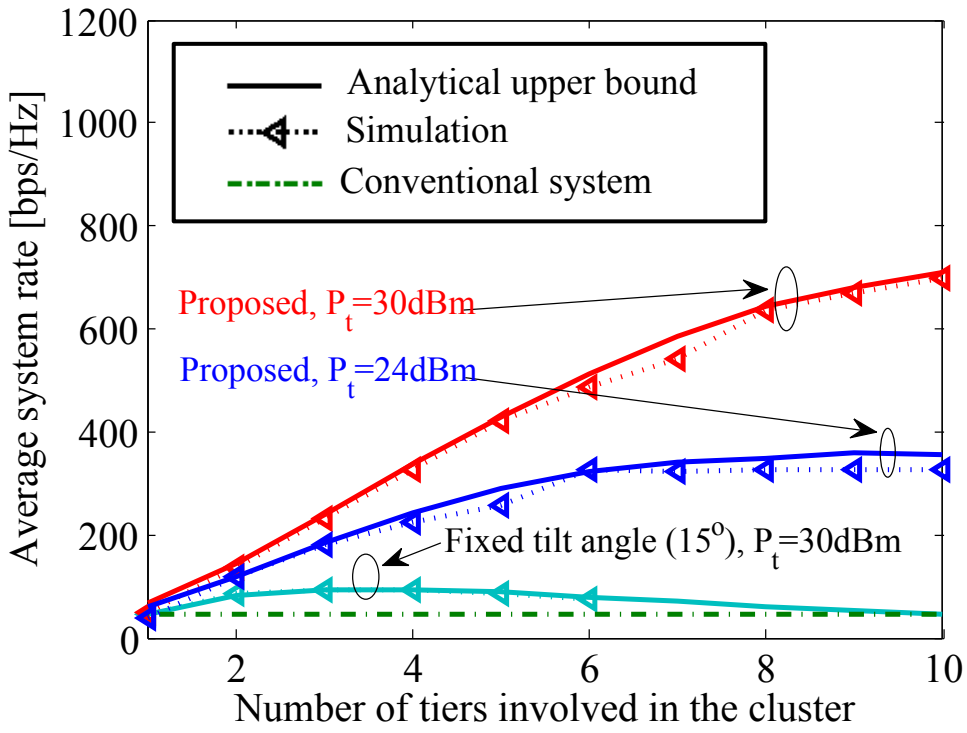

Figure 4.4: System rate vs. number of tiers in the clusters for single hotspot case as shown in Fig. 4.3.

In this figures, the analytical upper bound that is obtained from Eq. (4.13) is also shown. Calculation of this upper bound does not need any Monte Carlo iteration and therefore, for any cluster size it immediately reaches to an estimate. Quite the contrary, Monte Carlo simulation is a time consuming process and becomes slower as it analyzes larger clusters. It can be seen that the analytical upper bound reliably follows the trend of the system rate.

Figure 4.4 shows that the proposed scheme attains several times higher system rate than the conventional scheme. For the single hotspot scenario, the conventional scheme is equivalent to a 1-tier cluster in which only a few local BSs cooperatively perform intra-site CoMP. It is observed that even involving only two tiers

in the cooperative cluster can achieve more than four times higher system rate in our scenario. Besides, Fig. 4.4 shows the impact of antenna vertical tilt angle on the system rate. In fact, controlling BSs' antenna direction is the key factor that transfers network resources to the intended zone. Without such a dynamic coverage control, the gain in capacity would be very limited and vanish quickly when adding farther tiers to the cluster.

In Fig. 4.4, it is observed that with adding each tier to the cluster, at first the system rate increases linearly. However, the linear growth saturates at some tier. Especially for the lower transmit power of 24dBm, this saturation happens earlier. Naturally, the more is the distance between a BS and the hotspot zone, the less power is received from that BS in the hotspot. Therefore, it is expected that the system rate improvement eventually saturates at some tier.

4.4.2 Effect of shadowing

In all cases in Fig. 4.4 a log-normal shadowing is considered in the channel model. The log-normal shadowing parameters are selected according to 3GPP models as listed in Table 4.2. In this subsection, the effect of this shadowing on the system rate is studied. In Fig. 4.5, the system rate with and without shadowing are shown in the same graph. It is observed that although shadowing degrades the system performance, it does not change the system rate trend. This means that when a suitable model for shadowing and its parameters are not available, the case of no-shadowing can be examined as an upper bound which can show the trend of the performance.

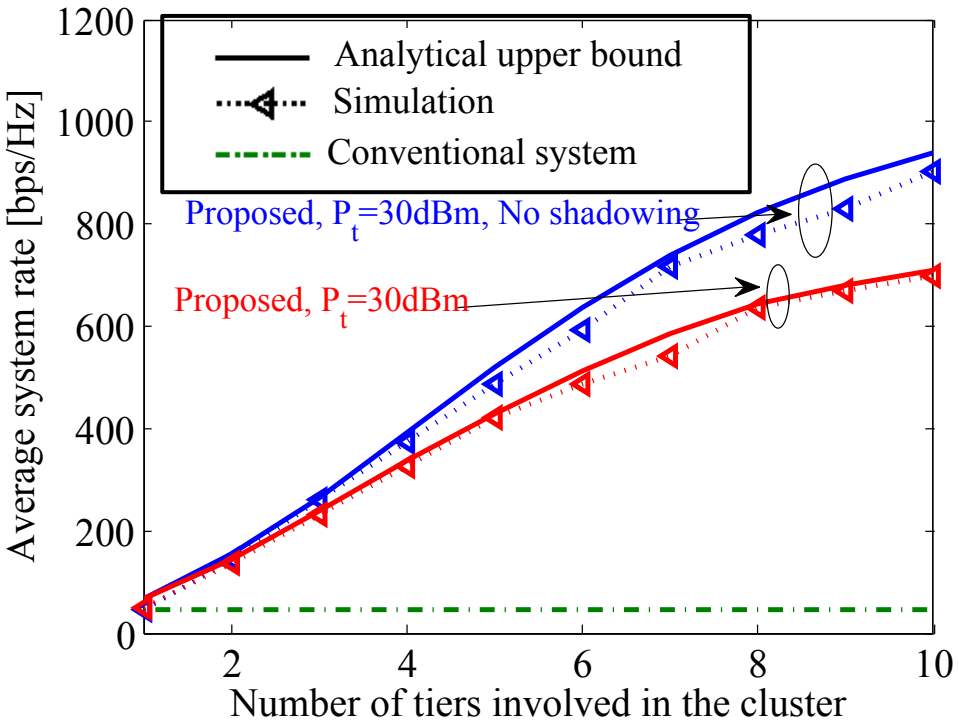

Figure 4.5: Shadowing degrades the system rate.

4.4.3 Effect of hotspot size

Our proposed clustering is designed based on the requirements of a limited hotspot zone. In order to examine the performance of this method in other cases, a certain large cluster is assumed and meanwhile the hotspot zone is expanded from a single point to the area which includes five tiers of small cells (Fig. 4.6). It can be seen that the cluster radius of kd is equivalent to $(k+1)$-tier cluster. Also, the hotspot radius of $0.5d$ means that the hotspot area is limited to a single cell which is equivalent to the scenario that is assumed for Figs. 4.4 and 4.5. In the extreme case, the hotspot area covers the whole area and the scenario becomes uniform user distribution case. In particular, when the radius of the hotspot approaches the radius of the large scale cluster, the scenario becomes equivalent to a network

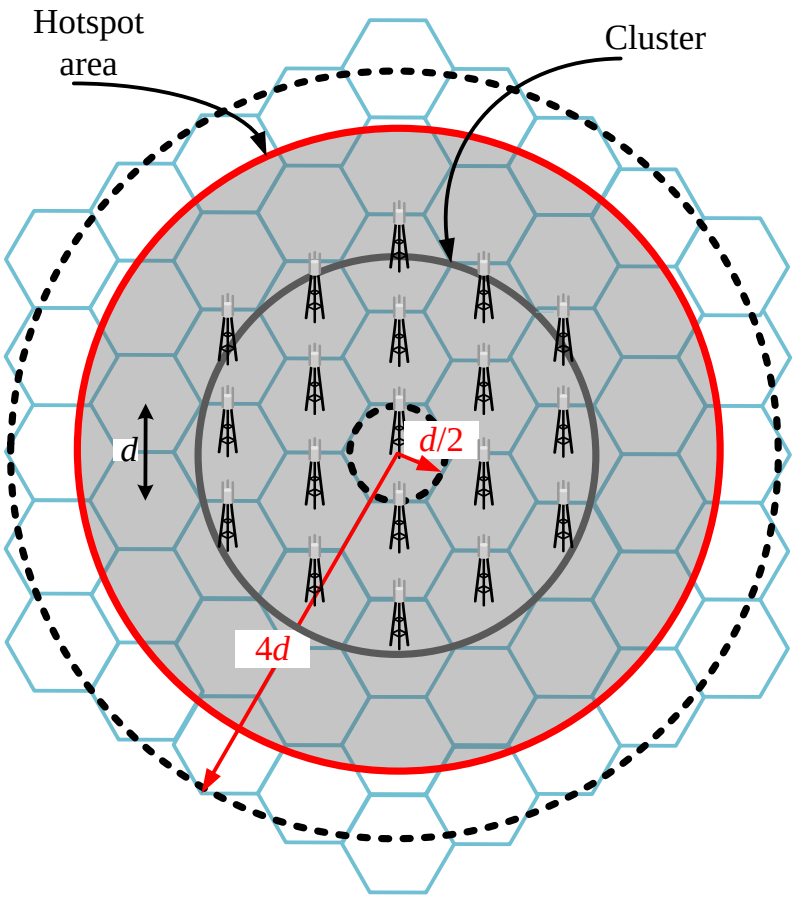

Figure 4.6: A certain cluster is considered and the radius of the hotspot is considered to vary from zero to 4d.

with uniform user distribution and full cooperation among all BSs within the user distribution area. The system rate for three different clusters is shown in Fig. 4.7. For comparison, the system rate of a single-cell (SC) transmission is also shown. In the SC transmission there is no coordination among BSs and each BS serves local UEs in its communication range. This is equivalent to the non-coordinated case with sectoral antennas that was studied in chapter 3 and Fig. 3.3.

In Fig. 4.7 in all cases the log-normal shadowing is not considered in the chan-

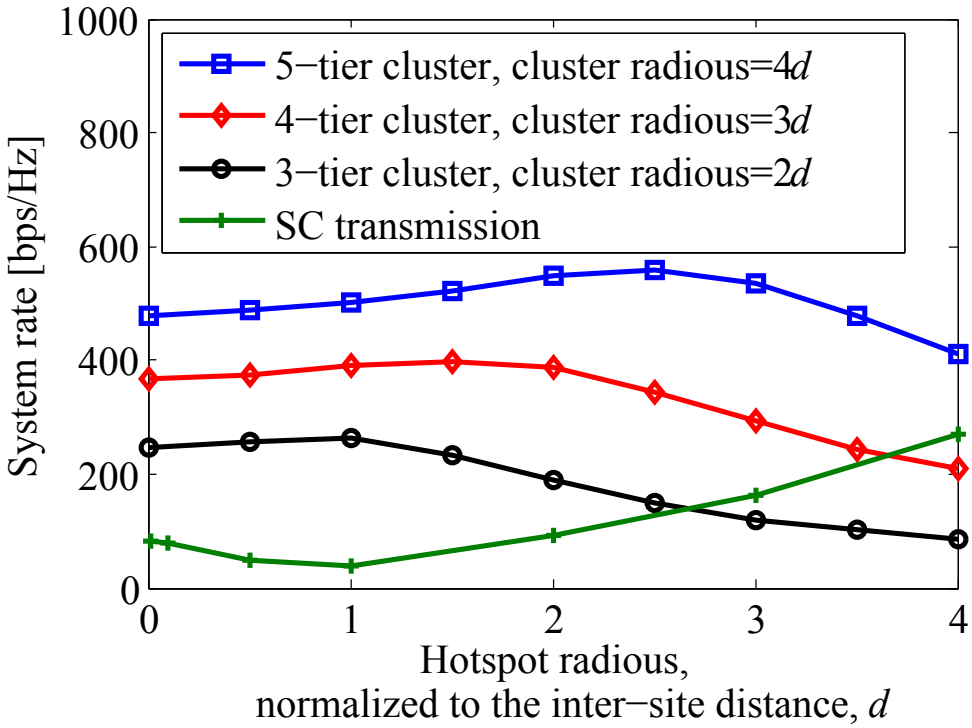

Figure 4.7: Effect of the hotspot radius on the system rate

nel modeling. The reason is that changing the size of the user distribution area alters the spatial correlation of the shadowing for different users. In the most extreme case, the hotspot radius is zero which means that all users are located in the same point and experience the same shadowing factor. The opposite extreme is the case of uniform user distribution in the the whole network area. In such a case, the shadowing factors for different users can be uncorrelated. Since the purpose is to study the effect of the hotspot expansion, in Fig. 4.7 the effect of shadowing is omitted.

In the SC transmission, when the radius of the hotspot is less than $0.5d$, only the BS in the central cell is transmitting and thus, no interference occurs. In this situation, the smaller is the hotspot, the higher is the received power and the system

rate. As the hotspot radius becomes larger than $0.5d$ some users are assigned to the BSs in the second tier. When these BSs start to transmit, the interference appears and degrades the whole system rate. In the SC transmission curve in Fig. 4.7 the point corresponding to the hotspot radius of $0.5d$ is the same as the conventional system case shown in Figs. 4.4 and 4.5.

It is expected that the large scale cooperation outperforms SC. However, if the large scale cooperative cluster is smaller than the area of user distribution, there exist BSs within the area that are not used in the cluster. In such a case, the SC scheme that uses all of the BSs, can utilize network resources more efficiently. In other words, the proposed large clusters do not utilize network resources efficiently unless the cluster is larger than the hotspot area. For example, in Fig. 4.7 at hotspot radius of $3d$, the system rate for the cluster radius of $2d$ drops below the system rate of SC.

Finally, it should be mentioned that when the cluster radius is larger than the hotspot radius, the optimal beam direction of the BSs follow almost the same trend as Fig. 4.3. On the other hand, when the hotspot radius exceeds the cluster radius, some disarray appears and some of the beam directions do not point to the center of the hotspot.

4.4.4 Two-hotspot scenario

In the scenario of single hotspot, only one cluster is formed in the network and since there is no active BS other than the cluster BSs, no interference exists. Therefore, such a scenario provides the upper bound of the performance of our proposed scheme. In this subsection, the proposed clustering method is applied to

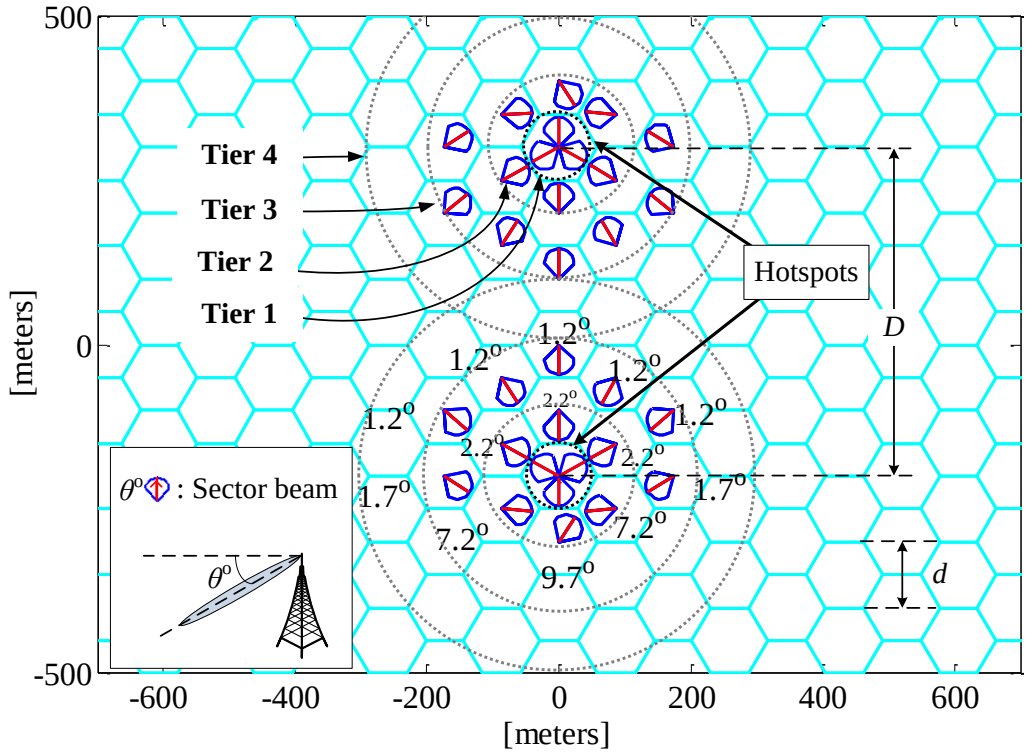

Figure 4.8: Two dense areas in the network and the proposed clusters with optimal beam directions around them; vertical tilt angles in degrees are also written beside corresponding BSs.

another scenario in which there are two similar hotspots in the distance of D from each other. This scenario provides a preliminary study of the effect of interference in practical networks. Apparently, the strength of the interference depends on D as well as the cluster size.

Figure 4.8 depicts the resultant cluster with optimized beam directions. It can be seen that the optimal clusters do not necessarily contain all BSs of a tier. In fact, BSs that produce high interference and reduce the overall system rate, may not join the clusters. Furthermore, this figure shows that in the presence of interference, the main lobe of the BS antenna does not necessarily point to the center of the hotspot zone. In this figure only the horizontal direction of the antennas' beams

can be seen graphically, yet the optimal vertical tilt angles are also written beside corresponding BSs. It can be seen that an unevenness happens in vertical tilt angles as well. Such inclinations in some of beam directions reduce the interference for the other hotspot.

In Fig. 4.9, the average system rate is examined versus the number of tiers in the cluster. For comparison, the average system rate in the single hotspot scenario is also shown. Since there is no interference in the scenario with only one hotspot, adding more tiers to the cluster increases the capacity dramatically. On the other hand for the scenario with two hotspots, increasing the tiers of the clusters improves the performance at first, but this will make neighboring clusters closer and at some point, the interference from neighboring clusters starts to degrade the performance. Therefore, although Fig. 4.9 confirms the significant superiority of the proposed clustering over the conventional system, the performance improvement saturates at some cluster-size. Also, as expected, the more is the distance between the hotspots, (D), the more capacity is obtained, which is because of less interfering power that reaches the users. Figure 4.9 shows that the proposed system attains three times higher system rate in the case of $D = 5d$. Furthermore, when $D = 10d$, almost six times higher capacity is obtained with 4-tier clusters.

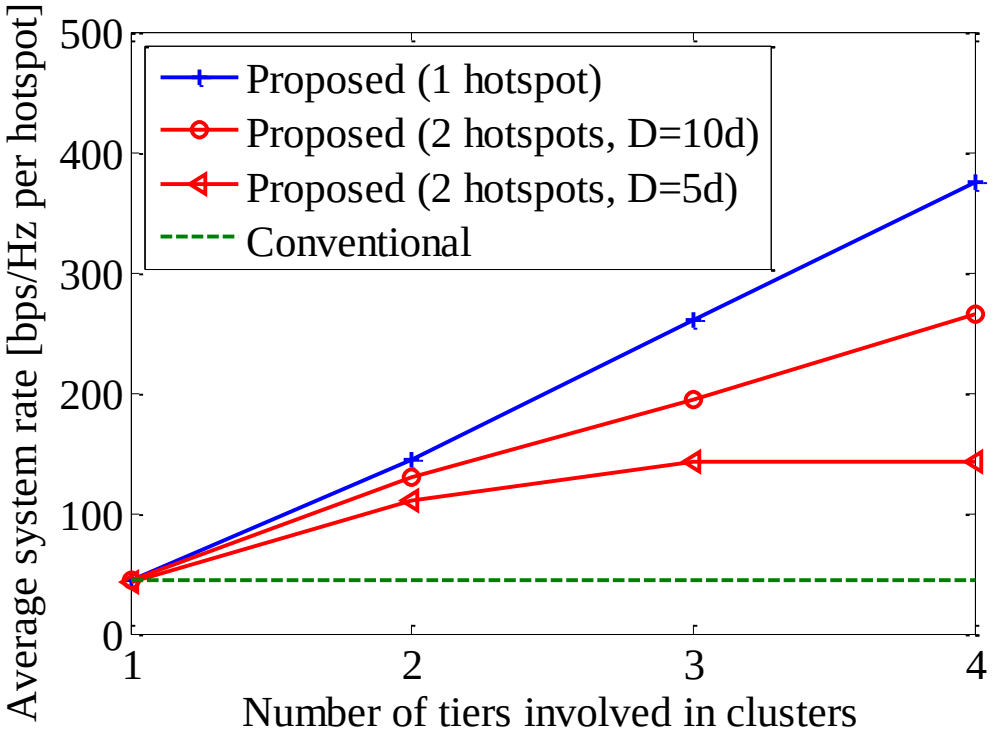

Figure 4.9: Average system rate of the proposed scheme and conventional scheme versus number of tiers in the clusters. The scenarios and corresponding parameters, D and d, are shown in Figs. 4.3 and 4.8. Here, P_t = 30 dBm for all cases.

4.4.5 Rank adaptation

So far, in all evaluations the number of UEs that are communicated simultaneously by the BSs in the cluster is set to the number of BSs: $K_{\text{UE}} = K_{\text{BS}}$. However, K_{UE} can vary between 1 and K_{BS} in general. Therefore, so far we have used the maximum possible K_{UE}. We call this case the full rank case because in this case the multiuser aggregated channel matrix in the cluster (**H** in Eq. (3.1)) is a square matrix and maximum possible parallel transmissions are utilized.

In this subsection we examine the effect of K_{UE} in the scenario of the single

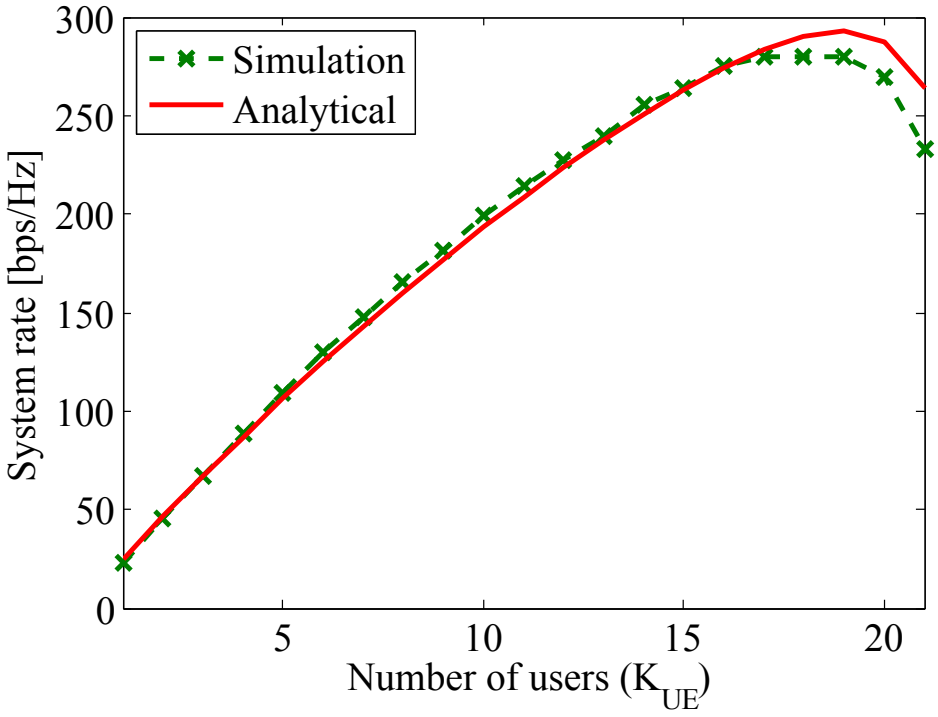

Figure 4.10: System rate vs. K_{UE} for a 3-tier cluster in the single hotspot scenario ($K_{BS} = 21$).

hotspot case in one small cell, i.e. Fig. 4.3. As an example, consider the case of the 3-tier cluster where $K_{BS} = 21$. The system rate versus K_{UE} is shown in Fig. 4.10. It is observed that picking the maximum K_{UE} does not necessarily produces maximum system rate.

The same study with different clusters show the same trend as Fig. 4.10. In fact, in each case an optimal K_{UE} that results in the maximum system rate can be obtained. In Fig. 4.11 the optimal K_{UE} is studied as a function of the cluster size. In this figure, K_{UE} is shown versus number of BSs in the cluster. This figure shows that K_{UE} changes almost linearly with K_{BS}. It also shows that in all cases $K_{UE} < K_{BS}$ except for the 1-tier cluster in which $K_{UE} = K_{BS} = 3$.

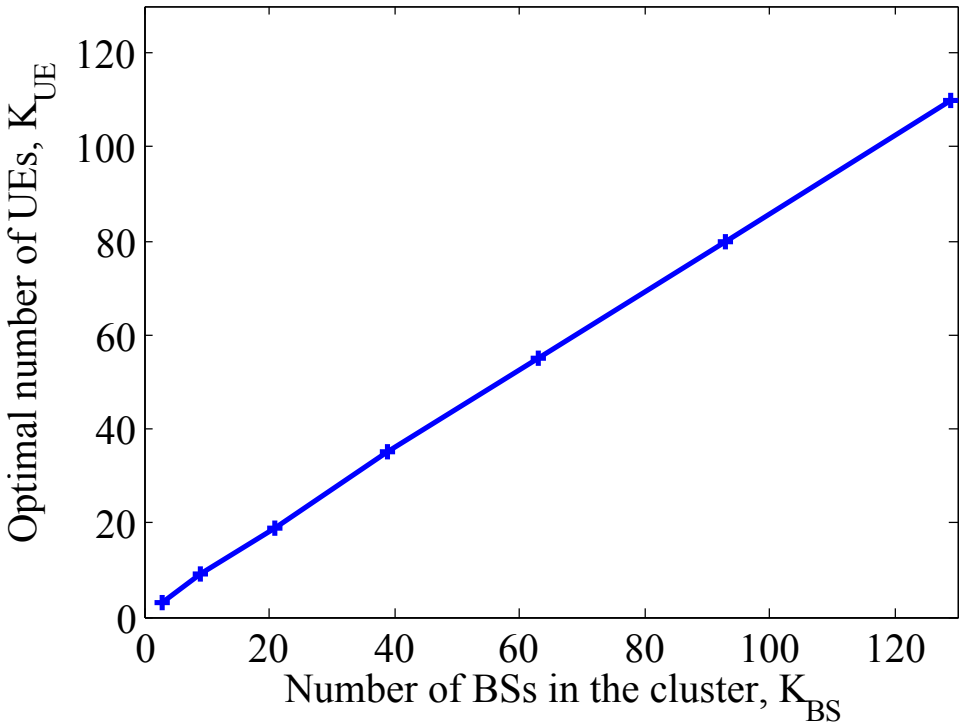

Figure 4.11: Optimal K_{UE} vs. number of BSs in the cluster, K_{BS}, in the single hotspot scenario.

Large scale clusters can use the optimal K_{UE} to get higher capacity than the full rank case. The selection of optimal K_{UE} is called rank adaptation here. In Fig. 4.12, the result of rank adaptation is compared to the full rank case. Rank adaptation results in a remarkable gain and prevents the performance saturation. Nonetheless, when the received power from a tier drops below the noise level it is still expected that the saturation happens eventually. However, prior to that tier, by selecting fewer UEs for multiuser transmission in the cluster each UE receives enough power and therefore the system rate continues to grow with the cluster size.

Also, Fig. 4.12 shows that the system rate is growing quadratically with the

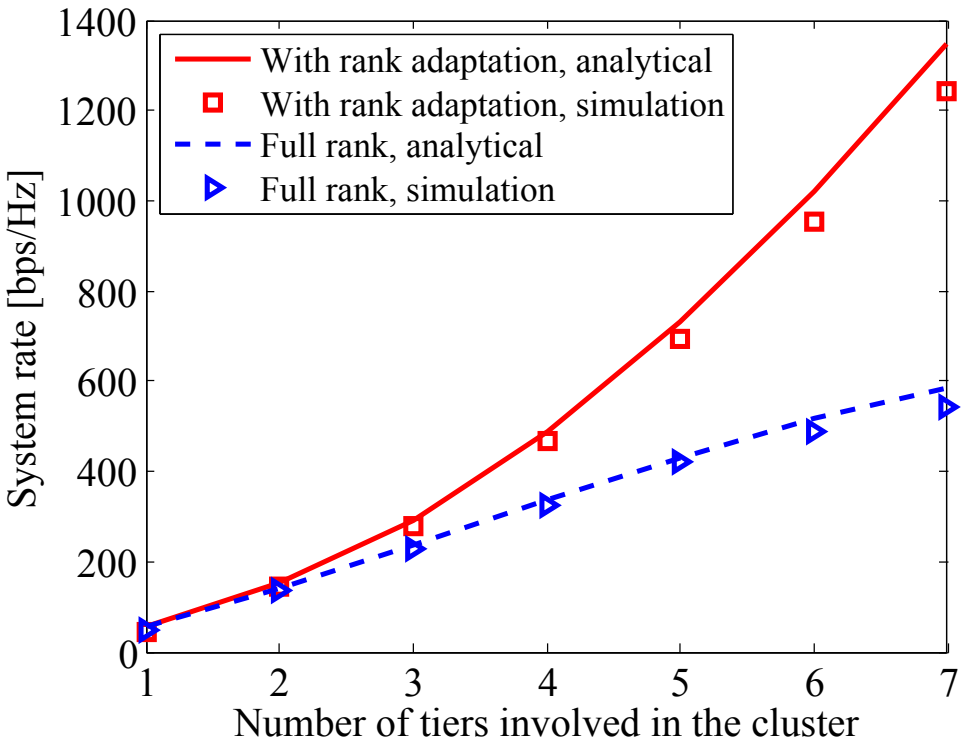

Figure 4.12: Effect of the rank adaptation for the single hotspot case.

number of tiers in the cluster. This means that the system rate is growing linearly with K_{BS} which is very favorable.

For the case when there are more than one hotspot in the network area, rank adaptation becomes even more important. In such a case, in the cluster formation phase, selecting optimal number of UEs may affect the decision of whether to add a BS to the cluster or not. To be more specific, addition of a BS to the cluster may increase the system rate with optimal rank, while with full rank the system rate is decreasing. Therefore, when a BS is examined to be added to the cluster, the system rate should be calculated for all possible values of K_{UE} ($1 \leq K_{\text{UE}} \leq K_{\text{BS}}$), and the maximum rate should be considered as the system rate or the decision criterion. Figure 4.13 shows the optimal clusters for the case of two hotspots when

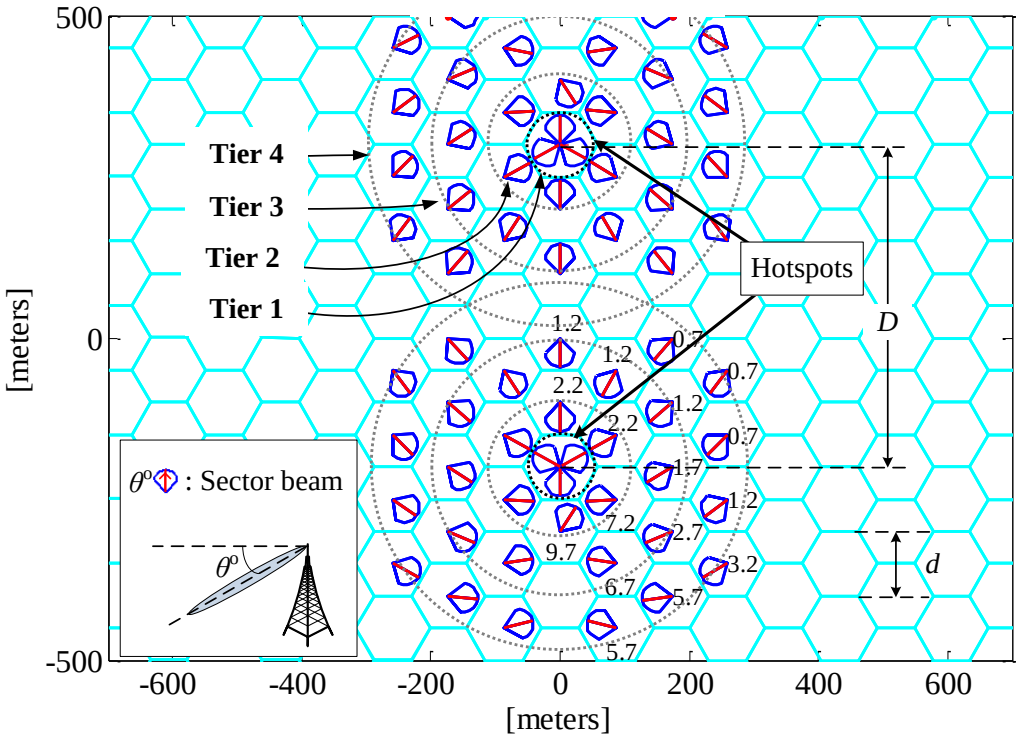

Figure 4.13: Optimal clusters with rank optimization for the two-hotspot scenario.

the rank optimization is considered in the cluster formation phase. The scenario is the same as the scenario of Fig. 4.8. Comparison of these two figures shows the difference of the optimal clusters with and without rank adaptation.

Figure 4.14 shows the optimal K_{UE}. This figure is obtained during cluster formation. At the time of examining each BS, the sum rate of the cluster is calculated to see if the addition of that BS increases the system rate or not. In this step, the optimal K_{UE} that maximizes the sum rate of the cluster is also obtained.

In Fig. 4.15, the system rate of optimal clusters with rank adaptation is shown for the two-hotspot scenario. Here, the distance between the hotspots is five times of the inter-site distance ($D = 5d$). In Fig. 4.15, the case of full rank is shown for

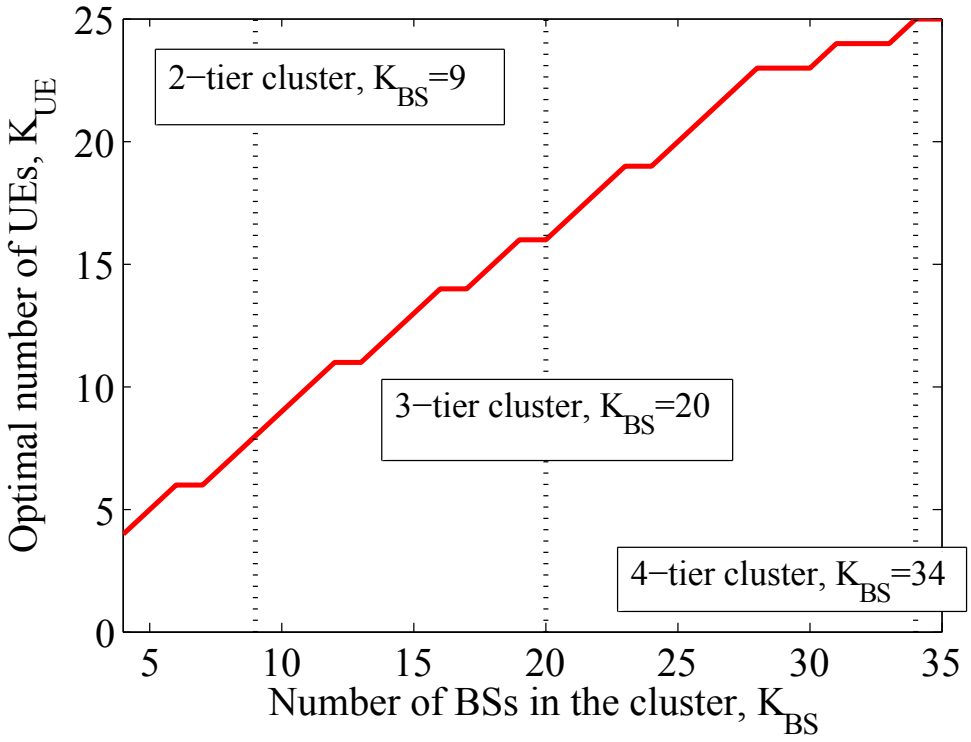

Figure 4.14: Optimal K_{UE} vs. number of BSs in the cluster, K_{BS}, for the two-hotspot scenario shown in Fig. 4.13.

comparison. Case of full rank has been analyzed in Fig. 4.9. Similar to the single hotspot scenario, rank adaptation provides a considerable gain and prevents the performance saturation.

4.5 Conclusion

This chapter introduced a scheme to dynamically direct idle network resources to the hotspot zones. For this purpose, a flexible clustering scheme along with dynamic cell structuring was used to form large clusters around user concentration zones. In order to utilize the network resources effectively, an optimization prob-

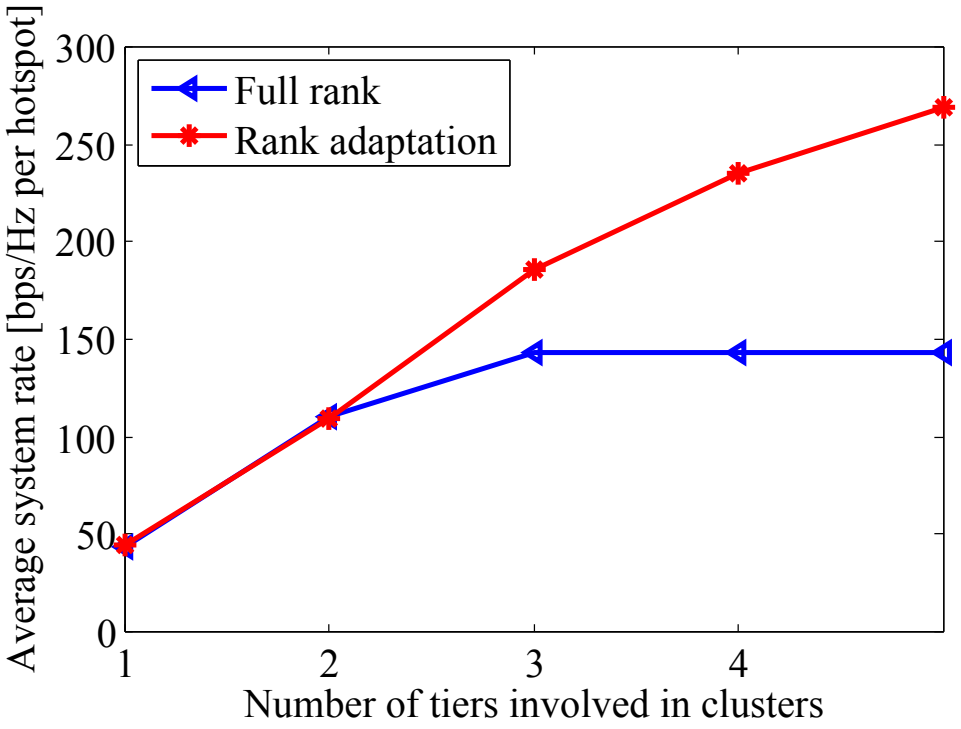

Figure 4.15: Effect of the rank adaptation for the two-hotspot scenario shown in Fig. 4.13.

lem was defined and solved to obtain optimal clusters. The BSs for each cluster and the antennas' beam angles of each BS were optimized subject to maximizing the average system rate of the network.

By means of large scale cooperation in each cluster, the system rate is multiplied several times mainly through multiplexing gain. In this chapter, the trend of capacity variations with cluster growth was studied and it was shown that even including a few tiers of BSs in the cluster, e.g. two or three tiers, combined with the optimized BS beam tilt angles, can result in an extraordinary gain in the system rate. Moreover, it was shown that including rank adaptation in the optimized clusters, increases the system rate even more.

This huge performance gain, suggests that it is worth further study, specially about the practical implementation aspects. Dynamic cell structuring and formation of optimal clusters require several measurement from the network. For instance, the received power from each SC-BS in the hotspot must be known. In the subsequent chapter the issue of signaling and collecting the required measurements is discussed in more details.

CHAPTER 5

PROTOCOL FOR DYNAMIC CLUSTER FORMATION

5.1 Introduction

The previous chapter, introduced an algorithm for cell structuring and formation of optimal large scale clusters around hotspot zones. Also the theoretical aspects of this algorithm was discussed and the boundaries of its performance was studied in different cases and versus different parameters. This chapter aims to complete that algorithm by providing a protocol for practical implementation. In order to implement the algorithm, a mechanism to collect the required measurements is necessary. Also, it is important to follow the measurement and feedback schemes that are accepted by the standardization bodies, especially 3GPP, as much as possible. In particular the C/U splitting concept affects the way that the required measurements can be collected. Therefore, here the concept of C/U splitting is described first. Also, since the proposed algorithm focuses on user-dense areas, a prior knowledge of UEs' positions can accelerate the cluster formation process. Based on the network conditions, e.g. outdoor or indoor environment, different positioning mechanisms of LTE and 3GPP can be employed. These mechanisms and their corresponding accuracies are also described before proceeding to discuss the protocol for the dynamic cluster formation.

The macro BS and SC-BSs play distinct roles in signaling and measurements. Therefore, in this chapter the type of a BS is explicitly mentioned.

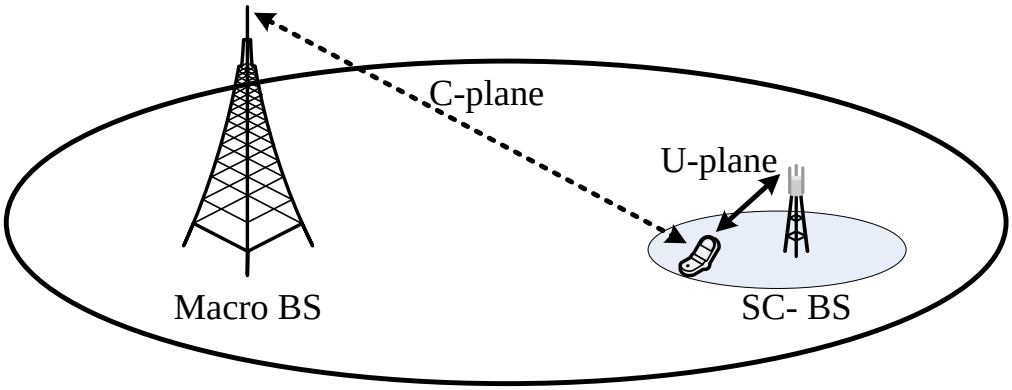

Figure 5.1: The concept of C/U splitting

5.1.1 The concept of C/U splitting

In LTE, the control plane (C-plane) is the protocol in radio resource control (RRC) layer that manages UE status and mobility. In this architecture, the control/ user-plane splitting (C/U splitting) means that only Master eNB (MeNB) has the RRC entity, and the RRC messages (such as RRC connection establishment and handover) can be transmitted only by the MeNB. On the other hand, the control signaling including positioning reference signal (PRS) and cell-specific reference signal (CRS) in MAC layer can be transmitted by both master and slave eNBs, MeNB and SeNB, independently.

In a HetNet consisting of a macro BS and several SC-BSs within the macro cell, the macro BS is qualified candidate of the MeNB to handles the C-plane. In this case thecontrol plane (C-plane) and user plane (U-plane) are splitted and only macro BS handle the control plane as demonstrated in Fig. 5.1 [27]. The advantage of this architecture is that the C-plane is maintained by the continuous and reliable coverage of the macro BS, while at the same time in the U-plane the UE can get

Table 5.1: Positioning methods in LTE and their accuracies

Method	3GPP Rel.	Category	Accuracy
A-GNSS	Rel. 9	UE-assisted, UE or LS-based	5-20 m (Outdoor)
E-CID	Rel. 9	UE or eNB-assisted, LS-based	cell size
OTDOA (DL)	Rel. 9	UE-assisted, LS-based	50-300 m
UTDOA (UL)	Rel. 11	eNB-assisted, LS-based	50-300 m
RF pattern matching	Rel. 11		

higher data rates by connecting to a local SC-BS.

5.1.2 Positioning in LTE

Several positioning methods are defined by 3GPP for LTE. These methods can be categorized based on two criteria: between BS and the UE, which one is the measurement entity, and secondly who is the position estimation entity. According to the measurement entity the method is either eNB-assisted or UE-assisted. On the other hand, according to the position estimation entity the method is called for example location server (LS)-based or UE-based.

Table 5.1 lists the different positioning methods of LTE [28]-[30]. A-GNSS

stands for autonomous and assisted global navigation satellite systems. In A-GNSS method the network provides some assisting information such as reference time and visible satellites list to the GPS-enabled UEs to improve their positioning performance. This method provides the highest accuracy among LTE positioning methods in outdoor environment, however, it is not useful in indoors or the area that the satellite signals may not reach due to tall buildings or other obstacles. In such environments, the use of other methods such as Enhanced Cell ID (E-CID), Observed Time Difference Of Arrival (OTDOA) or Uplink Time Difference-of-Arrival (UTDOA) is inevitable. Among these methods, E-CID is the easiest one. In E-CID the UE is localized to its serving BS and therefore the accuracy of the positioning is in the order of the cell size. In OTDOA the UE should detect position reference signals (PRS) of at least three BSs and according to the measured time differences in downlink the location of the UE is estimated. UTDOA is a newer technique that is introduced in Release 11 and measures the time differences in the uplink. The detail of the positioning methods is out of the scope of this research. In the analysis of in this chapter, selection of any method and its corresponding accuracy can be assumed.

5.2 Scenario and objectives

The ultimate goal of this chapter is to introduce a seamless clustering algorithm that dynamically adapts to the users distribution. A scenario with a macro cell with several SC-BSs is considered. It is assumed that the SC-BSs are randomly or arbitrarily placed in the macro cell area as shown in Fig. 5.2. A grid of uniform small hexagons is considered in the whole macro cell area. In general, some of the small hexagonal areas do not contain any SC-BS. The optimal clusters has to

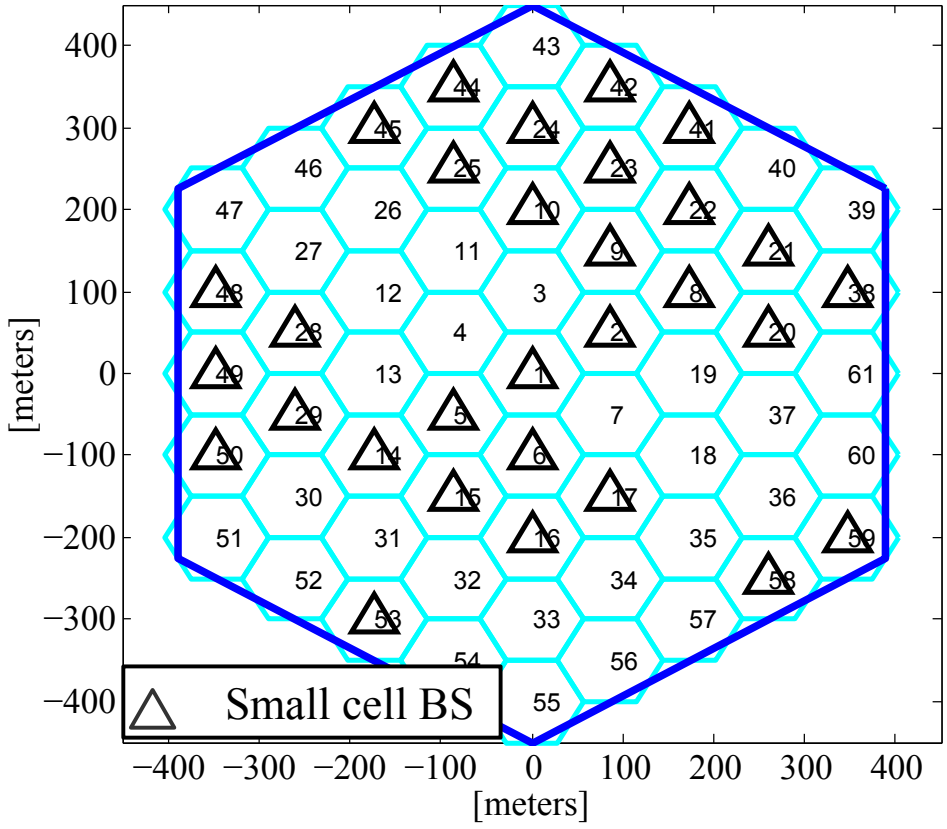

Figure 5.2: Scenario: There is a macro cell and several SC-BSs within the macro cell. The macro cell area is tiled by hexagonal small areas.

be formed around user-dense areas or the hotspots. Therefore, in the first step the objective is to detect any user-dense area within the macro cell.

The general overview of the protocol to detect the hotspots is shown in Fig. 5.3. This protocol benefits from positioning scheme as well as C/U splitting. First the macro BS obtains erroneous locations of all UEs in the macro cell area. On the other hands, the information of the exact locations of the SC-BSs is already available in the macro BS. Based on this information and the erroneous estimate of the positions of the UEs, the macro BS selects and commands some SC-BSs to trans-

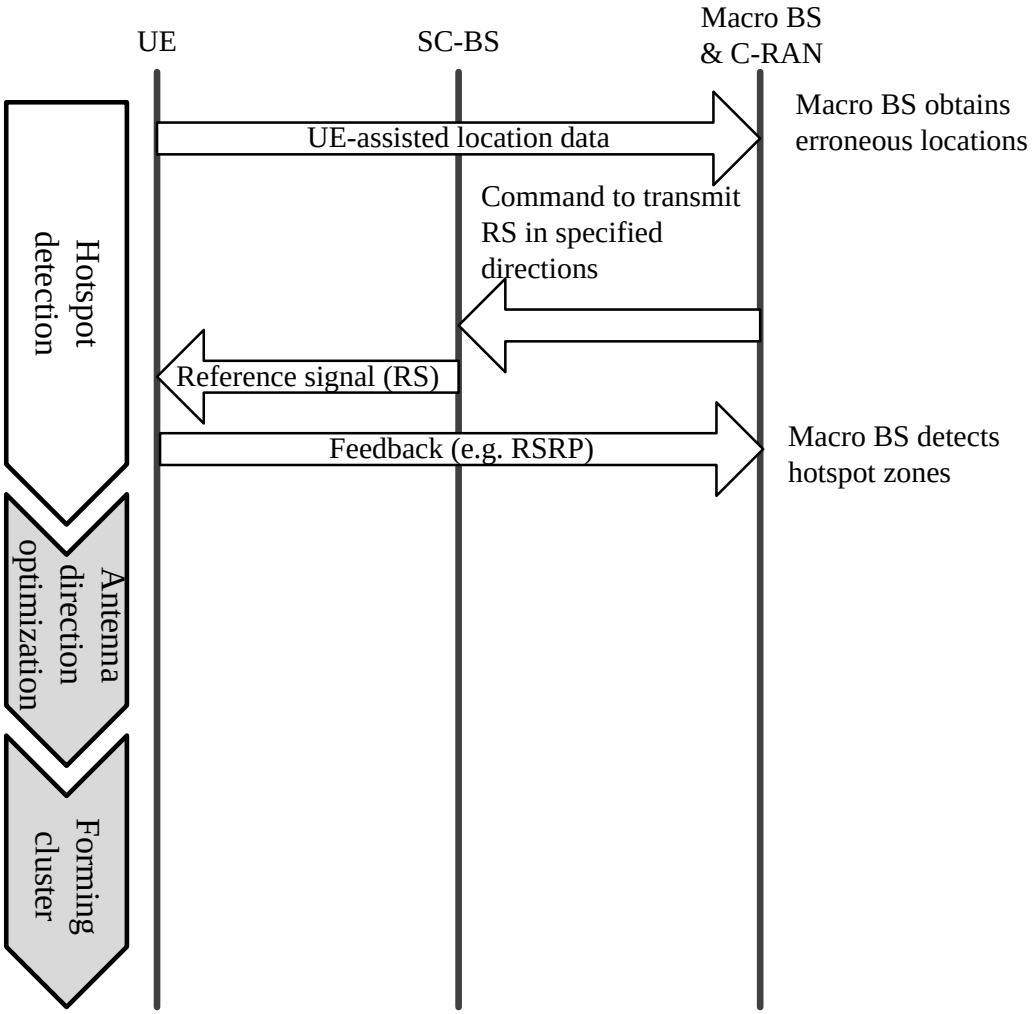

Figure 5.3: The protocol to detect the hotspot zones and its position with regard to the dynamic coverage control phase and cluster formation.

mit reference signals (RS). C/U splitting architecture is assumed and therefore the UEs send the feedback directly to the macro BS. Macro BS can detect the hotspot zones based on this feedback. Here some functions of the C-RAN are assumed in the macro BS implicitly.

As an example, assume that all users are concentrated in one small hexagonal area as shown in Fig. 5.4-(a). The UEs are connected to the macro BS, and therefore,

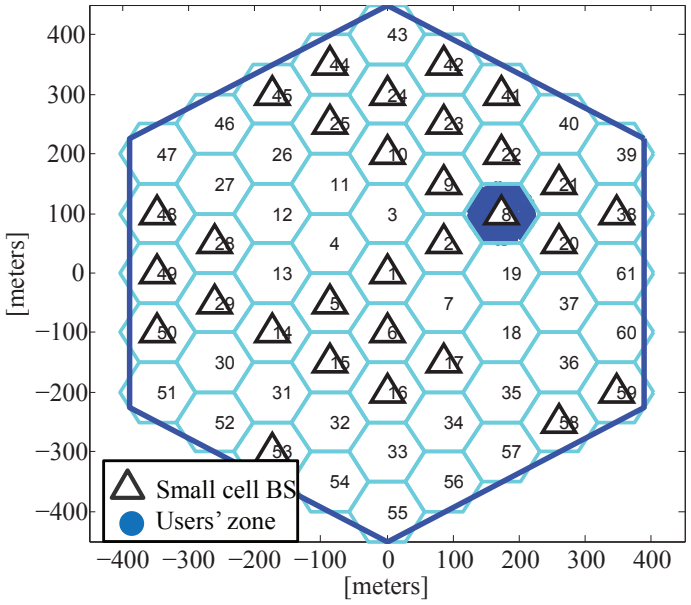

(a)

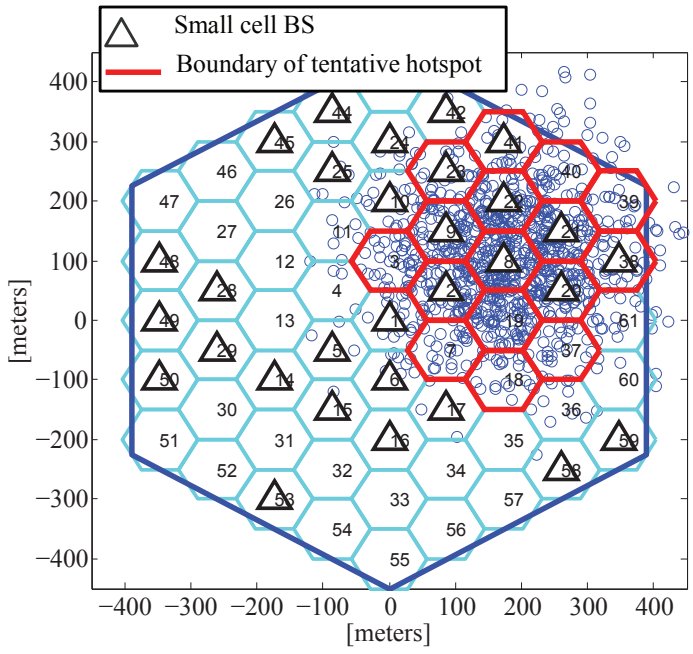

(b)

Figure 5.4: (a) A scenario with a single hotspot zone; (b) the macro BS recognizes tentative hotspot zones based on the estimated locations of UEs.

the macro BS has an approximate measurement of the locations of UEs:

$$\begin{aligned} \widetilde{\psi}_x\left(\mathrm{UE}_i\right) &= \psi_x\left(\mathrm{UE}_i\right) + \varepsilon_{x_i} \\ \widetilde{\psi}_y\left(\mathrm{UE}_i\right) &= \psi_y\left(\mathrm{UE}_i\right) + \varepsilon_{y_i} \end{aligned} \tag{5.1}$$

where $\psi_x(.)$ and $\psi_y(.)$ are the 2-dimensional Cartesian coordinates of a point.

The accuracy of the estimation depends on the environment and the estimation method as listed in Table 5.1. In this chapter in the numerical evaluations, it is assumed that the error terms, ε_{x_i} and ε_{y_i} follow a zero-mean Normal distribution with the standard deviation of 100 meters:

$$\varepsilon_{x_i}, \varepsilon_{y_i} \sim N\left(0, 100^2\right); \quad \forall i \tag{5.2}$$

Based on these erroneous estimates, the macro BS recognizes several tentative hotspot zones as shown in Fig. 5.4-(b). This will accomplish the first step of the hotspot protocol detection shown in Fig. 5.3. The next steps aim to detect the exact location of hotspots. The macro BS has to select some SC-BSs to transmit reference signals (RS). However, there are several issues that must be addressed to complete this protocol. Macro BS has to select the SC-BSs to transmit RS efficiently. Also, the type of the RS that is transmitted by the SC-BS should be specified. Furthermore, a suitable metric should be selected as the feedback of the UE to the macro BS. This metric must be a measurements that guides the macro BS to the correct detection of the hotspot zones.

The antenna pattern of the SC-BSs for control signal transmissions affects the structure of the protocol. If SC-BSs use directional antenna to transmit reference signals (RS), position of a UE related to a SC-BS can be determined upon receiving an RS that was transmitted by the SC-BS in a specific direction. Also, the optimal direction of the SC-BS for the data transmission may be determined concurrent

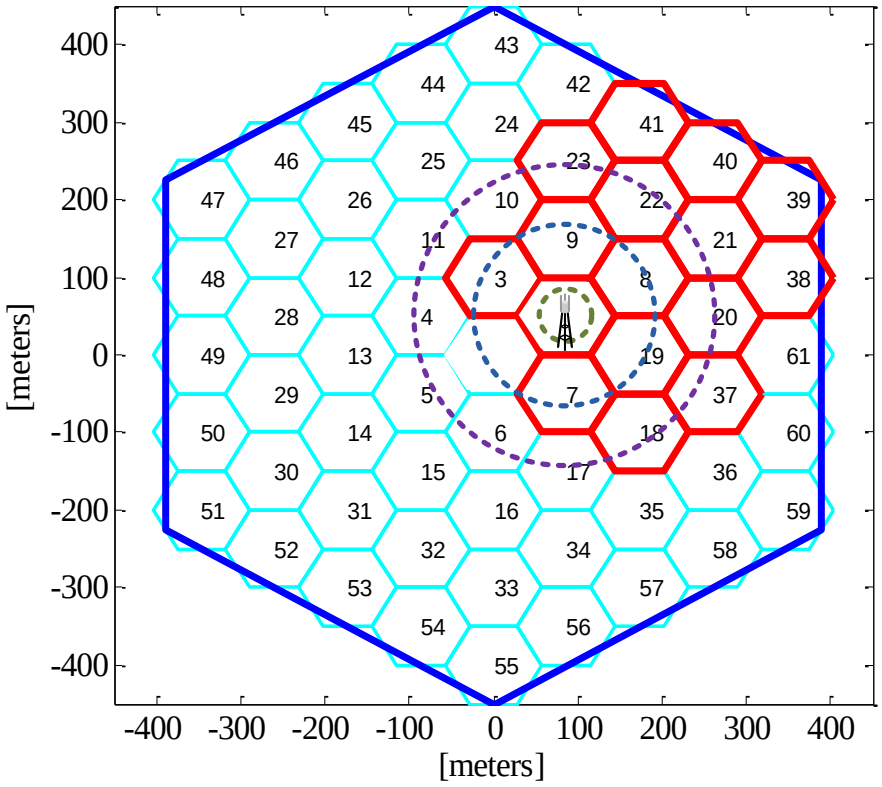

Figure 5.5: A SC-BS may use different antenna tilt angles to transmit control signals in order to target different tiers around it.

to hotspot detection step. However, a SC-BS might be required to transmit the RS several times to cover different directions in order to collect the feedback of probable nearby UEs. On the other hand, if RSs are transmitted through an omni-directional antennas, a UE should receive RSs from more than one SC-BS to obtain sufficient measurements that specify its location. Therefore, according to the antenna pattern of the SC-BSs for control signal transmissions, different strategies are followed to select and command some SC-BSs to transmit RSs.

Here omnidirectional transmission is assumed in horizontal plane. However,in the vertical plane the SC-BSs may need to transmit control signal with different tilt

angles to target different tiers around them (e.g. Fig. 5.5). The antenna specifications are picked from 3GPP specifications of a low power BS [31]. In this specifications, the horizontal pattern is omnidirectional and the vertical pattern, G_{v} is considered as follows:

$$G_{\mathrm{v}} = -\min\left(c\left(\frac{\theta-\theta_{\mathrm{o}}}{\theta_{3\mathrm{dB}}}\right)^2, A_{\mathrm{v}}\right), \tag{5.3}$$

where:

$$\begin{cases} c = 12, \\ A_{\mathrm{v}} = 20\mathrm{dB}. \end{cases}$$

Also, θ_{o} is the vertical beam tilt angle of the antenna and $\theta_{3\mathrm{dB}} = 40^{\mathrm{o}}$ is the 3dB beamwidth. The normalization factor of the antenna gain, G_{o}, is 5 dBi.

In the subsequent section, the scenario and assumptions that are defined here are considered and a mechanism is introduced to efficiently select several SC-BSs for RS transmissions.

5.3 Selection of SC-BSs for control signal transmissions

Based on the erroneous information of UEs' locations, several tentative hotspot zones are recognized by the macro BS. A tentative hotspot zone is a hexagonal small cell area that may contain a high density of users (Fig. 5.4). In the next step the exact locations of hotspots must be detected in order to direct network resources towards them. The macro BS is aware of the location of SC-BSs. It can use these knowledge beside the tentative information of hotspot areas to select and command several SC-BSs to transmit control signals so that each tentative hotspot area receives control signals of at least three SC-BSs. This will assure that the lo-

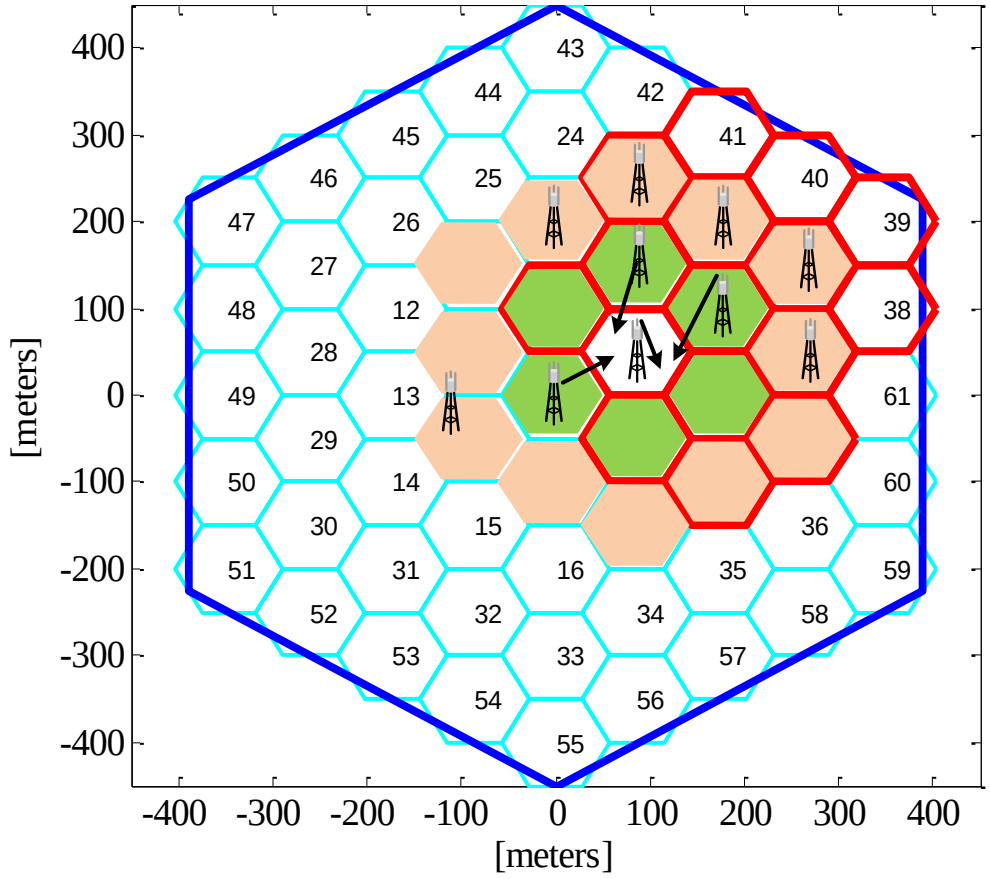

Figure 5.6: For a tentative hotspot, a list of SC-BSs in tiers around it are considered. Signal transmissions from these SC-BSs can cover some areas in the tentative hotspot control.

cations of probable UEs in each tentative hotspot area are estimated with higher accuracy and more accurate boundaries of hotspot zones is detected. The mechanism that is introduced in this section completes the hotspot detection protocol (Fig. 5.3).

A grid of uniform small hexagons tiles the whole macro cell area. The macro BS starts by listing all hexagonal areas that are recognized as tentative hotspot zones. Then for each of these tentative hotspots, the macro BS considers SC-BSs in tiers 1, 2, 3, etc. around that tentative hotspot as illustrated in Fig. 5.6. Afterwards,

the macro BS runs an algorithm to pick SC-BSs to transmit control signals in tiers around them.

The algorithm is described in Table 5.2. It starts by initializing the number of RSs that are going to cover any tentative hotspot area, N_{RS_k}, where k is the counter of tentative hotspots. In the beginning this number is zero for all areas. As the algorithm proceeds, when a SC-BS is selected to transmit RS to a tier around it, N_{RS_k} is incremented by one for the tentative hotspots that are covered by this transmission. The algorithm stops when $N_{RS_k} \geq 3, \forall k$. At first the SC-BSs that have got any tentative hotspot in their first tier are considered and one by one are added to the set of control signal transmitting SC-BSs. This set is called "Selected SC-BSs" set. After the addition of each SC-BS to the "Selected SC-BSs" set, the stop criterion is checked. If there are still tentative hotspots that cannot receive at least three RSs (i.e. $N_{RS_k} < 3, \exists k$) the selection of SC-BSs must continue.

When this algorithm is applied to the scenario shown in Fig. 5.4, the result is as shown in Fig. 5.7. Figure 5.7 shows the SC-BSs that are selected to transmit RSs towards different tiers around them. If the density of the SC-BSs in the area of interest is high, they will not be required to cover their farther tiers for control signal transmissions. Oppositely, if the density of SC-BSs is low, more SC-BSs may be commanded to cover farther tiers around them.

Once the set of SC-BSs is selected, they can start to transmit control signal to their required tiers. A SC-BS may need to tune the antenna tilt angle several times and repeat the transmission. Such a process will add to the cluster setup delay. Upon control signal transmission, each UE that receives the signal, reports the Reference Signal Received Power (RSRP) to the macro BS. The macro BS can use these data to estimate the locations of UEs and hotspots. One method which is

Table 5.2: The algorithm of SC-BS selection for control signal transmission

1. Initialization:
   1.1. For each tentative hotspot area initialize the counter of the control signals to 0: $N_{\mathrm{RS}_k} = 0$ $(\forall k)$;
   1.2. Set the tier counter to 1: $t = 1$.

2. Run the followings until $N_{\mathrm{RS}_k} \geq 3$ $(\forall k)$:
   2.1. Consider the set of SC-BSs that are in tier t of any tentative hotspot:
   $U = \left\{\text{SC-BS}_j \mid \text{SC-BS}_j \in \text{tier } t \text{ around } k^{\text{th}} \text{ tentative hotspot zone}, \quad \exists k\right\}$
   2.2. Sort the SC-BSs in set U according to the number of tentative hotspots that each SC-BS sees in its tier t. (A SC-BS that has more tentative hotspot zones in its tier t is given higher priority to join final "Selected SC-BSs" set, S.)
   2.3. Until $\exists k\ N_{\mathrm{RS}_k} \leq 3$, repeat this step for each $\text{SC-BS}_j \in U$:
      2.3.1. Add SC-BS_j to the "Selected SC-BSs" set, S,
      2.3.2. $N_{\mathrm{RS}_k} \leftarrow N_{\mathrm{RS}_k} + 1$,
         $\forall k$ that $\text{SC-BS}_j \in$ tier t around k^{th} tentative hotspot zone,
      2.3.3. Stop and exit the algorithm if $N_{\mathrm{RS}_k} \geq 3$ $(\forall k)$
   2.4. Set $t \leftarrow t + 1$, and return to step 2.

also used in this chapter is that the macro BS estimates the distance of the UE to at least three SC-BSs. This enables the macro BS to locate the UE with high accuracy. Our simulation shows that in the example shown in Fig. 5.4 at the end of this procedure the macro BS finds the exact location of the hotspot.

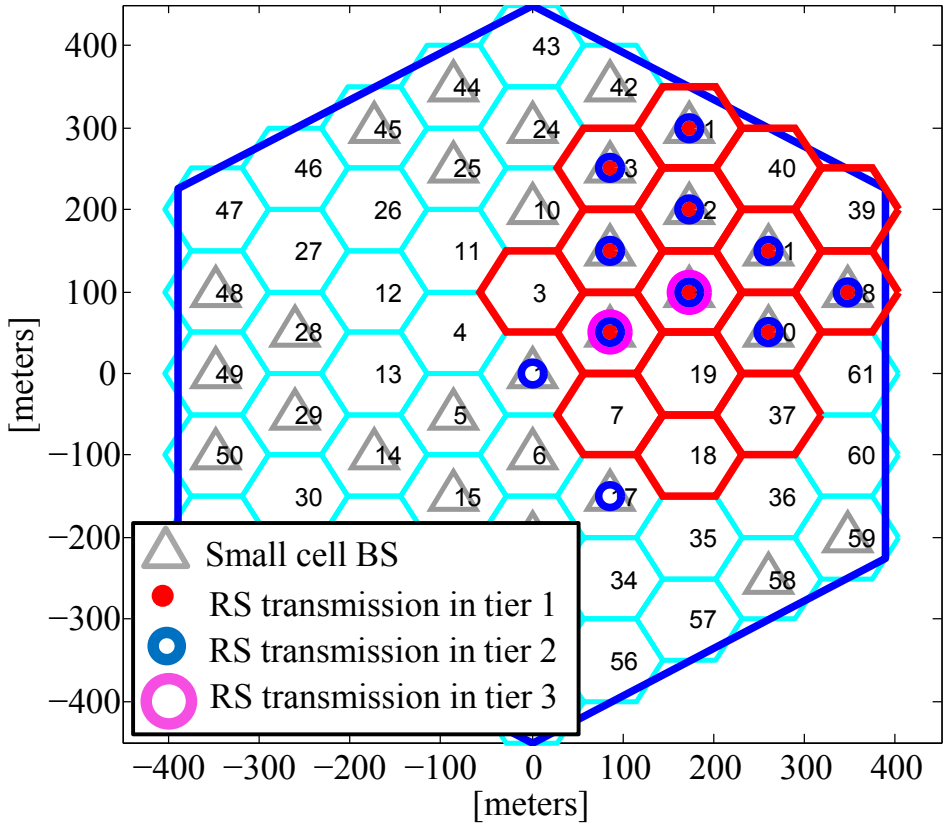

Figure 5.7: Several SC-BSs are selected to transmit reference signal (RS) to different tiers around them.

5.4 Optimal cluster formation

Now that the location of the hotspot zones has been pinpointed, the clustering algorithm of chapter 4 can be applied to direct idle network resources to hotspot areas. As described in section 4.3, formation of the optimal clusters has two phases. In the first phase, the antenna beam direction of each SC-BS is optimized and in the second phase, it is decided whether to add each SC-BS to the cluster or not.

Each SC-BS obtains its optimal antenna beam angles by maximizing the ratio of the signal power to the total interfering power that it produces (Eq. (4.26)). There-

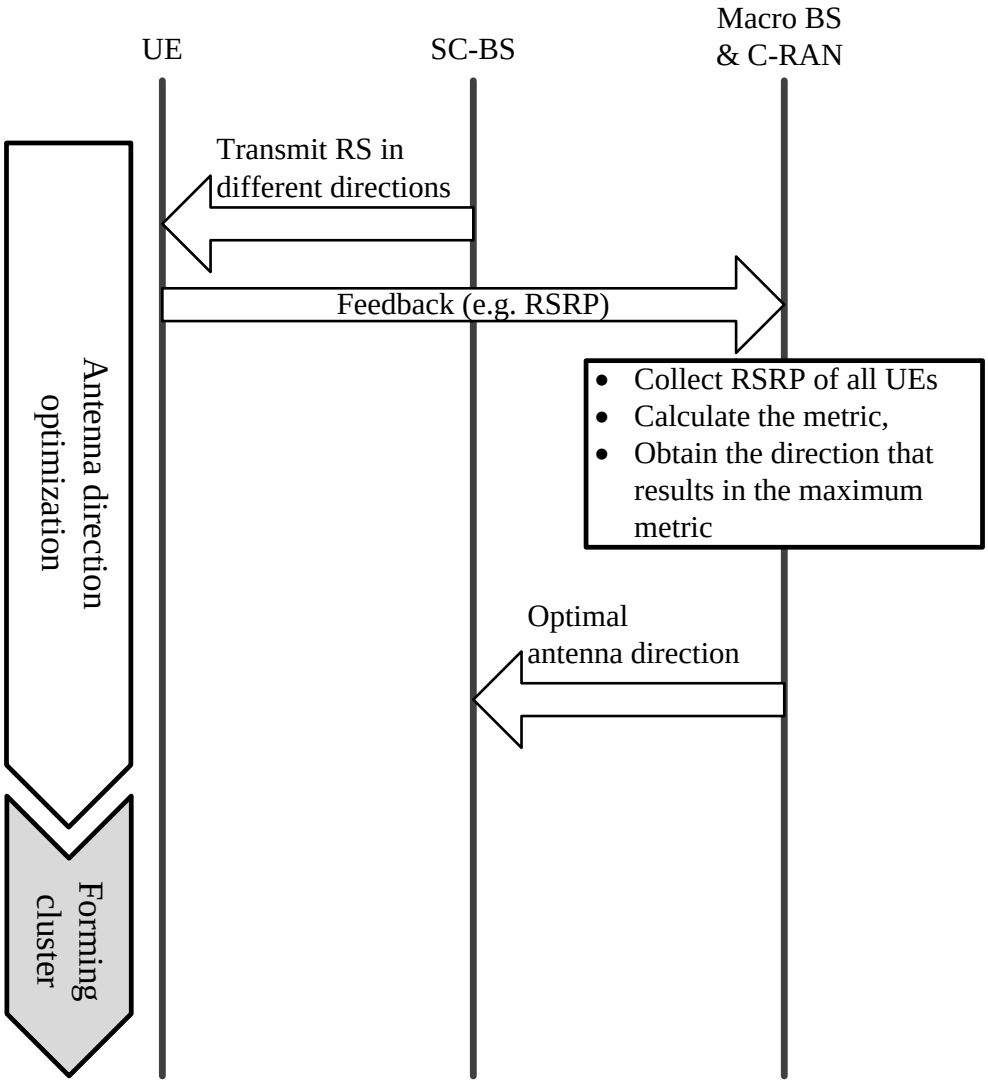

Figure 5.8: The protocol to obtain optimal antenna direction for a SC-BS.

fore, this phase requires the information of the powers that the UEs receive from each SC-BS when it is transmitting with different antenna beam directions. The simplest way is that the SC-BS sweeps all its possible transmission directions and the received powers by all the UEs are collected. These measurements can be used to estimate optimal antenna direction of that SC-BS. This protocol is summarized in Fig. 5.8.

This process slows down the initiation of the cluster. Each SC-BS needs to adjust its antenna to its all possible directions and transmit its RS several times. However, it is assumed that the hotspot locations and users' density does not change rapidly. In fact, the density of users may change a few times during a day. Thus, once the antenna directions are optimized the optimal clusters can be formed and the network can operate normally until the user distribution changes dramatically.

However, the antenna direction optimization can be accelerated if some prior information are available. For instance, if for every SC-BS the prior knowledge of the RF pattern in the whole area is available, the optimal antenna directions can be calculated without further measurements. In other words, for every SC-BS the calibrated power that is received from that SC-BS in all locations are collected in advance. Then at the time of clustering, these prior information are combined with the effect of the antenna pattern to estimate the signal to interference metric as defined in Eq. (4.25). Each SC-BS obtains the antenna beam direction that maximizes this metric. This will simplify the antenna direction optimization protocol as shown in Fig. 5.9.

As another alternative, the antenna directions may be adjusted according to an estimate of the received powers instead of measurements. If a channel model for the network area is available, it can be used to estimate the received powers based on the knowledge of the locations of BSs and UEs and the antenna patterns. Then the estimated powers are used to estimate the best antenna direction for each BS. Still, it might be necessary to fine tune the antenna beam direction by transmitting reference signals and measuring the received powers. In this case, a SC-BS tries beam angles around the estimated best angle value and transmits control signal. The feedbacks from UEs are then collected and the optimal beam direction in the tested range is found. In the next section the channel model and parameters of

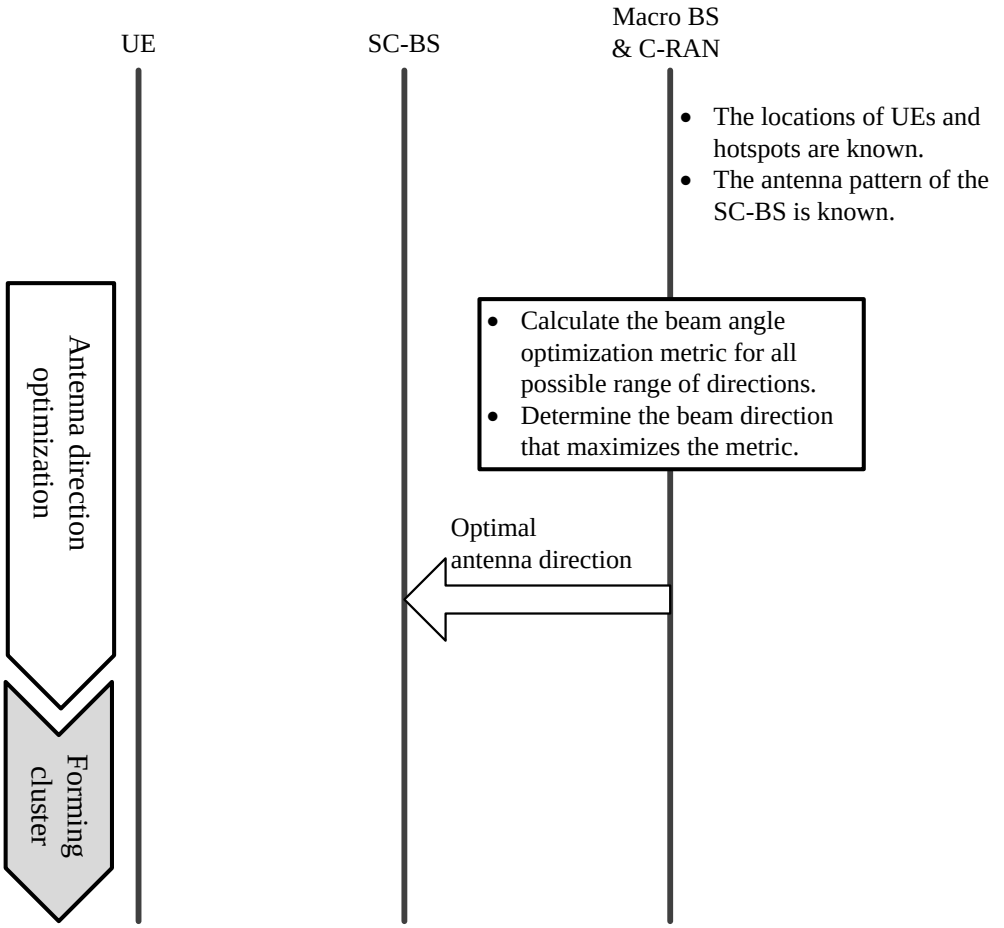

Figure 5.9: The protocol to obtain optimal antenna direction for a SC-BS in case when the prior knowledge of the calibrated RF pattern of the SC-BS in the whole area is available.

Table 4.2 are used to model the network and form optimal clusters.

After accomplishing the antenna direction optimization, the optimal clusters can be formed according to the algorithm of Table 4.1. This phase does not require additional measurements. In order to decide whether to add a SC-BS to the cluster or not the system rate with and without that SC-BS should be considered. Again in the estimation of the system rate, the information of the received powers from different BSs in hotspot areas are necessary. However, the same information that

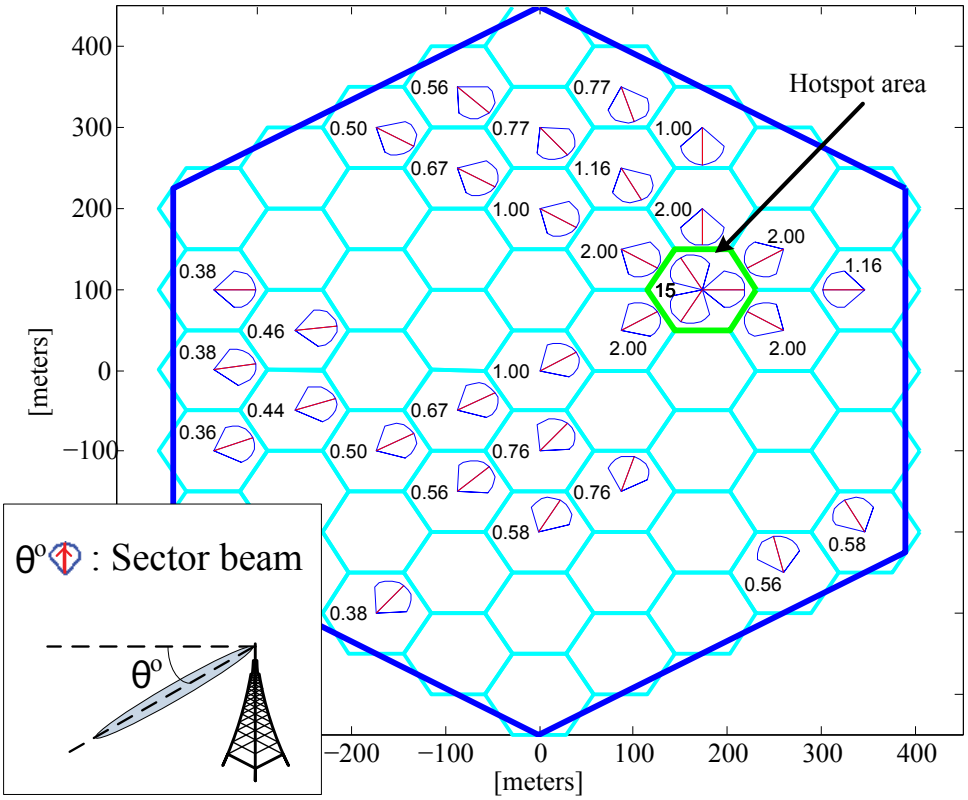

Figure 5.10: Optimal antenna beam directions: horizontal sector is shown in the figure and vertical tilt angle is written beside it.

were used to estimate the optimal antenna directions can be used again to estimate the system rate. In the end, it should be emphasized again that it is very beneficial to consider a mechanism to collect the calibrated received power measurements. Such a mechanism saves time and signaling requirements at the time of dynamic cell structuring and cluster formation.

5.5 Numerical results

In this section the clustering mechanism is evaluated for the network scenario shown in Fig. 5.4. As a result of the algorithm that was described in section 5.3 and Table 5.2, a few SC-BSs are selected to transmit reference signals as shown in Fig. 5.7. After collecting the feedback from UEs, the location of the hotspot area is detected. Assuming that the knowledge of the received powers from each BS is available through measurement, the optimal antenna beam direction is obtained as shown in Fig. 5.10. The beam angles in Fig. 5.10 has been obtained using the algorithm of Table 4.1. Here, no limitation on the possible beam angles is considered and it is assumed that the BSs can freely tune their antenna to any tilt angle.

According to the algorithm, the BSs need to be sorted and added one by one to the cluster. In Fig. 5.11 the order that the BSs are going to be considered for the cluster is shown. The BSs are added to the cluster one by one and the system rate at each stage is calculated. The trend of the system rate with cluster growth is shown in Fig. 5.12. Here, the rank adaptation is applied and for each case the optimal number of UEs is selected for multiuser communication as discussed in subsection 4.4.5.

5.6 Conclusion

In this chapter, the practical aspects of a heterogeneous cellular network with macro and small cells was considered and procedures required to implement the proposed cell structuring and large scale CoMP was discussed. Before formation of optimal clusters, several measurements and information of the location of the

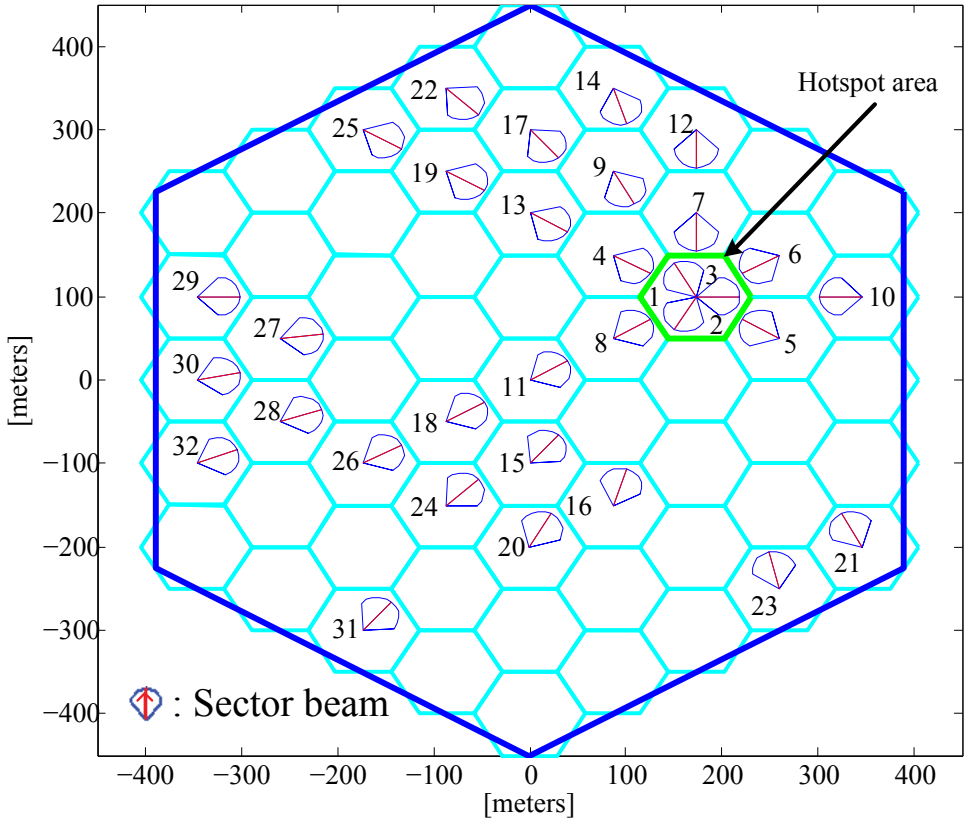

Figure 5.11: The order at which the BSs are going to be considered for the cluster.

hotspots as well as the received power from each BS is required. It is assumed that C/U splitting is implemented and the macro BS has got some erroneous preliminary estimation of the locations of UEs and hotspots via one of the available positioning schemes. Based on these information, the macro BS selects and command some SC-BSs to transmit control signals. The macro BS collects the feedback of the UEs and pinpoints the locations of UEs and hotspots with high accuracy. Afterwards, the clusters are formed around the hotspot zones to direct idle network resources to those area.

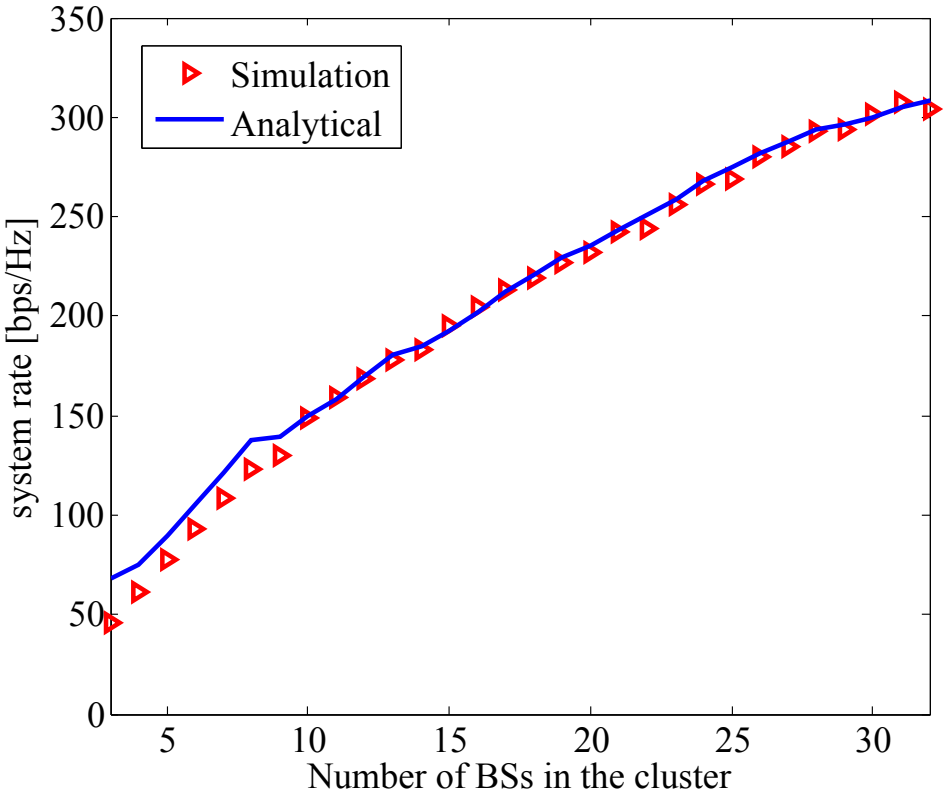

Figure 5.12: The result of cell structuring and large scale clustering for the scenario of Fig. 5.4.

In this chapter, the overview of a protocol for implementation of dynamic cell structuring and lare-scale CoMP was presented to show the feasibility of this scheme. However, more studies are required to obtain an efficient protocol. For instance, RS transmission with directional antenna should be examined and suitable algorithm for SC-BS selection in that case must be designed. The performance of such a scheme should be compared to the performance of the basic scheme that was provided in this chapter. In order to compare different protocols criteria of the efficiency of the protocols should be defined. One of these criteria could be the exact timing analysis of the protocols to determine the required time for whole the process of hotspot detection and cluster formation with some specified accu-

racy. The signaling load should also be considered. The exact signaling and the type of the RS, e.g. CRS, are still to be determined. The performance of the protocol should be examined in more realistic cases, such as the case of more than one hotspot and the case of a hotspot surrounded by sparse user areas. Finally, it should be mentioned that the mechanism that was introduced here for hotspot detection relies on detecting the high-population areas. A necessary extension to this scheme is to introduce a mechanism to include the traffic load of UEs instead of their population.

CHAPTER 6

CONCLUSION

6.1 Achievements of the thesis at a glance

In this thesis the capacity of wireless cellular networks was analyzed in different scenarios. Here a cellular network consists of a macro cell and several small cell base stations. For all cases a mathematical framework was developed to estimate the capacity without Monte Carlo iterations.

First the case of a random non-coordinated network was considered and analyzed. The network was modeled and the capacity was defined and formulated. Then, the statistics of the received signal to interference power ratio (SIR) was extracted and the cumulative distribution function (CDF) of SIR was analytically derived; and finally, the capacity was approximated.

Next, BS cooperation was added to the network. In general, BS cooperation can eliminate interference and improve the performance. However, this scheme is not sufficient for non-uniform user distributions in which congestion areas appear in the network.

The ultimate goal is to introduce a practical dynamic architecture/ scheme to utilize the network resources to the utmost extent and is capable of adapting to the data traffic requirements. The focus is especially on the cases of nonuniform user distributions where some limited congestion areas or hotspots exist. In this thesis, a HetNet scheme is developed step by step to direct the idle network resources of sparse areas towards hotspots. The final scheme relies on large CoMP clusters around hotspots along with dynamic cell structuring.

First of all, a mathematical framework was developed to analyze the system rate of a cooperative cluster around the hotspot. In brief, a cluster was modeled as a massive distributed MIMO system. Also, the spatial distribution of the antennas and different distances between antennas and the target user equipment (UE) were modeled.

Afterwards, the scheme for cell structuring and formation of optimal cooperative clusters was described. In this scheme, the coverage of BSs are transferred to hotspots by dynamically changing the antennas' beam angles, and then optimal large cooperative clusters are formed around hotspots. The mathematical framework to calculate the average system rate enables us to optimize and form clusters with no need to simulation iterations. An optimization problem is introduced and solved to form optimal clusters of SC-BSs within the whole macro cell area.

The effects of various parameters in different scenarios were also studied. Because of the huge multiplexing gain, the proposed scheme can achieve several times higher system rate. This scheme is especially beneficial in scenarios that contain distinct small congestion areas. When the hotspot area broadens the cluster should grow accordingly to keep the performance gain. Shadowing degrades the performance to some extent, but it does not affect the general trend of the capacity gain with cluster size. Also interference may limit the performance. Distinct clusters are formed around distinct hotspot zones. Beside the interference issue, distinct clusters limit each other's growth. The exact behavior and performance bounds of this scenario are still to be determined.

Among the studied parameters, rank adaptation greatly impacts the system rate. Here, rank adaptation means selection of optimal number of UEs to be communicated by a cooperative cluster simultaneously. The larger is the cluster, the

more impactive is the rank adaptation. Generally the number of UEs for a multiuser communication is limited by the number of BSs in the cluster. However, the study on the rank adaptation shows that picking maximum possible number of UEs does not necessarily lead to the maximum system rate. In the numerical results it was observed that the optimal number of UEs doubles the system rate compared to the full rank communication.

Finally, the last part of the thesis described the signaling method and protocols that facilitate the practical implementation of the cell structuring and clustering scheme. The objective of this part is to show a way to realize the huge gain of this scheme in cellular networks. Therefore, it is important to stick to the current standardization's framework as much as possible. The concept of C/U splitting, positioning methods and signaling were assumed the same as defined in 3GPP technical reports. Using these framework, the method to collect the required measurements to implement the proposed clustering scheme was discussed.

6.2 Open issues and future study

In this research a novel scheme was introduced to utilize network resources to the utmost extent. The huge theoretical gain was proved by various numerical analyses. The protocol for practical implementation of this scheme is yet to be completed. Here it was described that how the signaling and measurements should be used to implement the proposed scheme. However, the exact details of implementation steps are subjects of the more research. The time scale of the automatic organization of the network and dynamic cluster formation should be determined precisely. A mechanism to recognize the hotspot zones based on the traffic load

rather than the population of UEs should be developed. This might require some amendments to the current standardization protocols.

In this study, the focus was on the total sum rate or the system rate as the performance criterion. However, when the focus is on the system rate without considering fairness, some of the users may not receive sufficient quality of service. Therefore, fairness is another important metric that should be studied precisely in order to provide a reliable practical scheme.

Finally, it should be mentioned that in the capacity analysis perfect channel state information (CSI) was assumed. The method to obtain or estimate CSI is out of the scope of this study. However, for the practical implementation, it is important to analyze CSI feedback method and the effects of its limited accuracy on the system performance.

APPENDIX A

PDF OF THE EIGENVALUES OF A WISHART MATRIX

Consider a complex Gaussian matrix $\mathbf{H} \in \mathbb{C}^{q \times p}$, with $q \leq p$. Let $\mathbf{h}_j$ denote the j^{th} column of $\mathbf{H}$. If $\mathbf{h}_i$ and $\mathbf{h}_j$ are independent ($i \neq j$) and $\mathbf{\Sigma} = \mathrm{E}\{\mathbf{h}_j \mathbf{h}_j^{\mathrm{H}}\}\ \forall j$, the matrix $\mathbf{H}\mathbf{H}^{\mathrm{H}}$ is a Wishart matrix. Furthermore, when $\mathrm{E}\{h_{ij}\} = 0\ \forall i, j$ and $\mathbf{\Sigma} = \mathbf{I}$, the matrix $\mathbf{H}\mathbf{H}^{\mathrm{H}}$ becomes an uncorrelated central Wishart matrix. In this case the joint probability density function (PDF) of ordered eigen-values of $\mathbf{H}\mathbf{H}^{\mathrm{H}}$, $\lambda_1 \geq \lambda_2 \geq \cdots \geq \lambda_q$, is obtained as follows [24]:

$$f_{\underline{\lambda}}(\underline{\lambda}) = K \left|\mathbf{V}_1(\underline{\lambda})\right|^2 \prod_{l=1}^{q} \xi(\lambda_l) \tag{A.1}$$

where $\underline{\lambda} = \left[\lambda_1, \lambda_2, \cdots, \lambda_q\right]^T$. Also:

- K is the normalization factor:

  $K = \left[\prod_{i=1}^{q} (p-i)! \prod_{j=1}^{q} (q-j)!\right]^{-1}$;

- $\mathbf{V}_1(\underline{\lambda})$ denotes a Vandermonde matrix whose $(i, j)^{\text{th}}$ element is $(\lambda_j)^{i-1}$;

- And finally: $\xi(x) = x^{p-q} e^{-x}$.

In the case considered in chapters 4 and 5, $p = M_{\mathrm{T}} K_{\mathrm{BS}} - M_{\mathrm{R}} (K_{\mathrm{UE}} - 1)$ and $q = M_{\mathrm{R}}$.

APPENDIX B

PUBLICATIONS

B.1 Publications related to this thesis

B.1.1 Journal papers

- R. Rezagah, G. Khanh Tran, K. Sakaguchi, K. Araki, S. Konishi, "Large Scale Cooperation in Cellular Networks with Non-uniform User Distribution," accepted in IEICE transactions on Communications.
- R. E. Rezagah, A. Mohammadi, "Analyzing the Capacity of Wireless Ad Hoc Networks," Springer Telecommunication Systems Journal, vol. 55, Issue 1, pp. 159-167, Jan. 2014.
- R. E. Rezagah, A. Mohammadi, "Optimum Outage Threshold for Maximising the Capacity of Wireless Ad Hoc Networks," IET Communications, vol. 5, issue 6, pp. 811-818, April 2011.

B.1.2 Book chapter

- R. E. Rezagah, A. Mohammadi, "Chapter 05 - Capacity of Wireless Ad Hoc Networks" in the editorial book entitled "Dynamic Ad-Hoc Networks," published by IET Books in 2013.

B.1.3 Conference paper

- R. Rezagah, D. Matsuo, G. Khanh Tran, K. Sakaguchi, K. Araki, S. Konishi, "Large Scale Cooperation in Cellular Networks with Non-uniform User Distribution," IEEE Global Communications Conference 2013 Workshop - Emerging Technologies for LTE-Advanced and Beyond-4G, Globecom 2013.

B.1.4 Technical report

- R. Rezagah, D. Matsuo, G. Khanh Tran, K. Sakaguchi, K. Araki, S. Konishi, N. Miyazaki , "Large Scale Cooperation in Cellular Networks with Non-uniform User Distribution," IEICE Technical Report, Feb 27, 2013.

B.2 Others

- R. E. Rezagah, A. Mohammadi, "The Capacity Estimation of Wireless Ad Hoc Networks in Fading Channels," IET Communications journal, vol. 3, issue 2, pp. 293-302, 2009.
- R. E. Rezagah, A. Mohammadi, "Analyzing the Capacity of Wireless Ad Hoc Networks," in Proc. of 17th International Conference on Software Telecommunications and Computer Networks, SoftCom 2009.
- R. E. Rezagah, A. Mohammadi, "Analyzing the Capacity of Wireless Ad Hoc Networks with Rate Adaptation Capability," Accepted in International Conference on Ultra Modern Communications, ICUMT 2009.
- R. E. Rezagah, A. Mohammadi , "Characterization of the Scalability of Wireless Ad Hoc Networks under Channel Constraints," in Proc. of Innovations

in Information Technology, IIT 2006.

- R. EbrahimRezagah, A. Mohammadi, "The Capacity of Wireless Ad Hoc Networks Using Statistical Techniques," in Proc. of IEEE International Conference on Communications, ICC 2006.

BIBLIOGRAPHY

[1] CISCO Whitepaper, CISCO Visual Networking Index: Global Mobile Data Traffic Forecast Update, 2013-2018," Feb 2014.

[2] E. Hossain, D. I. Kim, V. K. Bhargava, "Cooperative Cellular Wireless Networks, Cambridge University press," April 2011.

[3] M.K. Karakayali, G.J. Foschini, and R.A.Valenzuela, "Network coordination for spectrally efficient communications in cellular systems," IEEE Wireless Commun. Mag., vol.13, no.4, pp.56-61, Aug. 2006.

[4] R. Irmer, H. Droste, P. Marsch, M. Grieger, G. Fettweis, S. Brueck, H.-P. Mayer, L. Thiele and V. Jungnickel, "Coordinated multipoint: concepts, performance, and field trial results," IEEE Commun. Mag., vol.49, no.2, pp.102-111, Feb. 2011.

[5] N. Kusashima, I.D. Garcia, K. Sakaguchi, K. Araki, S. Kaneko, Y. Kishi, "Dynamic fractional base station cooperation using shared distributed remote radio units for advanced cellular networks," IEICE Trans. Commun., vol. E94-B, no.12, pp. 3259-3271, Dec. 2011.

[6] 3GPP TR 36.819, "Coordinated multi-point operation for LTE physical layer aspects," 2011, available online: http://www.3gpp.org/ftp/ Specs/html-info/36819.htm

[7] P. Marsch, G. P. Fettweis, "Coordinated Multi-Point in Mobile Communications From Theory to Practice," Cambridge University Press, August 2011.

[8] T. Biermanna, L. Scaliaa, C. Choia, H. Karlb, W. Kellerera, "CoMP clustering and backhaul limitations in cooperative cellular mobile access networks," Pervasive and Mobile Computing, vol. 8, Issue 5, pp. 662-681, October 2012.

[9] W. Xiaoyun, H. Yuhong, C. Chunfeng, C. Kuilin, C. Mo, "C-RAN: evolution toward green radio access network," China mobile research institute, Beijing 100053, P.R. China, available online: http://labs.chinamobile.com/cran/wp-content/uploads/C-RAN Evolution toward Green Radio Access Network_Wang Xiaoyun.pdf

[10] J. Hoydis, M. Debbah, "David versus Goliath: Small Cells versus Massive MIMO," Available online: www-syscom.univ-mlv.fr/ najim/gdr-ecoradio/debbah.pdf

[11] E. Bjornson, M. Kountouris, M. Debbah, "Massive MIMO and Small Cells: Improving Energy Efciency by Optimal Soft-Cell Coordination," International Conference on Telecommunications (ICT 2013), Casablanca, Morocco, May 2013.

[12] K. Hosseini, J. Hoydis, S. T. Brink, M. Debbah, "Massive MIMO and small cells: How to densify heterogeneous networks," IEEE International Conference on Communications (ICC 2013), 5442-5447, Budapest, Hungary, June 2013.

[13] 3GPP TR 36.932 V12.1.0, "Scenarios and requirements for small cell enhancements for E-UTRA and E-UTRAN," Mar. 2013.

[14] 3GPP TR 36.872 V12.1.0, "Small cell enhancements for E-UTRA and E-UTRAN - Physical layer aspects," Dec. 2013.

[15] 3GPP TR 36.842 V12.0.0, "Study on Small Cell enhancements for E-UTRA and E-UTRAN; Higher layer aspects," Dec. 2013.

[16] J. Hoydis, M. Kobayashi, M. Debbah, "On the optimal number of cooperative base stations in network MIMO," submitted to IEEE Symposium on Information Theory 2010. Preprint available at http://arxiv.org/abs/0912.4595

[17] A. Lozano, R. W. Heath Jr., J. G. Andrews, "Fundamental limits of cooperation," Mar 2012, available at http://arxiv.org/abs/1204.0011

[18] J.-M. Moon, D.-H. Cho, "Efficient cell-clustering algorithm for inter-cluster interference mitigation in network MIMO systems," IEEE Communications Letters, vol. 15, no. 3, pp. 326-328, Mar. 2011.

[19] E. Pollakis, R. L. G. Cavalcante, S. Stanczak, "Base station selection for energy efficient network operation with the majorization-minimization algorithm," Proc. of IEEE 13th International Workshop on Signal Processing Advances in Wireless Communications (SPAWC), Jun. 2012.

[20] A. Muller, J. Hoydis, R. Couillet, M. Debbah, "Optimal 3D cell planning: a random matrix approach," Proc. of IEEE Global Communications Conference (GLOBECOM12), California, USA, 2012.

[21] 3GPP TR 36.814, "Evolved Universal Terrestrial Radio Access (E-UTRA); Further advancements for E-UTRA physical layer aspects" 2011, available online: http://www.3gpp.org/ftp/Specs/html-info/36814.htm

[22] D. Sugimura, M. Arai, K. Sakaguchi, K. Araki, T. Sotoyama, "A study on beam tilt angle of base station antennas for base station cooperation systems," Proc. of IEEE International Symposium on Personal Indoor and Mobile Radio Communications (PIMRC 2011), Toronto, Canada, Sept. 2011.

[23] M. Arai, K. Sakaguchi, K. Araki, T. Sotoyama, "Theoretical analysis of base station cooperation MIMO channel by using eigenvalue theory of Wishart matrix," IEEE APS/URSI, Jul. 2010.

[24] A. Zanella, M. Chiani, M.Z. Win, "On the Marginal Distribution of the Eigenvalues of Wishart Matrices," IEEE Transactions on Communications, vol. 57, no. 4, pp. 1050-1060, April 2009.

[25] T. Cover, J. Thomas, "Elements of information theory," John Wiley & Sons, Inc., 1991.

[26] M. Sadek, A. Tarighat, and A. H. Sayed, "A Leakage-Based Precoding Scheme for Downlink Multi-User MIMO Channels," IEEE Trans. Wireless Commun., vol. 6, no. 5, pp. 1711-1721, May 2007.

[27] H. Ishii, Y. Kishiyama, H. Takahashi, "A novel architecture for LTE-B: C-plane/U-plane split and Phantom Cell concept," Proc. of IEEE Global Communications Conference (GLOBECOM12): International Workshop on Emerging Technologies for LTE-Advanced and Beyond-4G, pp. 624-630, California, USA, 2012.

[28] 3GPP TS 36.355 "Evolved Universal Terrestrial Radio Access (E-UTRA); LTE Positioning Protocol (LPP)," Release 9.

[29] TS 36.214 "Evolved Universal Terrestrial Radio Access (E-UTRA); Physical Layer measurements," Release 9.

[30] S. Cherian, A. Rudrapatna, "A Primer on Location Technologies in LTE Networks," available online: http://www2.alcatel-lucent.com/techzine/a-primer-on-location-technologies-in-lte-networks

[31] 3GPP TR 36.819 "Coordinated multi-point operation for LTE physical layer aspects," Release 11.

[32] P. Gupta, P. R. Kumar, "The Capacity of Wireless Networks," IEEE Transactions on Information Theory, vol. 46, pp. 388-404, Mar. 2000.

[33] M. Grossglauser, D. Tse, "Mobility increases the capacity of ad-hoc wireless networks," IEEE/ACM Transactions on Networking, vol. 10, no. 4, pp. 477-486, Aug. 2002.

[34] A. C. Lozano, S. R. Kulkarni, P. Viswanath, "Throughput Scaling in Wireless Networks with Restricted Mobility," IEEE Transactions on Wireless Communications, vol. 6, no. 2, pp. 670-679, 2007.

[35] Liang-Liang Xie, P. R. Kumar, "A Network Information Theory for Wireless Communication: Scaling Laws and Optimal Operation," IEEE Transactions on Information Theory, vol. 50, no. 5, pp. 748-767, 2004.

[36] P. Gupta, P. R. Kumar, "Towards an Information Theory of Large Networks: An Achievable Rate Region," IEEE Transactions on Information Theory, vol. IT-49, pp. 1877-1894, 2003.

[37] W. H. Tranter, K. S. Shanmugan, T. Rappaport, K. L. Kosbar, "Principles of Communication System Simulation with Wireless Applications," Prentice Hall PTR, New Jersey, 2004.

[38] E. S. Sousa, J. A. Silvester, "Optimum Transmission Ranges in a Direct-Sequence Spread-Spectrum Multihop Packet Radio Network," IEEE Journal on Selected Areas in Communications, vol. 8, no. 5, pp. 762-771, 1990.

[39] C. Comaniciu, H. V. Poor, "On the capacity of mobile ad hoc networks with delay constraints," IEEE Transactions on Wireless Communications, vol. 5, no. 8, pp. 2061-2071, 2006.

[40] R. E. Rezagah, A. Mohammadi, "The Capacity Estimation of Wireless Ad Hoc Networks in Fading Channels," IET Communications, vol. 3, Issue 2, pp. 293-302, 2009.

[41] T. S. Rappaport, "Wireless Communications, Principles and Practice," Prentice Hall PTR, New Jersey 2nd edn.2002.

[42] S. Toumpis, A. Goldsmith,"Capacity regions for wireless ad hoc networks," IEEE Transactions on Wireless Communications, vol. 24, no. 5, pp. 736-748, 2003.

[43] A. Jovicic, P. Viswanath, S. Kulkarni, "Upper bounds to transport capacity of wireless networks," IEEE Transactions on Information Theory, vol. 50, no. 11, pp. 2555-2565, 2004.

[44] O. Leveque, I. E. Teletar, "Information-theoretic upper bounds on the capacity of large extended ad hoc wireless networks," IEEE Transactions on Information Theory, vol. 51, no. 3, pp. 858-865, 2005.

[45] M. Franceschetti, O. Dousse, D. Tse, P. Thiran, "Closing the gap in the capacity of wireless networks via percolation theory," IEEE Transactions on Information Theory, vol. 53, no. 3, pp. 1009-1018, 2007.

[46] N. Jindal, J. G. Andrews, S. Weber, "Energy-Limited vs. Interference-Limited Ad Hoc Network Capacity," Proceedings of ACSSC 2007- Forty First Asilomar Conference on Signals, Systems and Computers, pp. 148-152, Pacific Grove, CA, Nov. 2007.

[47] Canming Jiang, Yi Shi, Y. T. Hou, S. Kompella, "On the Asymptotic Capacity of Multi-Hop MIMO Ad Hoc Networks," IEEE Transactions on Wireless Communications, vol. 10, Issue 4, pp. 1032- 1037, Apr. 2011.

[48] Chun-Hung Liu, J. G. Andrews, "Ergodic Transmission Capacity of Wireless Ad Hoc Networks with Interference Management," IEEE Transactions on Wireless Communications, vol. 11, Issue 6, pp. 2136-2147, Jun. 2012.

[49] P. Li, M. Pan, Y. Fang, "Capacity Bounds of Three-Dimensional Wireless Ad Hoc Networks," IEEE/ACM Transactions on Networking, vol. 20, Issue 4, pp. 1304-1315, Aug. 2012.

[50] P. H. J. Nardelli, M. Kaynia, P. Cardieri, M. Latva-aho, "Optimal Transmission Capacity of Ad Hoc Networks with Packet Retransmissions," IEEE Transactions on Wireless Communications, vol. 11, Issue 8, pp. 2760- 2766, Aug. 2012.

[51] X. Chen, W. Huang, X. Wang, X. Lin, "Multicast Capacity in Mobile Wireless Ad Hoc Network with Infrastructure Support," Proceedings of IEEE INFOCOM, pp. 271-279, Mar. 2012.

[52] R. Vaze, R. W. Heath, "Transmission Capacity of Ad-hoc Networks with Multiple Antennas Using Transmit Stream Adaptation and Interference Cancellation," IEEE Transactions on Information Theory, vol. 58, Issue 2, pp. 780-792, Feb. 2012.